Who can believe what varies every day,
Nor ever was, nor will be at a stay?
John Dryden (1631-1700), Hind and the Panther

5

Variational Perturbation Theory

Most path integrals cannot be performed exactly. It is therefore necessary to develop approximation procedures which allow us to approach the exact result with any desired accuracy, at least in principle. The perturbation expansion of Chapter 3 does not serve this purpose since it diverges for any coupling strength. Similar divergencies appear in the semiclassical expansion of Chapter 4.

The present chapter develops a convergent approximation procedure to calculate Euclidean path integrals at a finite temperature. The basis for this procedure is a variational approach due to Feynman and Kleinert, which was recently extended to a systematic and uniformly convergent *variational perturbation expansion* [1].

5.1 Variational Approach to Effective Classical Partition Function

Starting point for the variational approach will be the path integral representation (3.816) for the effective classical potential introduced in Section 3.25. Explicitly, the effective classical Boltzmann factor $B(x_0)$ for a quantum system with an action

$$\mathcal{A}_{\rm e} = \int_0^{\hbar\beta} d\tau \left[\frac{M}{2}\dot{x}^2(\tau) + V(x(\tau))\right] \tag{5.1}$$

has the path integral representation [recall (3.816) and (3.809)]

$$B(x_0) \equiv e^{-V^{\rm eff\,cl}(x_0)/k_BT} = \oint \mathcal{D}'x\, e^{-\mathcal{A}_{\rm e}/\hbar} = \prod_{m=1}^{\infty}\left[\int \frac{dx_m^{\rm re}dx_m^{\rm im}}{\pi k_BT/M\omega_m^2}\right]\times \tag{5.2}$$
$$\times \exp\left[-\frac{M}{k_BT}\sum_{m=1}^{\infty}\omega_m^2|x_m|^2 - \frac{1}{\hbar}\int_0^{\hbar/k_BT} d\tau V\left(x_0 + \sum_{m=1}^{\infty}(x_m e^{-i\omega_m\tau} + \text{c.c.})\right)\right],$$

with the notation $x_m^{\rm re} = {\rm Re}\, x_m$, $x_m^{\rm im} = {\rm Im}\, x_m$. To make room for later subscripts, we shall in this chapter write $\mathcal{A}$ instead of $\mathcal{A}_{\rm e}$. In Section 3.25 we have derived a perturbation expansion for $B(x_0) = e^{-\beta V^{\rm eff\,cl}(x_0)}$. Here we shall find a simple but quite accurate approximation for $B(x_0)$ whose effective classical potential $V^{\rm eff\,cl}(x_0)$ approaches the exact expression always from above.

5.2 Local Harmonic Trial Partition Function

The desired approximation is obtained by comparing the path integral in question with a solvable trial path integral. The trial path integral consists of a suitable superposition of local harmonic oscillator path integrals centered at arbitrary average positions x_0, each with an own frequency $\Omega^2(x_0)$. The coefficients of the superposition and the frequencies are chosen in such a way that the effective classical potential of the trial system is an optimal upper bound to the true effective classical potential. In systems with a smooth or at least not too singular potential, the accuracy of the approximation will be very good. In Section 5.13 we show how to use this approximation as a starting point of a systematic variational perturbation expansion which permits improving the result to any desired accuracy.

As a local trial action we shall take the harmonic action (3.850), which may also be considered as the action of a harmonic oscillator centered around some point x_0:

$$\mathcal{A}_\Omega^{x_0} = \int_0^{\hbar/k_BT} d\tau M \left[\frac{\dot{x}^2}{2} + \Omega^2(x_0)\frac{(x-x_0)^2}{2}\right]. \tag{5.3}$$

However, instead of using the specific frequency $\Omega^2(x_0) \equiv V''(x_0)/M$ in (3.850), we shall choose $\Omega(x_0)$ to be an as yet unknown local trial frequency. The effective classical Boltzmann factor $B(x_0)$ associated with this trial action can be taken directly from (3.823). We simply replace the harmonic potential $M\omega^2x^2/2$ in the defining expression (3.816) by the local trial potential $\Omega(x_0)(x-x_0)^2/2$. Then the first term in the fluctuation expansion (3.817) of the action vanishes, and we obtain, instead of (3.823), the local Boltzmann factor

$$B_\Omega(x_0) \equiv e^{-V^{\text{eff cl}}(x_0)/k_BT} = \frac{\hbar\Omega(x_0)/2k_BT}{\sinh[\hbar\Omega(x_0)/2k_BT]} \equiv Z_\Omega^{x_0}. \tag{5.4}$$

The exponential $\exp(-\beta M\omega^2 x_0^2/2)$ in (3.823) is absent since the local trial potential vanishes at $x = x_0$. The local Boltzmann factor $B_\Omega(x_0)$ is a local partition function of paths whose temporal average is restricted to x_0, and this fact will be emphasized by the alternative notation $Z_\Omega^{x_0}$ which we shall now find convenient to use. The effective classical potential of the harmonic oscillators may also be viewed as a local free energy associated with the local partition function $Z_\Omega^{x_0}$ which we defined as

$$F_\Omega^{x_0} \equiv -k_BT \log Z_\Omega^{x_0}, \tag{5.5}$$

such that we may identify

$$V_\Omega^{\text{eff cl}}(x_0) = F_\Omega^{x_0} = k_BT \log\left\{\frac{\sinh[\hbar\Omega(x_0)/2k_BT]}{\hbar\Omega(x_0)/2k_BT}\right\}. \tag{5.6}$$

The harmonic path integral associated with the local partition function $Z_\Omega^{x_0}$ is

$$\begin{aligned} Z_\Omega^{x_0} &= \int \mathcal{D}x(\tau)\tilde{\delta}(\bar{x}-x_0)e^{-\mathcal{A}_\Omega^{x_0}/\hbar} \\ &= \prod_{m=1}^{\infty}\left[\int \frac{dx_m^{\text{re}}dx_m^{\text{im}}}{\pi k_BT/M\omega_m^2}\right] e^{-\frac{M}{k_BT}\sum_{m=1}^{\infty}[\omega_m^2+\Omega^2(x_0)]|x_m|^2}, \end{aligned} \tag{5.7}$$

where $\tilde{\delta}(\bar{x}-x_0)$ is the slightly modified δ-function introduced in Eq. (3.815).

We now define the *local expectation values* of an arbitrary functional $F[x(\tau)]$ within the harmonic path integral (5.7):

$$\langle F[x(\tau)]\rangle_\Omega^{x_0} \equiv [Z_\Omega^{x_0}]^{-1}\int \mathcal{D}x\,\tilde{\delta}(\bar{x}-x_0)e^{-\mathcal{A}_\Omega^{x_0}/\hbar}\,F[x(\tau)]. \tag{5.8}$$

The effective classical potential can then be re-expressed as a path integral

$$\begin{aligned} e^{-V^{\text{eff cl}}(x_0)/k_BT} &= Z^{x_0} = \int \mathcal{D}x\,\tilde{\delta}(\bar{x}-x_0)e^{-\mathcal{A}/\hbar} \\ &\equiv \int \mathcal{D}x\,\tilde{\delta}(\bar{x}-x_0)e^{-\mathcal{A}_\Omega^{x_0}/\hbar}e^{-(\mathcal{A}-\mathcal{A}_\Omega^{x_0})/\hbar} \\ &= Z_\Omega^{x_0}\left\langle e^{-(\mathcal{A}-\mathcal{A}_\Omega^{x_0})/\hbar}\right\rangle_\Omega^{x_0}. \end{aligned} \tag{5.9}$$

We now take advantage of the fact that the expectation value on the right-hand side possesses an easily calculable bound given by the *Jensen-Peierls inequality*:

$$\left\langle e^{-(\mathcal{A}-\mathcal{A}_\Omega^{x_0})/\hbar}\right\rangle_\Omega^{x_0} \geq e^{-\left\langle \mathcal{A}/\hbar-\mathcal{A}_\Omega^{x_0}/\hbar\right\rangle_\Omega^{x_0}}. \tag{5.10}$$

This implies that the effective classical potential has an upper bound

$$V^{\text{eff cl}}(x_0) \leq F_\Omega^{x_0}(x_0) + k_BT\,\langle \mathcal{A}/\hbar - \mathcal{A}_\Omega^{x_0}/\hbar\rangle_\Omega^{x_0}. \tag{5.11}$$

The Jensen-Peierls inequality is a consequence of the *convexity* of the exponential function: The average of two exponentials is always larger than the exponential at the average point (see Fig. 5.1):

$$\frac{e^{-x_1}+e^{-x_2}}{2} \geq e^{-\frac{x_1+x_2}{2}}. \tag{5.12}$$

This convexity property of the exponential function can be generalized to an exponential functional. Let $\mathcal{O}[x]$ be an arbitrary functional in the space of paths $x(\tau)$, and

$$\langle \mathcal{O}[x]\rangle \equiv \int \mathcal{D}\mu[x]\mathcal{O}[x] \tag{5.13}$$

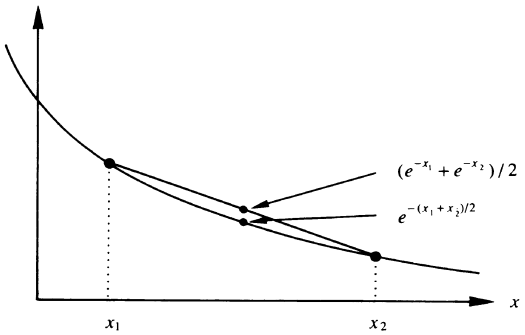

Figure 5.1 Illustration of convexity of exponential function e^{-x}, satisfying $\langle e^{-x}\rangle \geq e^{-\langle x\rangle}$ everywhere.

an expectation value in this space. The measure of integration $\mu[x]$ is supposed to be normalized so that $\langle 1 \rangle = 1$. Then (5.12) generalizes to

$$\left\langle e^{-\mathcal{O}} \right\rangle \geq e^{-\langle \mathcal{O} \rangle}. \tag{5.14}$$

To prove this we first observe that the inequality (5.12) remains valid if x_1, x_2 are replaced by the values of an arbitrary function $\mathcal{O}(x)$:

$$\frac{e^{-\mathcal{O}(x_1)} + e^{-\mathcal{O}(x_2)}}{2} \geq e^{-\frac{\mathcal{O}(x_1)+\mathcal{O}(x_2)}{2}}. \tag{5.15}$$

This inequality is then generalized with the help of any positive measure $\mu(x)$, with unit normalization, $\int d\mu(x) = 1$, to

$$\int d\mu(x) e^{-\mathcal{O}(x)} \geq e^{\int d\mu(x) e^{-\mathcal{O}(x)}}, \tag{5.16}$$

and further to

$$\int \mathcal{D}\mu[x] e^{-\mathcal{O}[x]} \geq e^{\int \mathcal{D}\mu[x] e^{-\mathcal{O}[x]}}, \tag{5.17}$$

where $\mu[x]$ is any positive functional measure with the normalization $\int \mathcal{D}\mu[x] = 1$. This shows that Eq. (5.14) is true, and hence also the Jensen-Peierls inequality (5.10).

Since the kinetic energies in the two actions $\mathcal{A}$ and $\mathcal{A}_\Omega^{x_0}$ in (5.11) are equal, the inequality (5.11) can also be written as

$$V^{\text{eff cl}}(x_0) \leq F_\Omega^{x_0} + \frac{k_B T}{\hbar} \int_0^{\hbar/k_B T} d\tau \left\langle \left[V(x(\tau)) - M \frac{\Omega^2(x_0)}{2} (x(\tau) - x_0)^2 \right] \right\rangle_\Omega^{x_0}. \tag{5.18}$$

The local expectation value on the right-hand side is easily calculated. Recalling the definition (3.856) we have to use the correlation functions of $\eta(\tau)$ without the zero frequency in Eq. (3.842):

$$\langle \eta(\tau)\eta(\tau') \rangle_\Omega^{x_0} \equiv a^2_{\tau\tau'}(x_0) = \frac{\hbar}{M} \left[\frac{1}{2\Omega(x_0)} \frac{\cosh \Omega(x_0)(|\tau - \tau'| - \hbar\beta/2)}{\sinh(\Omega(x_0)\hbar\beta/2)} - \frac{1}{\hbar\beta\Omega^2} \right], \tag{5.19}$$

valid for arguments $\tau, \tau' \in [0, \hbar\beta]$. By analogy with (3.806) we may denote this quantity by $a^2_{\Omega(x_0)}(\tau, \tau')$, which we have shortened to $a^2_{\tau\tau'}(x_0)$, to avoid a pile-up of indices.

All subtracted correlation functions can be obtained from the functional derivatives of the local generating functional

$$Z_\Omega^{x_0}[j] \equiv \int \mathcal{D}x(\tau) \tilde{\delta}(\bar{x} - x_0)\, e^{-(1/\hbar)\int_0^{\hbar\beta} d\tau \left[\frac{M}{2} \left\{ \dot{x}^2(\tau) + \Omega^2(x_0)[x(\tau) - x_0]^2 \right] - j(\tau)[x(\tau) - x_0] \right\}}, \tag{5.20}$$

whose explicit form was calculated in (3.847):

$$Z_\Omega^{x_0}[j] = Z_\Omega^{x_0} \exp \left\{ \frac{1}{2M\hbar} \int_0^{\hbar\beta} d\tau \int_0^{\hbar\beta} d\tau' j(\tau) G^{\text{p}\prime}_{\Omega^2(x_0),\text{e}}(\tau - \tau') j(\tau') \right\}. \tag{5.21}$$

If desired, the Green function can be continued analytically to the real-time retarded Green function

$$G^R_{\Omega^2}(t,t') = \frac{M}{\hbar}\Theta(t-t')\,\langle x(t)x(t')\rangle \tag{5.22}$$

in a way to be explained later in Section 18.2.

With the help of the spectral decomposition of these correlation functions to be derived in Section 18.2, it is possible to show that the lowest frequency content of the zero-temperature Green function (5.22) contains the information on the lowest excitation energy of a physical system. For the frequncy ω of an oscillator Green function this is trivially true. It is then obvious that in the above approximation where the Green function is a superposition of oscillator Green functions of frequencies $\Omega(x_0)$, the minimal zero-temperature value of $\hbar\Omega(x_0)$ gives an approximation to the energy difference between ground and first excited states. In Table 5.1 we see that for the anharmonic oscillator, this approximation is quite good.

As shown in Fig. 3.14, the *local fluctuation square width*

$$\Big\langle \eta^2(\tau)\Big\rangle^{x_0}_{\Omega} = \Big\langle (x(\tau)-x_0)^2\Big\rangle^{x_0}_{\Omega} = a^2_{\tau\tau}(x_0) \equiv a^2_{\Omega(x_0)}, \tag{5.23}$$

with the explicit form (3.806),

$$a^2_{\Omega(x_0)} = \frac{2}{M\beta}\sum_{m=1}^{\infty}\frac{1}{\omega_m^2+\Omega^2(x_0)} = \frac{1}{M\beta\Omega^2(x_0)}\left[\frac{\hbar\beta\Omega(x_0)}{2}\coth\frac{\hbar\beta\Omega(x_0)}{2}-1\right], \tag{5.24}$$

goes to zero for high temperature like

$$a^2_{\Omega(x_0)} \xrightarrow[T\to\infty]{} \hbar^2/12Mk_BT. \tag{5.25}$$

This is in contrast to the unrestricted expectation $\langle (x(\tau)-x_0)^2\rangle_{\Omega(x_0)}$ of the harmonic oscillator which includes the $\omega_m = 0$ -term in the spectral decomposition (3.803):

$$a^2_{\rm tot} \equiv \Big\langle (x(\tau)-x_0)^2\Big\rangle_{\Omega(x_0)} = a^2_{\Omega(x_0)} + \frac{k_BT}{M\Omega^2(x_0)}. \tag{5.26}$$

This grows linearly with T following the equipartition theorem (3.803).

As discussed in Section 3.25, this difference is essential for the reliability of a perturbation expansion of the effective classical potential. It will also be essential for the quality of the variational approach in this chapter.

The local fluctuation square width $a^2_{\Omega(x_0)}$ measures the importance of quantum fluctuations at nonzero temperatures. These decrease with increasing temperatures. In contrast, the square width of the $\omega_0 = 0$ -term grows with the temperature showing the growing importance of classical fluctuations.

This behavior of the fluctuation width is in accordance with our previous observation after Eq. (3.840) on the finite width of the Boltzmann factor $B(x_0) = e^{-V^{\rm eff\,cl}(x_0)/k_BT}$ for low temperatures in comparison to the diverging width of the

alternative Boltzmann factor (3.841) formed from the partition function density $\tilde{B}(x_0) \equiv l_{\rm e}(\hbar\beta)\, z(x) = e^{-\tilde{V}^{\rm eff\,cl}(x_0)/k_BT}$.

Since $a^2_{\Omega(x_0)}$ is finite at *all* temperatures, the quantum fluctuations can be treated approximately. The approximation improves with growing temperatures where $a^2_{\Omega(x_0)}$ tends to zero. The thermal fluctuations, on the other hand, diverge at high temperatures. Their evaluation requires a numeric integration over x_0 in the final effective classical partition function (3.811).

Having determined $a^2_{\Omega(x_0)}$, the calculation of the local expectation value $\langle V(x(\tau))\rangle^{x_0}_{\Omega}$ is quite easy following the steps in Subsection 3.25.8. The result is the smearing formula analogous to (3.875): We write $V(x(\tau))$ as a Fourier integral

$$V(x(\tau)) = \int_{-\infty}^{\infty} \frac{dk}{2\pi} e^{ikx(\tau)} \tilde{V}(k), \tag{5.27}$$

and obtain with the help of Wick's rule (3.307) the expectation value

$$\langle V(x(\tau))\rangle^{x_0}_{\Omega} = V_{a^2}(x_0) \equiv \int_{-\infty}^{\infty} \frac{dk}{2\pi} \tilde{V}(k) e^{ikx_0 - a^2(x_0)k^2/2}. \tag{5.28}$$

For brevity, we have used the shorter notation $a^2(x_0)$ for $a^2_{\Omega(x_0)}$, and shall do so in the remainder of this chapter. Reinsert the Fourier coefficients of the potential

$$\tilde{V}(k) = \int_{-\infty}^{\infty} dx\, V(x) e^{-ikx}, \tag{5.29}$$

we may perform the integral over k and obtain the convolution integral

$$\langle V(x(\tau))\rangle^{x_0}_{\Omega} = V_{a^2}(x_0) \equiv \int_{-\infty}^{\infty} \frac{dx_0'}{\sqrt{2\pi a^2(x_0)}} e^{-(x_0'-x_0)^2/2a^2(x_0)}\; V(x_0'). \tag{5.30}$$

As in (3.875), the convolution integral smears the original potential $V(x_0)$ out over a length scale $a(x_0)$, thus accounting for the effects of quantum-statistical path fluctuations.

The expectation value $\langle (x(\tau) - x_0)^2\rangle^{x_0}_{\Omega}$ in Eq. (5.26) is, of course, a special case of this general *smearing rule*:

$$(x - x_0)^2_{a^2} = \int_{-\infty}^{\infty} \frac{dx'}{\sqrt{2\pi a^2}} e^{-(1/2a^2)(x'-x_0)^2} (x' - x_0)^2 = a^2(x_0). \tag{5.31}$$

Hence we obtain for the effective classical potential the approximation

$$W_1^{\Omega}(x_0) \;\equiv\; F^{x_0}_{\Omega} + V_{a^2}(x_0) - \frac{M}{2}\Omega^2(x_0)a^2(x_0), \tag{5.32}$$

which by the Jensen-Peierls inequality lies always above the true result:

$$W_1^{\Omega}(x_0) \geq V^{\rm eff\,cl}(x_0). \tag{5.33}$$

A minimization of $W_1^\Omega(x_0)$ in $\Omega(x_0)$ produces an optimal variational approximation to be denoted by $W_1(x_0)$.

For the harmonic potential $V(x) = M\omega^2 x^2/2$, the smearing process leads to $V_{a^2}(x_0) = M\omega^2(x_0^2 + a^2)/2$. The extremum of $W_1^\Omega(x_0)$ lies at $\Omega(x_0) \equiv \omega$, so that the optimal upper bound is

$$W_1(x_0) = F_\omega^{x_0} + M\omega^2 \frac{x_0^2}{2}. \tag{5.34}$$

Thus, for the harmonic oscillator, $W_1^\Omega(x_0)$ happens to coincide with the exact effective classical potential $V_\omega^{\text{eff cl}}(x_0)$ found in (3.830).

5.3 The Optimal Upper Bound

We now determine the frequency $\Omega(x_0)$ of the local trial oscillator which optimizes the upper bound in Eq. (5.33). The derivative of $W_1^\Omega(x_0)$ with respect to $\Omega^2(x_0)$ has two terms:

$$\frac{dW_1^\Omega(x_0)}{d\Omega^2(x_0)} = \frac{\partial W_1^\Omega(x_0)}{\partial \Omega^2(x_0)} + \left.\frac{\partial W_1^\Omega(x_0)}{\partial a^2(x_0)}\right|_{\Omega(x_0)} \frac{\partial a^2(x_0)}{\partial \Omega^2(x_0)}.$$

The first term is

$$\frac{\partial W_1(x_0)}{\partial \Omega^2(x_0)} = \frac{M}{2}\left\{\frac{k_B T}{M\Omega^2(x_0)}\left[\frac{\hbar\Omega}{2k_BT}\coth\left(\frac{\hbar\Omega}{2k_BT}\right) - 1\right] - a^2(x_0)\right\}. \tag{5.35}$$

It vanishes automatically due to (5.24). Thus we only have to minimize $W_1^\Omega(x_0)$ with respect to $a^2(x_0)$ by satisfying the condition

$$\frac{\partial W_1^\Omega(x_0)}{\partial a^2(x_0)} = 0. \tag{5.36}$$

Inserting (5.32), this determines the trial frequency

$$\Omega^2(x_0) = \frac{2}{M}\frac{\partial V_{a^2}(x_0)}{\partial a^2(x_0)}. \tag{5.37}$$

In the Fourier integral (5.28) for $V_{a^2}(x_0)$, the derivative $2(\partial/\partial a^2)V_{a^2}$ is represented by a factor $-k^2$ which, in turn, is equivalent to $\partial/\partial x_0^2$. This leads to the alternative equation:

$$\Omega^2(x_0) = \frac{1}{M}\left[\frac{\partial^2}{\partial x_0^2} V_{a^2}(x_0)\right]_{a^2 = a^2(x_0)}. \tag{5.38}$$

Note that the partial derivatives must be taken at *fixed* a^2 which is to be set equal to $a^2(x_0)$ at the end.

The potential $W_1^\Omega(x_0)$ with the extremal $\Omega^2(x_0)$ and the associated $a^2(x_0)$ of (5.24) constitutes the *Feynman-Kleinert approximation* $W_1(x_0)$ to the effective classical potential $V^{\text{eff cl}}(x_0)$.

It is worth noting that due to the vanishing of the partial derivative $\partial W_1^\Omega(x_0)/\partial\Omega^2(x_0)$ in (5.35) we may consider $\Omega^2(x_0)$ and $a^2(x_0)$ as arbitrary variational parameters in the expression (5.32) for $W_1^\Omega(x_0)$. Then the *independent* variation of $W_1^\Omega(x_0)$ with respect to these two parameters yields both (5.24) *and* the minimization condition (5.37) for $\Omega^2(x_0)$.

From the extremal $W_1^\Omega(x_0)$ we obtain the approximation for the partition function and the free energy [recall (3.837)]

$$Z_1 = e^{-F_1/k_BT} = \int_{-\infty}^{\infty} \frac{dx_0}{l_{\rm e}(\hbar\beta)} e^{-W_1(x_0)/k_BT} \leq Z, \tag{5.39}$$

where $l_{\rm e}(\hbar\beta)$ is the thermal de Broglie length defined in Eq. (2.353). We leave it to the reader to calculate the second derivative of $W_1^\Omega(x_0)$ with respect to $\Omega^2(x_0)$ and to prove that it is nonnegative, implying that the above extremal solution is a local *minimum*.

5.4 Accuracy of Variational Approximation

The accuracy of the approximate effective classical potential $W_1(x_0)$ can be estimated by the following observation: In the limit of high temperatures, the approximation is perfect by construction, due the shrinking width (5.25) of the nonzero frequency fluctuations. This makes $W_1(x_0)$ in (5.31) converge against $V(x_0)$, just as the exact effective classical potential in Eq. (3.812).

In the opposite limit of low temperatures, the integral over x_0 in the general expression (3.811) is dominated by the minimum of the effective classical potential. If its position is denoted by $x_{\rm m}$, we have the saddle point approximation (see Section 4.2)

$$Z \xrightarrow[T\to 0]{} e^{-V^{\rm eff\,cl}(x_{\rm m})/k_BT} \int \frac{dx_0}{l_{\rm e}(\hbar\beta)} e^{-[V^{\rm eff\,cl}(x_{\rm m})]''(x_0-x_{\rm m})^2/2k_BT}. \tag{5.40}$$

The exponential of the prefactor yields the leading low-temperature behavior of the free energy:

$$F \xrightarrow[T\to 0]{} V^{\rm eff\,cl}(x_{\rm m}). \tag{5.41}$$

The Gaussian integral over x_0 contributes a term

$$\Delta F = k_BT \log\left\{ \frac{\hbar}{k_BT}\sqrt{\frac{[V^{\rm eff\,cl}(x_{\rm m})]''}{M}} \right\}, \tag{5.42}$$

which accounts for the entropy of x_0 fluctuations around $x_{\rm m}$ [recall Eq. (1.568)]. Moreover, at zero temperature, the free energy F converges against the ground state energy $E^{(0)}$ of the system, so that

$$E^{(0)} = V^{\rm eff\,cl}(x_{\rm m}). \tag{5.43}$$

The minimum of the approximate effective classical potential, $W_1^\Omega(x_0)$ with respect to $\Omega(x_0)$ supplies us with a variational approximation to the free energy F_1, which in the limit $T \to 0$ yields a variational approximation to the ground state energy

$$E_1^{(0)} = F_1|_{T=0} \equiv W_1(x_{\rm m})|_{T=0}\,. \tag{5.44}$$

By taking the $T \to 0$ limit in (5.32) we see that

$$\lim_{T\to 0} W_1^\Omega(x_0) = \frac{1}{2}\left[\hbar\Omega(x_0) - M\Omega^2(x_0)a^2(x_0)\right] + V_{a^2}(x_0). \tag{5.45}$$

In the same limit, Eq. (5.24) gives

$$\lim_{T\to 0} a^2(x_0) = \frac{\hbar}{2M\Omega(x_0)}, \tag{5.46}$$

so that

$$\lim_{T\to 0} W_1^\Omega(x_0) = \frac{1}{4}\hbar\Omega(x_0) + V_{a^2}(x_0) = \frac{1}{8}\frac{\hbar^2}{Ma^2(x_0)} + V_{a^2}(x_0)\,. \tag{5.47}$$

The right-hand side is recognized as the expectation value of the Hamiltonian operator

$$\hat H = \frac{\hat p^2}{2M} + V(x) \tag{5.48}$$

in a normalized Gaussian wave packet of width a centered at x_0:

$$\psi(x) = \frac{1}{(2\pi a^2)^{1/4}} \exp\left[-\frac{1}{4a^2}(x-x_0)^2\right]. \tag{5.49}$$

Indeed,

$$\left\langle \hat H \right\rangle_\psi \equiv \int_{-\infty}^{\infty} dx \psi^*(x)\hat H\psi(x) = \frac{1}{8}\frac{\hbar^2}{Ma^2} + V_{a^2}(x_0). \tag{5.50}$$

Let E_1 be the minimum of this expectation under the variation of x_0 and a^2:

$$E_1 = \min_{x_0,a^2} \left\langle \hat H \right\rangle_\psi. \tag{5.51}$$

This is the variational approximation to the ground state energy provided by the *Rayleigh-Ritz method*.

In the low temperature limit, the approximation F_1 to the free energy converges toward E_1:

$$\lim_{T\to 0} F_1 = E_1. \tag{5.52}$$

The approximate effective classical potential $W_1(x_0)$ is for all temperatures and x_0 more accurate than the estimate of the ground state energy E_0 by the minimal expectation value (5.51) of the Hamiltonian operator in a Gaussian wave packet. For potentials with a pronounced unique minimum of quadratic shape, this estimate is known to be excellent.

Table 5.1 Comparison of variational energy $E_1 = \lim_{T\to 0} F_1$, obtained from Gaussian trial wave function, with exact ground state energy $E_{\rm ex}^{(0)}$. The energies of the first two excited states $E_{\rm ex}^{(1)}$ and $E_{\rm ex}^{(2)}$ are listed as well. The level splitting $\Delta E_{\rm ex}^{(0)} = E_{\rm ex}^{(1)} - E_{\rm ex}^{(0)}$ to the first excited state is shown in column 6. We see that it is well approximated by the value of $\Omega(0)$, as it should (see the discussion after Eq. (5.21).

$g/4$	E_1	$E_{\rm ex}^{(0)}$	$E_{\rm ex}^{(1)}$	$E_{\rm ex}^{(2)}$	$\Delta E_{\rm ex}^{(0)}$	$\Omega(0)$	$a^2(0)$
0.1	0.5603	0.559146	1.76950	3.13862	1.21035	1.222	0.4094
0.2	0.6049	0.602405	1.95054	3.53630	1.34810	1.370	0.3650
0.3	0.6416	0.637992	2.09464	3.84478	1.45665	1.487	0.3363
0.4	0.6734	0.668773	2.21693	4.10284	1.54816	1.585	0.3154
0.5	0.7017	0.696176	2.32441	4.32752	1.62823	1.627	0.2991
0.6	0.7273	0.721039	2.42102	4.52812	1.69998	1.749	0.2859
0.7	0.7509	0.743904	2.50923	4.71033	1.76533	1.819	0.2749
0.8	0.7721	0.765144	2.59070	4.87793	1.82556	1.884	0.2654
0.9	0.7932	0.785032	2.66663	5.03360	1.86286	1.944	0.2572
1.0	0.8125	0.803771	2.73789	5.17929	1.93412	2.000	0.2500
10	1.5313	1.50497	5.32161	10.3471	3.81694	4.000	0.1250
50	2.5476	2.49971	8.91510	17.4370	6.41339	6.744	0.0741
100	3.1924	3.13138	11.1873	21.9069	8.05590	8.474	0.0590
500	5.4258	5.31989	19.0434	37.3407	13.7235	14.446	0.0346
1000	6.8279	6.69422	23.9722	47.0173	17.2780	18.190	0.0275

In Table 5.1 we list the energies $E_1 = W_1(0)$ for a particle in an anharmonic oscillator potential. Its action will be specified in Section 5.7, where the approximation $W_1(x_0)$ will be calculated and discussed in detail. The table shows that this approximation promises to be quite good [2].

With the effective classical potential having good high- and low-temperature limits, it is no surprise that the approximation is quite reliable at all temperatures.

Even if the potential minimum is not smooth, the low-temperature limit can be of acceptable accuracy. An example is the three-dimensional Coulomb system for which the limit (5.51) becomes (with the obvious optimal choice $x_0 = 0$)

$$E_1 = \min_a \left(\frac{3}{8} \frac{\hbar^2}{Ma^2} - \frac{2}{\sqrt{\pi}} \frac{e^2}{\sqrt{2a^2}} \right) = -\frac{3}{8} \frac{\hbar^2}{Ma_{\rm min}^2}. \tag{5.53}$$

The minimal value of a is $a_{\rm min} = \sqrt{9\pi/32}a_H$ where $a_H = \hbar^2/Me^2$ is the Bohr radius (4.376) of the hydrogen atom. In terms of it, the minimal energy has the value $E_1 = -(4/3\pi)e^2/a_H$. This is only 15% percent different from the true ground state energy of the Coulomb system $E_{\rm ex}^{(0)} = -(1/2)e^2/a_H$. Such a high degree of accuracy may seem somewhat surprising since the exact Coulomb wave function $\psi(\mathbf{x}) = (\pi a_H^3)^{-1/2} \exp(-r/a_H)$ is far from being a Gaussian.

The partition function of the Coulomb system can be calculated only after subtracting the free-particle partition function and screening the $1/r$ -behavior down to a finite range. The effective classical free energy F_1 of the Coulomb potential

obtained by this method is, at any temperature, more accurate than the difference between E_1 and $E_{\rm ex}^{(0)}$. More details will be given in Section 5.10.

5.5 Weakly Bound Ground State Energy in Finite-Range Potential Well

The variational approach allows us to derive a simple approximation for the bound-state energy in an arbitrarily shaped potential of finite range, for which the binding energy is very weak. Precisely speaking, the falloff of the ground state wave function has to lie outside the range of the potential. A typical example for this situation is the binding of electrons to Cooper pairs in a superconductor. The attractive force comes from the electron-phonon interaction which is weakened by the Coulomb repulsion. The potential has a complicated shape, but the binding energy is so weak that the wave function of a Cooper pair reaches out to several thousand lattice spacings, which is much larger than the range of the potential, which extends only over maximally a hundred lattice spacings. In this case one may practically replace the potential by an equivalent δ-function potential.

The present considerations apply to this situation. Let us assume the absolute minimum of the potential to lie at the origin. The first-order variational energy at the origin is given by

$$W_1(0) = \frac{\Omega}{2} + V_{a^2}(0), \tag{5.54}$$

where by (5.30)

$$V_{a^2}(0) = \int_{-\infty}^{\infty} \frac{dx_0'}{\sqrt{2\pi a^2}} e^{-x_0'^2/2a^2}\ V(x_0'). \tag{5.55}$$

By assumption, the binding energy is so small that the ground state wave function does not fall off within the range of $V(x_0)$. Hence we can approximate

$$V_{a^2}(0) \approx \sqrt{\frac{\Omega}{\pi}} \int_{-\infty}^{\infty} dx_0'\ V(x_0'), \tag{5.56}$$

where we have inserted $a^2 = 1/2\Omega$. Extremizing this in Ω yields the approximate ground state energy

$$E_1^{(0)} \approx -\frac{1}{2\pi} \left[-\int_{-\infty}^{\infty} dx_0'\ V(x_0') \right]^2. \tag{5.57}$$

By applying this result to a simple δ-function potential at the origin,

$$V(x) = -g\delta(x), \quad g > 0, \tag{5.58}$$

we find an approximate ground state energy

$$E_1^{(0)} = -\frac{1}{2\pi} g^2. \tag{5.59}$$

The exact value is

$$E^{(0)} = -\frac{1}{2} g^2. \tag{5.60}$$

The failure of the variational approximation is due to the fact that outside the range of the potential, the wave function is a simple exponential $e^{-k|x|}$ with $k = \sqrt{-2E^{(0)}}$, and not a Gaussian. In fact, if we consider the expectation value of the Hamiltonian operator

$$H = -\frac{1}{2}\frac{d^2}{dx^2} - g\delta(x) \tag{5.61}$$

for a normalized trial wave function

$$\psi(x) = \sqrt{K}e^{-K|x|}, \tag{5.62}$$

we obtain a variational energy

$$W_1 = \frac{K^2}{2} - gK, \tag{5.63}$$

whose minimum gives the exact ground state energy (5.60). Thus, problems of the present type call for the development of a variational perturbation theory for which Eq. (5.54) and (5.55) read

$$W(0) = \frac{K^2}{2} + V_K(0), \tag{5.64}$$

where

$$V_K(0) = K\int_{-\infty}^{\infty}\frac{dx_0'}{a}e^{-K|x_0|}\ V(x_0). \tag{5.65}$$

For an arbitrary attractive potential whose range is much shorter than a, this leads to the correct energy for a weakly bound ground state

$$E_1^{(0)} \approx -\frac{1}{2}\left[-\int_{-\infty}^{\infty}dx_0'\ V(x_0)\right]^2. \tag{5.66}$$

5.6 Possible Direct Generalizations

Let us remark that there is a possible immediate generalization of the above variational procedure. One may treat higher components x_m with $m > 0$ accurately, say up to $m = \bar{m} - 1$, where $\bar{m}$ is some integer > 1, using the ansatz

$$\begin{aligned} Z_{\bar{m}} \equiv \int \mathcal{D}x(\tau)\exp\left\{-\frac{1}{\hbar}\int_0^{\hbar/k_BT}\frac{M}{2}\left[\frac{\dot{x}^2(\tau)}{2} + \Omega^2(x_0,\ldots,x_{\bar{m}})\right.\right. \\ \left.\left.\times\left(x(\tau) - x_0 - \sum_{m=1}^{\bar{m}-1}(x_m e^{-i\omega_m\tau} + \text{c.c.})\right)^2\right]\right\} e^{-(1/k_BT)L_{\bar{m}}(x_0,\ldots,x_{\bar{m}})} \\ = \int_{-\infty}^{\infty}\frac{dx_0}{l_{\rm e}(\hbar\beta)}\prod_{n=1}^{\bar{m}-1}\left[\int\frac{dx_m^{\rm re}\,dx_m^{\rm im}}{\pi k_BT/M\omega_m^2}\frac{\omega_m^2+\Omega^2(x_0)}{\omega_m^2}\right] \\ \times\frac{\hbar\Omega(x_0)/2k_BT}{\sinh(\hbar\Omega(x_0)/2k_BT)}e^{-L_{\bar{m}}(x_0,\ldots,x_{\bar{m}})/k_BT}, \end{aligned} \tag{5.67}$$

with the trial function $L_{\bar{m}}$:

$$L_{\bar{m}}(x_0,\ldots,x_{\bar{m}}) = \frac{k_BT}{\hbar}\int_0^{\hbar/k_BT}d\tau\ V_{a_{\bar{m}}^2}\left(x_0 + \sum_{m=1}^{\bar{m}-1}(x_m e^{-i\omega_m\tau} + \text{c.c.})\right) - \frac{M}{2}\Omega^2(x_0,\ldots,x_{\bar{m}})a_{\bar{m}}^2, \tag{5.68}$$

and a smearing square width of the potential

$$a^2_{\bar{m}} = \frac{2k_BT}{M}\sum_{m=\bar{m}}^{\infty}\frac{1}{\omega_m^2+\Omega^2} \tag{5.69}$$
$$= \frac{k_BT}{M\Omega^2}\left(\frac{\hbar\Omega}{2k_BT}\coth\frac{\hbar\Omega}{2k_BT}-1\right)-\frac{2k_BT}{M}\sum_{m=1}^{\bar{m}-1}\frac{1}{\omega_m^2+\Omega^2}.$$

For the partition function alone the additional work turns out to be not very rewarding since it renders only small improvements. It turns out that in the low-temperature limit $T\to 0$, the free energy is still equal to the optimal expectation of the Hamiltonian operator in the Gaussian wave packet (5.49).

Note that the ansatz (5.7) [as well as (5.67)] cannot be improved by allowing the trial frequency $\Omega(x_0)$ to be a matrix $\Omega_{mm'}(x_0)$ in the space of Fourier components x_m [i.e., by using $\sum_{m,m'}\Omega_{mm'}(x_0)x^*_m x_{m'}$ instead of $\Omega(x_0)\sum_m|x_m|^2$]. This would also lead to an exactly integrable trial partition function. However, after going through the minimization procedure one would fall back to the diagonal solution $\Omega_{mm'}(x_0)=\delta_{mm'}\Omega(x_0)$.

5.7 Effective Classical Potential for Anharmonic Oscillator and Double-Well Potential

For a typical application of the approximation method consider the Euclidean action

$$\mathcal{A}[x]=\int_0^{\hbar/k_BT}d\tau\left[\frac{M}{2}\left(\dot{x}^2+\omega^2x^2\right)+\frac{g}{4}x^4\right]. \tag{5.70}$$

Let us write $1/k_BT$ as β and use natural units with $M=1$, $\hbar=k_B=1$. We have to distinguish two cases:

a) Case $\omega^2>0$, Anharmonic Oscillator

Setting $\omega^2=1$, the smeared potential (5.30) is according to formula (3.879):

$$V_{a^2}(x_0)=\frac{x_0^2}{2}+\frac{g}{4}x_0^4+\frac{a^2}{2}+\frac{3}{2}gx_0^2a^2+\frac{3g}{4}a^4. \tag{5.71}$$

Differentiating this with respect to $a^2/2$ gives, via (5.37),

$$\Omega^2(x_0)=[1+3gx_0^2+3ga^2(x_0)]. \tag{5.72}$$

This equation is solved at each x_0 by iteration together with (5.24),

$$a^2(x_0)=\frac{1}{\beta\Omega^2(x_0)}\left[\frac{\beta\Omega(x_0)}{2}\coth\frac{\beta\Omega(x_0)}{2}-1\right]. \tag{5.73}$$

An initial approximation such as $\Omega(x_0)=0$ is inserted into (5.73) to find $a^2(x_0)\equiv\beta/12$, which serves to calculate from (5.72) an improved $\Omega^2(x_0)$, and so on. The iteration converges rapidly. Inserting the final $a^2(x_0),\Omega^2(x_0)$ into (5.71) and (5.32),

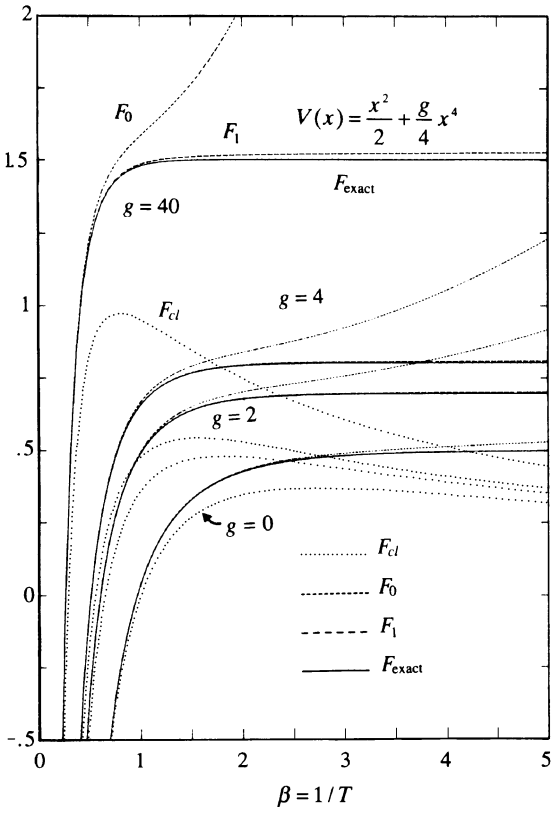

Figure 5.2 Approximate free energy F_1 of anharmonic oscillator as compared with the exact energy F_{ex}, the classical limit $F_{\text{cl}} = -(1/\beta)\log\int_{-\infty}^{\infty}(dx/\sqrt{2\pi\beta})e^{-\beta V(x)}$, as well as an earlier approximation $F_0 = -(1/\beta)\log Z_0$ of Feynman's corresponding to F_1 for the nonoptimal choice $\Omega = 0$, $a^2 = \beta/12$. Note that F_0, F_1 satisfy the inequality $F_{0,1} \geq F$, while F_{cl} does not.

we obtain the desired approximation $W_1(x_0)$ to the effective classical potential $V^{\text{eff cl}}(x_0)$. By performing the integral (5.39) in x_0 we find the approximate free energy F_1 plotted as a function of β in Fig. 5.2. The exact free-energy values are obtained from the known energy eigenvalues of the anharmonic oscillator. They are seen to lie closely below the approximate F_1 curve. For comparison, we have also plotted the classical approximation $F_{\text{cl}} = -(1/\beta)\log Z_{\text{cl}}$ which does not satisfy the Jensen-Peierls inequality and lies *below* the exact curve.

In his book on statistical mechanics [3], Feynman gives another approximation, called here F_0, which can be obtained from the present $W_1(x_0)$ by ending the iteration of (5.72), (5.73) after the first step, i.e., by using the constant nonminimal variational parameters $\Omega(x_0) \equiv 0$, $a^2(x_0) \equiv \hbar^2\beta/12M$. This leads to the approximation

$$V_{a^2}(x_0) \approx V(x_0) + \frac{1}{2}\frac{\hbar^2\beta}{12M}V''(x_0) + \frac{1}{8}\left(\frac{\hbar^2\beta}{12M}\right)^2 V^{(4)}(x_0) + \dots\ , \tag{5.74}$$

referred to as Wigner's expansion [4]. The approximation F_0 is good only at higher temperatures, as seen in Fig. 5.2. Just like F_1, the curve F_0 lies also above the exact curve since it is subject to the Jensen-Peierls inequality. Indeed, the inequality holds for the potential $W_1(x_0)$ in the general form (5.32), i.e., irrespective of the minimization in $a^2(x_0)$. Thus it is valid for arbitrary $\Omega^2(x_0)$, in particular for $\Omega^2(x_0) \equiv 0$.

In the limit $T \to 0$, the free energy F_1 yields the following approximation for the ground state energy $E^{(0)}$ of the anharmonic oscillator:

$$E_1^{(0)} = \frac{1}{4\Omega} + \frac{\Omega}{4} + \frac{3}{4}\frac{g}{4\Omega^2}. \tag{5.75}$$

This approximation is very good for all coupling strengths, including the strong-coupling limit. In this limit, the optimal frequency and energy have the expansions

$$\Omega_1 \;=\; \left(\frac{g}{4}\right)^{1/3}\left[6^{1/3} + \frac{1}{2^{1/3}3^{4/3}}\frac{1}{(g/4)^{2/3}} + \dots\right], \tag{5.76}$$

and

$$\begin{aligned} E_1^{(0)}(g) \approx &\quad \left(\frac{g}{4}\right)^{1/3}\left[\left(\frac{3}{4}\right)^{4/3} + \frac{1}{2^{7/3}3^{1/3}}\frac{1}{(g/4)^{2/3}} + \dots\right] \\ \approx &\quad \left(\frac{g}{4}\right)^{1/3}\left[0.681420 + 0.13758\frac{1}{(g/4)^{2/3}} + \dots\right]. \end{aligned} \tag{5.77}$$

The coefficients are quite close to the precise limiting expression to be calculated in Section 5.15 (listed in Table 5.9).

b) Case $\omega^2 < 0$: The Double-Well Potential

For $\omega^2 = -1$, we slightly modify the potential by adding a constant $1/4g$, so that it becomes

$$V(x) = -\frac{x^2}{2} + \frac{g}{4}x^4 + \frac{1}{4g}. \tag{5.78}$$

The additional constant ensures a smooth behavior of the energies in the limit $g \to 0$. Since the potential possesses now two symmetric minima, it is called the *double-well potential*. Its smeared version $V_{a^2}(x_0)$ can be taken from (5.71), after a sign change in the first and third terms (and after adding the constant $1/4g$).

Now the trial frequency

$$\Omega^2(x_0) = -1 + 3gx_0^2 + 3ga^2(x_0) \tag{5.79}$$

can become negative, although it turns out to remain always larger than $-4\pi^2/\beta^2$, since the solution is incapable of crossing the first singularity in the sum (5.24)

from the right. Hence the smearing square width $a^2(x_0)$ is always positive. For $\Omega^2 \in (-4\pi^2/\beta^2, 0)$, the sum (5.24) gives

$$\begin{aligned} a^2(x_0) &= \frac{2}{\beta}\sum_{m=1}^{\infty}\frac{1}{\omega_m^2+\Omega^2(x_0)} \\ &= \frac{1}{\beta\Omega^2(x_0)}\left(\frac{\beta|\Omega(x_0)|}{2}\cot\frac{\beta|\Omega(x_0)|}{2}-1\right), \end{aligned} \tag{5.80}$$

which is the expression (5.73), continued analytically to imaginary $\Omega(x_0)$. The above procedure for finding $a^2(x_0)$ and $\Omega^2(x_0)$ by iteration of (5.79) and (5.80) is not applicable near the central peak of the double well, where it does not converge. There one finds the solution by searching for the zero of the function of $\Omega^2(x_0)$

$$f(\Omega^2(x_0)) \equiv a^2(x_0) - \frac{1}{3g}[1+\Omega^2(x_0)-3gx_0^2], \tag{5.81}$$

with $a^2(x_0)$ calculated from (5.80) or (5.73). At $T=0$, the curves have for $g \le g_c$ two symmetric nontrivial minima at $\pm x_m$ with

$$x_m = \sqrt{\frac{1-3ga^2}{g}}, \tag{5.82}$$

where Eq. (5.79) becomes

$$\Omega^2(x_m) = 2 - 6ga^2(x_m). \tag{5.83}$$

These disappear for

$$g > g_c = \frac{4}{9}\sqrt{\frac{2}{3}} \approx 0.3629\ . \tag{5.84}$$

The resulting effective classical potentials and the free energies are plotted in Figs. 5.3 and 5.4.

It is useful to compare the approximate effective classical potential $W_1(x)$ with the true one $V^{\text{eff cl}}(x)$ in Fig. 5.5. The latter was obtained by Monte Carlo simulations of the path integral of the double-well potential, holding the path average $\bar{x} = (1/\beta)\int_0^\beta d\tau x(\tau)$ fixed at x_0. The coupling strength is chosen as $g = 0.4$, where the worst agreement is expected.

In the limit $T \to 0$, the approximation F_1 yields an approximation $E_1^{(0)}$ for the ground state energy. In the strong-coupling limit, the leading behavior is the same as in Eq. (5.77) for the anharmonic oscillator.

Let us end this section with the following remark. The entire approximation procedure can certainly also be applied to a time-sliced path integral in which the time axis contains $N+1$ discrete points $\tau_n = n\epsilon,\ n = 0, 1, \ldots N$. The only change in the above treatment consists in the replacement

$$\omega_m^2 \to \Omega_m\bar{\Omega}_m = \frac{1}{\epsilon^2}[2-2\cos(\epsilon\omega_m)]. \tag{5.85}$$

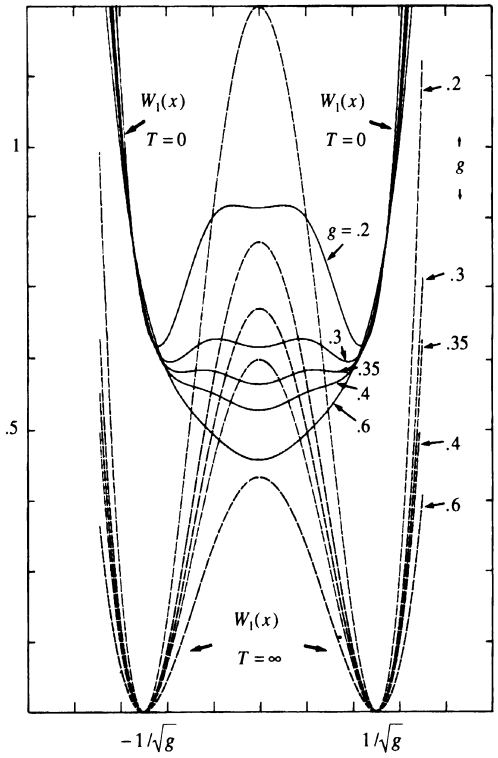

Figure 5.3 Effective classical potential of double well $V(x) = -x^2/2 + gx^4/4 + 1/4g$ at various g for $T = 0$ and $T = \infty$ [where it is equal to the potential $V(x)$ itself]. The quantum fluctuations at $T = 0$ smear out the double well completely if $g \gtrsim 0.4$, but not if $g = 0.2$.

Hence the expression for the smearing square width parameter $a^2(x_0)$ of (5.24) is replaced by

$$\begin{aligned} a^2(x_0) &= \frac{2k_BT}{M}\frac{\partial}{\partial\Omega^2(x_0)}\log\prod_{m=1}^{m_{\max}}\left[\Omega_m\overline{\Omega}_m+\Omega^2(x_0)\right] \\ &= \frac{k_BT}{M}\frac{1}{\Omega}\frac{\partial}{\partial\Omega}\log\frac{\sinh(\hbar\Omega_N(x_0)/2k_BT)}{\hbar\Omega(x_0)/2k_BT} \\ &= \frac{k_BT}{M\Omega^2(x_0)}\left[\frac{\hbar\Omega(x_0)}{2k_BT}\coth\frac{\hbar\Omega_N(x_0)}{2k_BT}\frac{1}{\cosh(\epsilon\Omega_N(x_0)/2)}-1\right], \end{aligned} \tag{5.86}$$

where $m_{\max} = N/2$ for even and $(N-1)/2$ for odd N [recall (2.391)], and $\Omega_N(x_0)$ is defined by

$$\sinh[\epsilon\Omega_N(x_0)/2] \equiv \epsilon\Omega(x_0)/2 \tag{5.87}$$

[see Eq. (2.399)]. The trial potential $W_1(x_0)$ now reads

$$W_1(x_0) \equiv k_BT\log\frac{\sinh\hbar\Omega_N(x_0)/2k_BT}{\hbar\Omega(x_0)/2k_BT} + V_{a^2(x_0)}(x_0) - \frac{M}{2}\Omega^2(x_0)a^2(x_0), \tag{5.88}$$

rather than (5.32). Minimizing this in $a^2(x_0)$ gives again (5.37) and (5.38) for $\Omega^2(x_0)$.

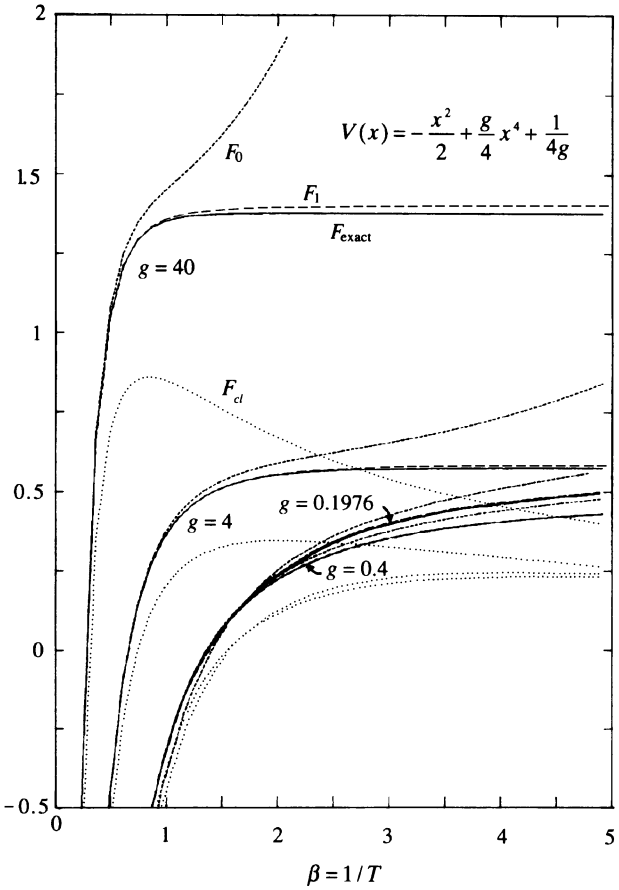

Figure 5.4 Free energy F_1 in double-well potential (5.78), compared with the exact free energy $F_{\rm ex}$, the classical limit $F_{\rm cl}$, and Feynman's approximation F_0 (which coincides with F_1 for the nonminimal values $\Omega = 0$, $a^2 = \beta/12$).

In Fig. 5.6 we have plotted the resulting approximate effective classical potential $W_1(x_0)$ of the double-well potential (5.78) with $g = 0.4$ at a fixed large value $\beta = 20$ for various numbers of lattice points $N + 1$. It is interesting to compare these plots with the exact curves, obtained again from Monte Carlo simulations. For $N = 1$, the agreement is exact. For small N, the agreement is good near and outside the potential minima. For larger N, the exact effective classical potential has oscillations which are not reproduced by the approximation.

5.8 Particle Densities

It is possible to find approximate particle densities from the optimal effective classical potential $W_1(x_0)$ [5, 6]. Certainly, the results cannot be as accurate as those for the free energies. In Schrödinger quantum mechanics, it is well known that variational methods can give quite accurate energies even if the trial wave functions are only of moderate quality. This has also been seen in the Eq. (5.53) estimate to the ground state energy of the Coulomb system by a Gaussian wave packet. The energy

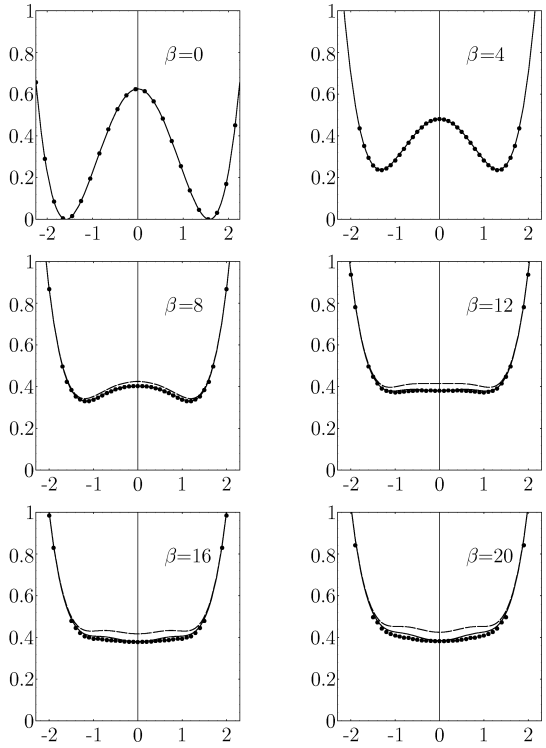

Figure 5.5 Comparison of approximate effective classical potential $W_1(x_0)$ (dashed curves) and $W_3(x_0)$ (solid curves) with exact $V^{\text{eff cl}}(x_0)$ (dots) at various inverse temperatures $\beta = 1/T$. The data dots are obtained from Monte Carlo simulations using 10^5 configurations [W. Janke and H. Kleinert, Chem. Phys. Lett. *137*, 162 (1987) (`http://www.physik.fu-berlin.de/~kleinert/154`)]. We have picked the worst case, $g = 0.4$. The solid lines represent the higher approximation $W_3(x_0)$, to be calculated in Section 5.13.

is a rather global property of the system. For physical quantities such as particle densities which contain local information on the wave functions, the approximation is expected to be much worse. Let us nevertheless calculate particle densities of a quantum-mechanical system. For this we tie down the periodic particle orbit in the trial partition function Z_1 for an arbitrary time at a particular position, say x_a. Mathematically, this is enforced with the help of a δ-function:

$$\begin{aligned}\delta(x_a - x(\tau)) &= \delta(x_a - x_0 - \sum_{m=1}^{\infty}(x_m e^{-i\omega_m \tau} + \text{c.c.})) \\ &= \int_{-\infty}^{\infty}\frac{dk}{2\pi}\exp\left\{ik\left[x_a - x_0 - \sum_{m=1}^{\infty}(x_m e^{-i\omega_m\tau} + \text{c.c.})\right]\right\}. \end{aligned} \tag{5.89}$$

ref(2.353) With this, we write the path integral for the particle density [compare (2.353)]
lab(2.length)
est(2.234)

$$\rho(x_a) = Z^{-1}\oint \mathcal{D}x\,\delta(x_a - x(\tau))e^{-\mathcal{A}/\hbar} \tag{5.90}$$

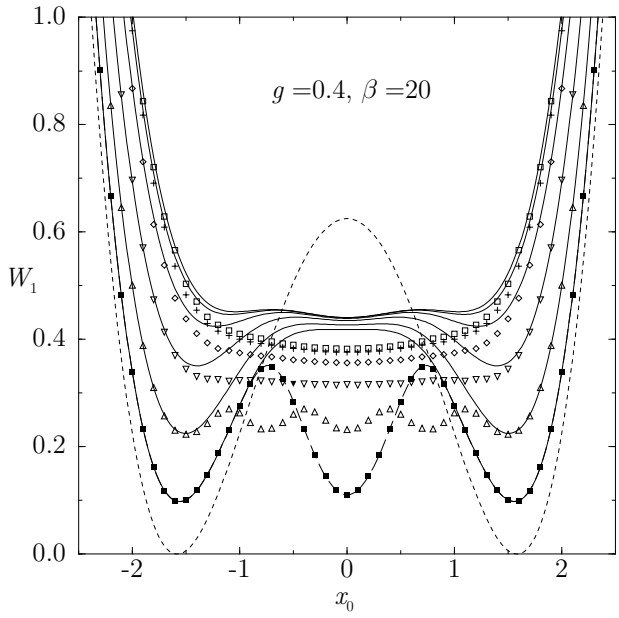

Figure 5.6 Effective classical potential $W_1(x_0)$ for double-well potential (5.78) with $g = 0.4$ at fixed low temperature $T = 1/\beta = 1/20$, for various numbers of time slices $N+1 = 2$ (■), 4 (△), 8 (▽), 16 (◇), 32 (+), 64 (□). The dashed line represents the original potential $V(x_0)$. For the source of the data points, see the previous figure caption.

and decompose

$$\begin{aligned}\rho(x_a) &= Z^{-1}\int_{-\infty}^{\infty}\frac{dx_0}{l_{\rm e}(\hbar\beta)}\int\frac{dk}{2\pi}e^{ik(x_a-x_0)} \\ &\quad\times\int\mathcal{D}x\tilde{\delta}(\bar{x}-x_0)e^{-ik\Sigma_{m=1}^{\infty}(x_m+\text{c.c.})}e^{-\mathcal{A}/\hbar}.\end{aligned} \tag{5.91}$$

The approximation $W_1(x_0)$ is based on a quasiharmonic treatment of the x_m-fluctuations for $m > 0$. For harmonic fluctuations we use Wick's rule of Section 3.10 to evaluate

$$\left\langle e^{-ik\Sigma_{m=1}^{\infty}(x_m e^{-i\omega_m\tau}+\text{c.c.})}\right\rangle_{\Omega}^{x_0} \approx e^{-k^2\Sigma_{m=1}^{\infty}\left\langle|x_m|^2\right\rangle_{\Omega}^{x_0}} \equiv e^{-k^2a^2/2}, \tag{5.92}$$

which is true for any τ. Thus we could have chosen any τ in the δ-function (5.89) to find the distribution function. Inserting (5.92) into (5.91) we can integrate out k and find the approximation to the particle density

$$\rho(x_a) \approx Z^{-1}\int_{-\infty}^{\infty}\frac{dx_0}{l_{\rm e}(\hbar\beta)}\frac{e^{-(x_a-x_0)^2/2a^2(x_0)}}{\sqrt{2\pi a^2(x_0)}}e^{-V^{\rm eff\,cl}(x_0)/k_BT}. \tag{5.93}$$

By inserting for $V^{\rm eff\,cl}(x_0)$ the approximation $W_1(x_0)$, which for Z yields the approximation Z_1, we arrive at the corresponding approximation for the particle distribution function:

$$\rho_1(x_a) = Z_1^{-1}\int_{-\infty}^{\infty}\frac{dx_0}{l_{\rm e}(\hbar\beta)}\frac{e^{-(x_a-x_0)^2/2a^2(x_0)}}{\sqrt{2\pi a^2(x_0)}}e^{-W_1(x_0)/k_BT}. \tag{5.94}$$

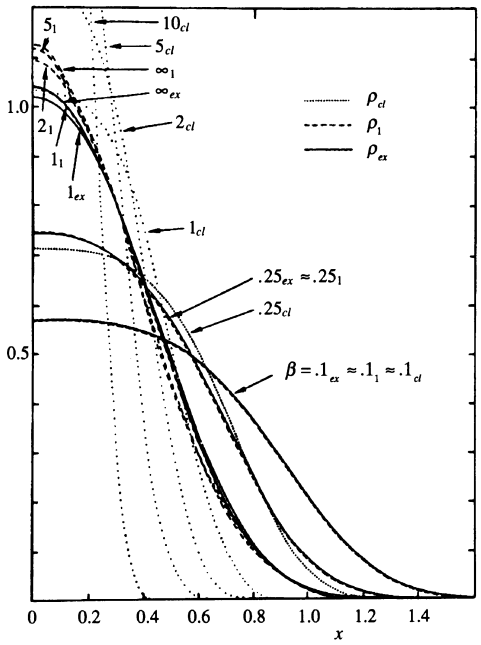

Figure 5.7 Approximate particle density (5.94;r:5.63,a:5.93) of anharmonic oscillator for $g = 40$, as compared with the exact density $\rho(x) = Z^{-1} \sum_n |\psi_n(x)|^2 e^{-\beta E_n}$, obtained by integrating the Schrödinger equation numerically. The curves are labeled by their β values with the subscripts 1, ex, cl indicating the approximation.

This has obviously the correct normalization $\int_{-\infty}^{\infty} dx_a \rho_1(x_a) = 1$. Figure 5.7 shows a comparison of the approximate particle distribution functions of the anharmonic oscillator with the exact ones. Both agree reasonably well with each other. In Fig. 5.8, the same plot is given for the double-well potential at a coupling $g = 0.4$. Here the agreement at very low temperature is not as good as in Fig. 5.7. Compare, for example, the zero-temperature curve ∞_1 with the exact curve $\infty_{\rm ex}$. The first has only a single central peak, the second a double peak. The reason for this discrepancy is the correspondence of the approximate distribution to an optimal Gaussian wave function which happens to be centered at the origin, in spite of the double-well shape of the potential. In Fig. 5.3 we see the reason for this: The approximate effective classical potential $W_1(x_0)$ has, at small temperatures up to $T \sim 1/10$, only one minimum at the origin, and this becomes the center of the optimal Gaussian wave function. For larger temperatures, there are two minima and the approximate distribution function $\rho_1(x)$ corresponds roughly to two Gaussian wave packets centered around these minima. Then, the agreement with the exact distribution becomes better. We have intentionally chosen the coupling $g = 0.4$, where the result would be about the worst. For $g \gg 0.4$, both the true and the approximate distributions have a single central peak. For $g \ll 0.4$, both have two peaks at small temperatures. In both limits, the approximation is acceptable.

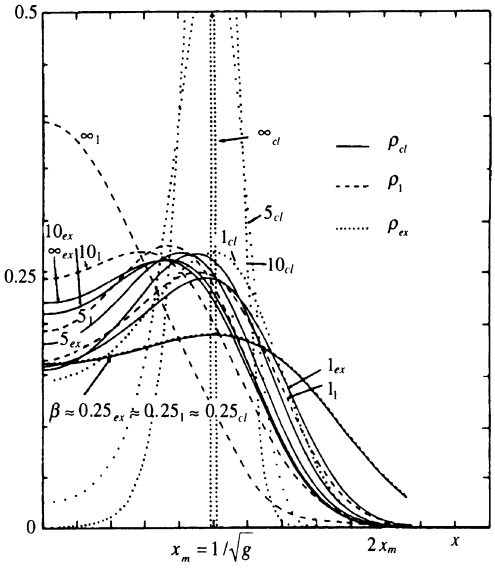

Figure 5.8 Particle density (5.94) in double-well potential (5.78) for the worst choice of the coupling constant, $g = 0.4$. Comparison is made with the exact density $\rho(x) = Z^{-1}\sum_n |\psi_n(x)|^2 e^{-\beta E_n}$ obtained by integrating the Schrödinger equation numerically. The curves are labeled by their β values with the subscripts 1, ex, cl indicating the approximation. For $\beta \to \infty$, the distribution tends to the Gaussian $e^{-x^2/2a^2}/\sqrt{2\pi a^2}$ with $a^2 = 1.030$ (see Table 5.1).

5.9 Extension to D Dimensions

The method can easily be extended to approximate the path integral of a particle moving in a D-dimensional $\mathbf{x}$-space. Let x_i be the D components of $\mathbf{x}$. Then the trial frequency $\Omega_{ij}^2(\mathbf{x}_0)$ in (5.7) must be taken as a $D \times D$ -matrix. In the special case of $V(\mathbf{x})$ being rotationally symmetric and depending only on $r = \sqrt{\mathbf{x}^2}$, we may introduce, as in the discussion of the effective action in Eqs. (3.684)–(3.689), longitudinal and transverse parts of $\Omega_{ij}^2(\mathbf{x}_0)$ via the decomposition

$$\Omega_{ij}^2(\mathbf{x}_0) = \Omega_L^2(r_0) P_{Lij}(\mathbf{x}_0) + \Omega_T^2(r_0) P_{Tij}(\mathbf{x}_0), \tag{5.95}$$

where

$$P_{Lij}(\hat{\mathbf{x}}_0) = x_{0i}x_{0j}/r_0^2, \qquad P_{Tij}(\hat{\mathbf{x}}_0) = \delta_{ij} - x_{0i}x_{0j}/r_0^2, \tag{5.96}$$

are projection matrices into the longitudinal and transverse directions of $\mathbf{x}_0$. Analogous projections of a vector are defined by $\mathbf{x}_L \equiv P_L(\mathbf{x}_0)\,\mathbf{x}$, $\mathbf{x}_T \equiv P_T(\mathbf{x}_0)\,\mathbf{x}$. Then the anisotropic generalization of $W_1^{\Omega}(\mathbf{x}_0)$ becomes

$$\begin{aligned} W_1^{\mathbf{\Omega}}(r_0) \;&=\; k_B T \left[\log \frac{\sinh \hbar\Omega_L/2k_BT}{\hbar\Omega_L/2k_BT} + (D-1)\log \frac{\sinh \hbar\Omega_T/2k_BT}{\hbar\Omega_T/2k_BT} \right] \\ &\quad - \frac{M}{2}\left[\Omega_L^2 a_L^2 + (D-1)\Omega_T^2 a_T^2\right] + V_{a_L,a_T}, \end{aligned} \tag{5.97}$$

with all functions on the right-hand side depending only on r_0. The bold-face superscript indicates the presence of two variational frequencies $\mathbf{\Omega} \equiv (\Omega_L, \Omega_T)$. The smeared potential is now given by

$$\begin{aligned} V_{a_L,a_T}(r_0) &= \frac{1}{\sqrt{2\pi a_L^2}} \frac{1}{\sqrt{2\pi a_T^2}^{D-1}} \prod_{i=1}^{D} \left[\int_{-\infty}^{\infty} d\delta x_i\right] \\ &\times \exp\left[-\frac{1}{2}\left(a_L^{-2}\delta x_L^2 + a_T^{-2}\delta \mathbf{x}_T^2\right)\right] V(\mathbf{x}_0 + \delta\mathbf{x}), \end{aligned} \tag{5.98}$$

which can also be written as

$$V_{a_L,a_T}(r_0) = \frac{1}{\sqrt{(2\pi)^D a_L^2 a_T^{2D-2}}} \int d\delta x_L \int d^{D-1}\delta x_T \exp\left[-\frac{\delta x_L^{\,2}}{2a_L^2} - \frac{\delta x_T^{\,2}}{2a_T^2}\right] V(\mathbf{x}_0 + \delta\mathbf{x}). \tag{5.99}$$

For higher temperatures where the smearing widths a_L^2, a_T^2 are small, we set $V(\mathbf{x}) \equiv v(r^2)$, so that

$$\begin{aligned} V(\mathbf{x}) &= v(r_0^2 + 2r_0\delta x_L + \delta x_L^2 + \delta \mathbf{x}_T^2) = \sum_{n=0}^{\infty} \frac{1}{n!} v^{(n)}(r_0^2) \left(2r_0\delta x_L + \delta x_L^2 + \delta \mathbf{x}_T^2\right)^n \\ &= \left[v(r_0^2 + \partial_\lambda) e^{\lambda\left(2r_0\delta x_L + \delta x_L^2 + \delta \mathbf{x}_T^2\right)}\right]_{\lambda=0}. \end{aligned} \tag{5.100}$$

Inserting this into the right-hand side of (5.98), we find

$$V_{a_L,a_T}(r_0) = \left[v(r_0^2 + \partial_\lambda) \frac{1}{\sqrt{1 - 2a_L^2\lambda}} \frac{1}{\sqrt{1 - 2a_T^2\lambda}^{D-1}} e^{2r_0^2\lambda^2 a_L^2/(1-2a_L^2\lambda)}\right]_{\lambda=0}, \tag{5.101}$$

which has the expansion

$$\begin{aligned} V_{a_L,a_T}(r_0) &= v(r_0^2) + v'(r_0^2)[a_L^2 + (D-1)a_T^2] \\ &+ \frac{1}{2} v''(r_0^2)[3a_L^4 + 2(D-1)a_L^2 a_T^2 + (D^2-1)a_T^4 + 4r_0^2 a_L^2] + \ldots. \end{aligned} \tag{5.102}$$

The prime abbreviates the derivative with respect to r_0^2.

In general it is useful to insert into (5.98) the Fourier representation for the potential

$$V(\mathbf{x}) = \int \frac{d^D k}{(2\pi)^D} e^{i\mathbf{k}\mathbf{x}} V(\mathbf{k}), \tag{5.103}$$

which makes the $\mathbf{x}$-integration Gaussian, so that (5.99) becomes

$$V_{a_L^2,a_T^2}(r_0) = \int \frac{d^D k}{(2\pi)^D} V(\mathbf{k}) \exp\left(-\frac{a_L^2}{2}k_L^2 - \frac{a_T^2}{2}k_T^2 - ir_0 k_L\right). \tag{5.104}$$

Exploiting the rotational symmetry of the potential by writing $V(\mathbf{k}) \equiv v(k^2)$, we decompose the measure of integration as

$$\int \frac{d^D k}{(2\pi)^D} = \frac{S_{D-1}}{(2\pi)^D} \int_{-\infty}^{\infty} dk_L \int_0^{\infty} dk_T\, k_T^{D-2}, \tag{5.105}$$

where

$$S_D = \frac{2\pi^{D/2}}{\Gamma(D/2)} \tag{5.106}$$

is the surface of a sphere in D dimensions, and further with $k_L = k\cos\phi$, $k_T = k\sin\phi$:

$$\int \frac{d^D k}{(2\pi)^D} = \frac{S_{D-1}}{(2\pi)^D}\int_{-1}^{1} d\cos\phi \int_0^\infty dk\, k^{D-1}. \tag{5.107}$$

This brings (5.104) to the form

$$\begin{aligned} V_{a_L^2,a_T^2}(r_0) &= \frac{S_{D-1}}{(2\pi)^D}\int_{-1}^{1} du \int_{-1}^{\infty} dk\, k^{D-1} v(k^2) \\ &\quad \times \exp\left\{-\frac{1}{2}\left[\left(a_L^2 u^2 + a_T^2(1-u^2)\right)k^2 - ir_0 u\right]\right\}. \end{aligned} \tag{5.108}$$

The final effective classical potential is found by minimizing $W_1(r_0)$ at each r_0 in $a_L, a_T, \Omega_L, \Omega_T$. To gain a rough idea about the solution, it is usually of advantage to study first the *isotropic approximation* obtained by assuming $a_T^2(r_0) = a_L^2(r_0)$, and to proceed later to the anisotropic approximation.

5.10 Application to Coulomb and Yukawa Potentials

The effective classical potential can be useful also for singular potentials as long as the smearing procedure makes sense. An example is the Yukawa potential

$$V(r) = -(e^2/r)e^{-mr}, \tag{5.109}$$

which reduces to the Coulomb potential for $m \equiv 0$. Using the Fourier representation

$$V(r) = 4\pi \int \frac{d^3k}{(2\pi)^3}\frac{e^{i\mathbf{kx}}}{k^2+m^2} = 4\pi\int_0^\infty d\tau \int \frac{d^3k}{(2\pi)^3} e^{-\tau(k^2+m^2)}, \tag{5.110}$$

we easily calculate the isotropically smeared potential

$$\begin{aligned} V_{a^2}(r_0) &= -e^2 \int \frac{d^3x}{\sqrt{2\pi a^2}^3}\exp\left[-\frac{1}{2a^2}(\mathbf{x}_0-\mathbf{x})^2\right] V(r) \\ &= -e^2\, 2\pi e^{m^2a^2/2}\int_{a^2}^\infty da'^2 \frac{1}{\sqrt{2\pi a'^2}^3}\exp\left(-r_0^2/2a'^2 - m^2a'^2/2\right) \\ &= -e^2\,\frac{2e^{m^2a^2/2}}{\sqrt{\pi}}\frac{1}{r_0}\int_0^{r_0/\sqrt{2a^2}} dt e^{-(t^2+m^2r_0^2/4t^2)}. \end{aligned} \tag{5.111}$$

In the Coulomb limit $m \to 0$, the smeared potential becomes equal to the Coulomb potential multiplied by an error function,

$$V_{a^2}(r_0) = -\frac{e^2}{r_0}\mathrm{erf}(r_0/\sqrt{2a^2}), \tag{5.112}$$

where the error function is defined by

$$\mathrm{erf}(z) \equiv \frac{2}{\sqrt{\pi}} \int_0^z dx e^{-x^2}. \tag{5.113}$$

The smeared potential is no longer singular at the origin,

$$V_{a^2}(0) = -\frac{e^2}{a}\sqrt{\frac{2}{\pi}} e^{m^2 a^2/2}. \tag{5.114}$$

The singularity has been removed by quantum fluctuations. In this way the effective classical potential explains the stability of matter in quantum physics, i.e., the fact that atomic electrons do not fall into the origin. The effective classical potential of the Coulomb system is then by the isotropic version of (5.97)

$$W_1^{\Omega}(\mathbf{x}_0) = \frac{3}{\beta} \ln \frac{\sinh[\hbar\beta\Omega(\mathbf{x}_0)/2]}{\hbar\beta\Omega(\mathbf{x}_0)/2} - \frac{e^2}{|\mathbf{x}_0|} \mathrm{erf}\left[\frac{|\mathbf{x}_0|}{\sqrt{2a^2(\mathbf{x}_0)}}\right] - \frac{3}{2} M\Omega^2(\mathbf{x}_0) a^2(\mathbf{x}_0). \tag{5.115}$$

Minimizing $W_1(r_0)$ with respect to $a^2(r_0)$ gives an equation analogous to Eq. (5.37) determining the frequency $\Omega^2(r_0)$ to be

$$\Omega^2(r_0) = e^2 \frac{2}{3} \frac{1}{\sqrt{2\pi}} \frac{1}{(a^2)^{3/2}} e^{-r_0^2/2a^2}. \tag{5.116}$$

We have gone to atomic units in which $e = M = \hbar = k_B = 1$, so that energies and temperatures are measured in units of $E_0 = Me^4/M\hbar^2 \approx 4.36 \times 10^{-11}$erg ≈ 27.21eV and $T_0 = E_0/k_B \approx 31575$K, respectively. Solving (5.116) together with (5.24), we find $a^2(r_0)$ and the approximate effective classical potential (5.32). The result is shown in Fig. 5.9 as a dashed curve. The above approximation may now be improved by treating the fluctuations anisotropically, as described in the previous section, with different $\Omega^2(\mathbf{x}_0)$ for radial and tangential fluctuations $\delta\mathbf{x}_L$ and $\delta\mathbf{x}_T$, and the effective potential following Eqs. (5.97) and (5.98). For the anisotropically smeared Coulomb potential we calculate from (5.108):

$$V_{a_L^2, a_T^2}(r_0) = -\sqrt{\frac{1}{2\pi}} \int_{-1}^{1} du \frac{e^2}{\sqrt{a_L^2 u^2 + a_T^2(1-u^2)}} \exp\left\{-\frac{r_0^2 u^2}{2\left[a_L^2 u^2 + a_T^2(1-u^2)\right]}\right\}. \tag{5.117}$$

Introducing the variable $\lambda = \sqrt{a_L^2}u/\sqrt{a_L^2\lambda^2 + a_T^2(1-\lambda^2)}$, which runs through the same interval $[-1, 1]$ as u, we rewrite this as

$$V_{a_L^2, a_T^2}(r_0) = -e^2 \sqrt{\frac{a_L^2}{2\pi}} \int_{-1}^{1} d\lambda \frac{\exp[-(r_0^2/2a_L^2)\lambda^2]}{a_L^2(1-\lambda^2) + a_T^2\lambda^2}. \tag{5.118}$$

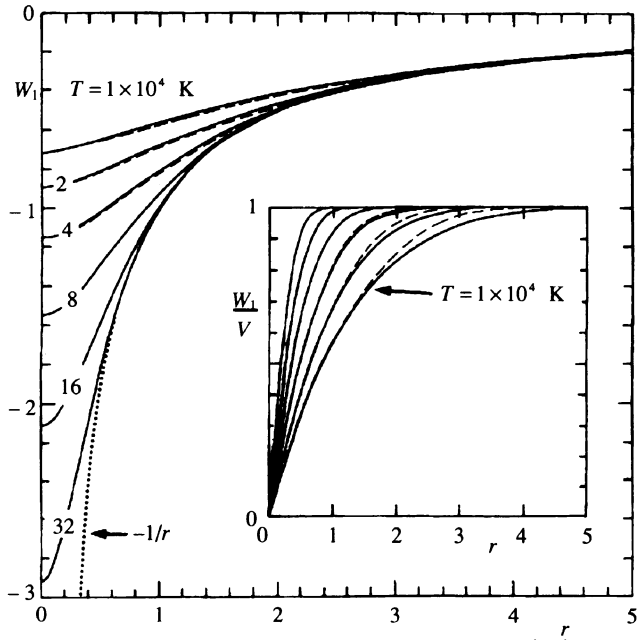

Figure 5.9 Approximate effective classical potential $W_1(r_0)$ of Coulomb system at various temperatures (in multiples of 10^4K). It is calculated once in the isotropic (dashed curves) and once in the anisotropic approximation. The improvement is visible in the insert which shows W_1/V. The inverse temperature values of the different curves are $\beta = 31.58$, 15.78, 7.89, 3.945, 1.9725, 0.9863, 0 atomic units, respectively.

Extremization of $W_1(r_0)$ in Eq. (5.97) yields the equations for the trial frequencies

$$\Omega_T^2(r_0) \equiv \frac{\partial}{\partial a_T^2} V_{a_T^2, a_L^2} = e^2 \sqrt{\frac{a_L^2}{2\pi}} \int_{-1}^{1} d\lambda \frac{\lambda^2 \exp[-(r_0^2/2a_L^2)\lambda^2]}{[a_L^2(1-\lambda^2) + a_T^2\lambda^2]^2}, \tag{5.119}$$

$$\begin{aligned} \Omega^2(r_0) &\equiv \frac{1}{3}[\Omega_L^2 + 2\Omega_T^2] = \frac{1}{3}\left[\frac{\partial}{\partial a_L^2} + 2\frac{\partial}{\partial a_T^2}\right] V_{a_T^2, a_L^2} \\ &= e^2 \frac{2}{3} \frac{1}{\sqrt{2\pi}} \frac{1}{\sqrt{a_L^2 a_T^4}} \exp(-r_0^2/2a_L^2). \end{aligned} \tag{5.120}$$

These equations have to be solved together with

$$a_{L,T}^2(r_0) = \frac{1}{\beta\Omega_{L,T}^2(r_0)} \left[\frac{\beta\Omega_{L,T}(r_0)}{2} \coth \frac{\beta\Omega_{L,T}(r_0)}{2} - 1\right]. \tag{5.121}$$

Upon inserting the solutions into (5.97), we find the approximate effective classical potential plotted in Fig. 5.9 as a solid curve. Let us calculate the approximate particle distribution functions using a three-dimensional anisotropic version of Eq. (5.94). With the potential $W_1(r_0)$, we arrive at the integral [6]

$$\rho_1(r) = \int d^3x_0 \frac{e^{-(z_0-r)^2/2a_L^2}}{\sqrt{2\pi a_L^2(r_0)}} \frac{e^{-(x_0^2+y_0^2)/2a_T^2}}{2\pi a_T^2(r_0)} \frac{e^{-\beta W_1(r_0)}}{(2\pi\beta)^{3/2}}$$

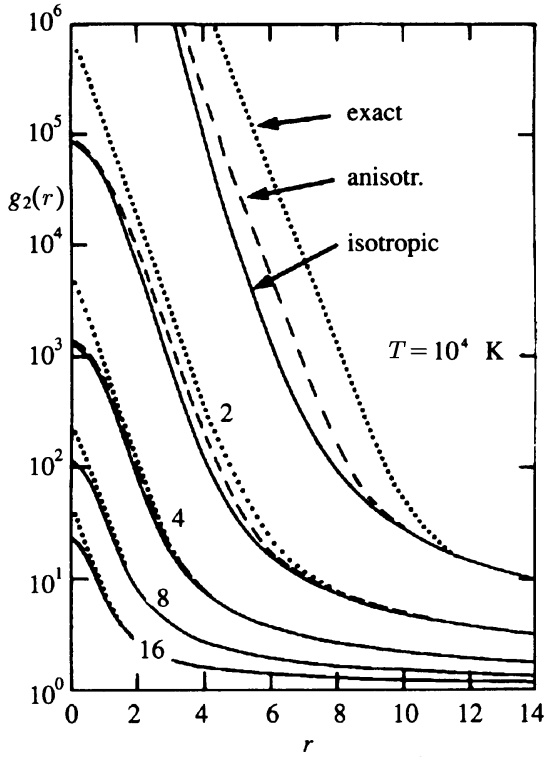

Figure 5.10 Particle distribution $g(r) \equiv \sqrt{2\pi\beta}^3\rho(r)$ in Coulomb potential at different temperatures T (the same as in Fig. 5.9), calculated once in the isotropic and once in the anisotropic approximation. The dotted curves show the classical distribution. For low and intermediate temperatures the exact distributions of R.G. Storer, J. Math. Phys. *9*, 964 (1968) are well represented by the two lowest energy levels for which $\rho(r)=\pi^{-1}e^{-2r}e^{\beta/2}+(1/8\pi)(1-r+r^2/2)e^{-r}e^{\beta/8}+(1/3^8\pi)(243-324r+216r^2-48r^3+4r^4)e^{-2r/3}e^{\beta/18}$.

$$= 2\pi\int_0^\infty dr_0\int_{-1}^1 d\lambda\frac{e^{-(\lambda r_0-r)^2/2a_L^2}}{\sqrt{2\pi a_L^2(r_0)}}\frac{e^{-r_0^2(1-\lambda^2)/2a_T^2}}{2\pi a_T^2(r_0)}\frac{e^{-\beta W_1(r_0)}}{(2\pi\beta)^{3/2}}. \tag{5.122}$$

The resulting curves to different temperatures are plotted in Fig. 5.10 and compared with the exact distribution as given by Storer. The distribution obtained from the earlier isotropic approximation (5.116) to the trial frequency $\Omega^2(r_0)$ is also shown.

5.11 Hydrogen Atom in Strong Magnetic Field

The recent discovery of magnetars [7] has renewed interest in the behavior of charged particle systems in the presence of extremely strong external magnetic fields. In this new type of neutron stars, electrons and protons from decaying neutrons produce magnetic fields B reaching up to 10^{15} G, much larger than those in neutron stars and white dwarfs, where B is of order $10^{10}-10^{12}$ G and 10^6-10^8 G, respectively.

Analytic treatments of the strong-field properties of an atomic system are difficult, even in the zero-temperature limit. The reason is a logarithmic asymptotic behavior of the ground state energy to be derived in Eq. (5.132). In the weak-field

limit, on the other hand, perturbative approaches yield well-known series expansions in powers of B^2 up to B^{60} [8]. These are useful, however, only for $B \ll B_0$, where B_0 is the atomic magnetic field strength $B_0 = e^3M^2/\hbar^3 \approx 2.35 \times 10^5\,\mathrm{T} = 2.35 \times 10^9\,\mathrm{G}$.

So far, the most reliable values for strong uniform fields were obtained by numerical calculations [9].

The variational approach can be used to derive a single analytic expression for the effective classical potential applicable to all field strengths and temperatures [10]. The Hamiltonian of the electron in a hydrogen atom in a uniform external magnetic field pointing along the positive z-axis is the obvious extension of the expression in Eq. (2.646) by a Coulomb potential:

$$H(\mathbf{p},\mathbf{x}) = \frac{1}{2M}\mathbf{p}^2 + \frac{M}{2}\omega_B^2\mathbf{x}^2 - \omega_B l_z(\mathbf{p},\mathbf{x}) - \frac{e^2}{|\mathbf{x}|}, \tag{5.123}$$

where ω_B denotes the B-dependent magnetic frequency $\omega_L/2 = eB/2Mc$ of Eq. (2.651), i.e., half the Landau or cyclotron frequency. The magnetic vector potential has been chosen in the symmetric gauge (2.640). Recall that l_z is the z-component of the orbital angular momentum $l_z(\mathbf{p},\mathbf{x}) = (\mathbf{x}\times\mathbf{p})_z$ [see (2.647)].

At first, we restrict ourselves here to zero temperature. From the imaginary-time version of the classical action (2.640) we see that the particle distribution function in the orthogonal direction of the magnetic field is, for $x_b = 0, y_b = 0$, proportional to

$$\exp\left(-\frac{M}{2}\omega_B\mathbf{x}_a^2\right). \tag{5.124}$$

This is the same distribution as for a transverse harmonic oscillator with frequency ω_B. Being at zero temperature, the first-order variational energy requires knowing the smeared potential at the origin. Allowing for a different smearing width $a_\parallel^2$ and $a_\perp^2$ along an orthogonal to the magnetic field, we may use Eq. (5.118) to write

$$V_{a_\parallel^2,a_\perp^2}(0) = -e^2\sqrt{\frac{1}{2\pi a_\parallel^2}}\int_{-1}^{1}d\lambda\frac{1}{(1-\lambda^2)+\lambda^2 a_\perp^2/a_\parallel^2}\,. \tag{5.125}$$

Performing the integral yields

$$V_{a_\parallel^2,a_\perp^2}(0) = -e^2\sqrt{\frac{1}{2\pi(a_\parallel^2-a_\perp^2)}}\,2\,\mathrm{arccosh}\frac{a_\parallel}{a_\perp}\,. \tag{5.126}$$

Since the ground state energies of the parallel and orthogonal oscillators are $\Omega_\parallel/2$ and $2\times\Omega_\perp/2$, we obtain immediately the first-order variational energy

$$W_1(\mathbf{0}) = \Omega_\perp + \frac{\Omega_\parallel}{2} + V_{a_\parallel^2,a_\perp^2}(\mathbf{0}) + \frac{M}{2}(\omega_\parallel^2-\Omega_\parallel^2)a_\parallel^2 + M(\omega_B^2-\Omega_\perp^2)a_\perp^2\,, \tag{5.127}$$

with $\omega_\parallel = 0$ and $a_{\parallel,\perp}^2 = 1/2\Omega_{\parallel,\perp}$. In this expression we have ignored the second term in the Hamiltonian (5.123), since the angular momentum l_z of the ground state must have a zero expectation value.

For very strong magnetic fields, the transverse variational frequency Ω_T will become equal to $\omega_B = \hbar e/2Mc$, such that in this limit

$$W(\mathbf{0}) \approx \omega_B + \frac{\Omega_\parallel}{4} - e^2\sqrt{\frac{\Omega_\parallel}{\pi}}\log\frac{8\omega_B}{\Omega_\parallel}. \tag{5.128}$$

Extremizing this in $\Omega_\parallel$ yields

$$\Omega_\parallel \approx \frac{4e^4}{\pi}\log^2\frac{2\pi\omega_B}{e^4}, \tag{5.129}$$

and thus an approximate ground state energy

$$E_1^{(0)} \approx \omega_B - \frac{e^4}{\pi}\log^2\frac{2\pi\omega_B}{e^4}. \tag{5.130}$$

The approach to very strong fields can be found by extremizing the energy (5.127) also in $\Omega_\perp$. Going over to atomic units with $e = 1$ and $M = 1$, where energies are measured in units of $\epsilon_0 = Me^4/\hbar^2 \equiv 2\,\mathrm{Ryd} \approx 27.21\,\mathrm{eV}$, temperatures in $\epsilon_0/k_B \approx 3.16\times10^5\,\mathrm{K}$, distances in Bohr radii $a_B = \hbar^2/Me^2 \approx 0.53\times10^{-8}\,\mathrm{cm}$, and magnetic field strengths in $B_0 = e^3M^2/\hbar^3 \approx 2.35\times10^5\,\mathrm{T} = 2.35\times10^9\,\mathrm{G}$, the extremization yields

$$\Omega_\parallel \approx \frac{B}{2}, \qquad \sqrt{\Omega_\perp} = \frac{2}{\sqrt{\pi}}\left(\ln B - 2\mathrm{lnln}\,B + \frac{2a}{\ln B} + \frac{a^2}{\ln^2 B} + b\right) + \mathcal{O}(\ln^{-3}B), \tag{5.131}$$

with abbreviations $a = 2 - \ln 2 \approx 1.307$ and $b = \ln(\pi/2) - 2 \approx -1.548$. The associated optimized ground state energy is, up to terms of order $\ln^{-2}B$,

$$E^{(0)}(B) = \frac{B}{2} - \frac{1}{\pi}\Big\{\ln^2 B - 4\ln B\,\mathrm{lnln}\,B + 4\ln^2\!\mathrm{ln}\,B - 4b\,\mathrm{lnln}\,B + 2(b+2)\ln B + b^2 - \frac{1}{\ln B}\left[8\ln^2\!\mathrm{ln}\,B - 8b\,\mathrm{lnln}\,B + 2b^2\right]\Big\} + \mathcal{O}(\ln^{-2}B). \tag{5.132}$$

The prefactor $1/\pi$ of the leading $\ln^2 B$-term using a variational ansatz of the type (5.64), (5.65) for the transverse degree of freedom is in contrast to the value $1/2$ calculated in the textbook by Landau and Lifshitz [11]. The calculation of higher orders in variational perturbation theory would drive our value towards $1/2$.

The convergence of the expansion (5.132) is quite slow. At a magnetic field strength $B = 10^5 B_0$, which corresponds to $2.35\times10^{10}\,\mathrm{T} = 2.35\times10^{14}\,\mathrm{G}$, the contribution from the first six terms is $22.87\,[2\,\mathrm{Ryd}]$. The next three terms suppressed by a factor $\ln^{-1}B$ contribute $-2.29\,[2\,\mathrm{Ryd}]$, while an estimate for the $\ln^{-2}B$-terms yields nearly $-0.3\,[2\,\mathrm{Ryd}]$. Thus we find $\varepsilon^{(1)}(10^5) = 20.58 \pm 0.3\,[2\,\mathrm{Ryd}]$.

Table 5.2 lists the values of the first six terms of Eq. (5.132). This shows in particular the significance of the second term in (5.132), which is of the same order of the leading first term, but with an opposite sign.

Table 5.2 Example for competing leading six terms in large-B expansion (5.132) at $B = 10^5 B_0 \approx 2.35 \times 10^{14}$ G.

$(1/\pi)\ln^2 B$	$-(4/\pi)\ln B \,\mathrm{lnln}\, B$	$(4/\pi)\ln^2 \ln B$	$-(4b/\pi)\,\mathrm{lnln}\, B$	$[2(b+2)/\pi]\ln B$	b^2/π
42.1912	−35.8181	7.6019	4.8173	3.3098	0.7632

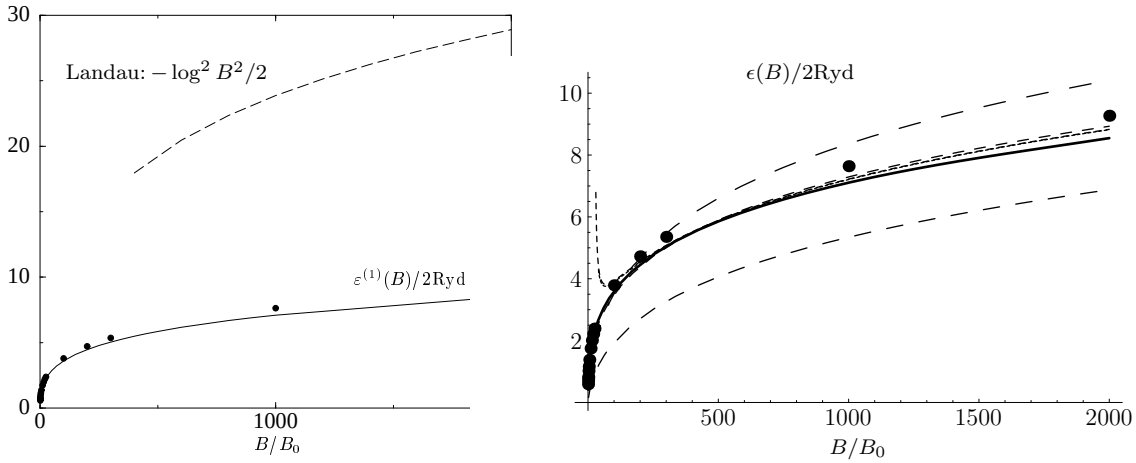

Figure 5.11 First-order variational result for binding energy (5.133) as a function of the strength of the magnetic field. The dots indicate the values derived in the reference given in Ref. [12]. The long-dashed curve on the left-hand side shows the simple estimate $0.5\ln^2 B$ of the textbook by Landau and Lifshitz [11]. The right-hand side shows the successive approximations from the strong-field expansion (5.134) for $N = 0, 1, 2, 3, 4$, with decreasing dash length. Fat curve is our variational approximation.

The field dependence of the binding energy

$$\varepsilon(B) \equiv \frac{B}{2} - E^{(0)} \tag{5.133}$$

is plotted in Fig. 5.11, where it is compared with the results of other authors who used completely different methods, with satisfactory agreement [12]. On the strong-coupling side we have plotted successive orders of a strong-field expansion [24]. The curves result from an iterative solution of the sequence of implicit equations for the quantity $w(B) = \sqrt{\epsilon(4B)/2}$ for $N = 1, 2, 3, 4$:

$$w = \frac{1}{2}\log\frac{B}{w^2} + \sum_{n=1}^{N} a_n(B, w), \tag{5.134}$$

where

$$a_1 \equiv -\frac{1}{2}(\gamma + \log 2),\ a_2 \equiv \frac{\pi^2}{12w},\ a_3 \equiv -\sqrt{\frac{2}{B}}\left(\log\frac{B}{2w^2} - \sqrt{\pi}w\right),\ a_4 = \sqrt{\frac{2}{B}}\frac{\sqrt{\pi}}{2}D, \tag{5.135}$$

and D denotes the integral $D \equiv \gamma - 2\int_0^\infty dy\,(y/\sqrt{y^2+1}-1)\log y \approx -0.03648$, where $\gamma \approx 0.5773$ is the Euler-Mascheroni constant (2.469).

Our results are of similar accuracy as those of other first-order calculations based on an operator optimization method [25]. The advantage of our variational approach is that it yields good results for all magnetic field strengths and temperatures, and that it can be improved systematically by methods to be developed in Section 5.13, with rapid convergence. The figure shows also the energy of Landau and Lifshitz which grossly overestimates the binding energies even at very large magnetic fields, such as $2000B_0 \propto 10^{12}\,\mathrm{G}$. Obviously, the nonleading terms in Eq. (5.132) give important contributions to the asymptotic behavior even at such large magnetic fields. As an peculiar property of the asymptotic behavior, the absolute value of the difference between the Landau-Lifshitz result and our approximation (5.132) diverges with increasing magnetic field strengths B. Only the relative difference decreases.

5.11.1 Weak-Field Behavior

Let us also calculate the weak-field behavior of the variational energy (5.127). Setting $\eta \equiv \Omega_\parallel/\Omega_\perp$, we rewrite $W_1(\mathbf{0})$ as

$$W_1(\mathbf{0}) = \frac{\Omega_\perp}{2}\left(1+\frac{\eta}{2}\right) + \frac{B^2}{8\Omega_\perp} + \sqrt{\frac{\eta\Omega_\perp}{\pi}}\frac{1}{\sqrt{1-\eta}}\ln\frac{1-\sqrt{1-\eta}}{1+\sqrt{1-\eta}}. \tag{5.136}$$

This is minimized in η and $\Omega_\perp$ by expanding $\eta(B)$ and $\Omega(B)$ in powers of B^2 with unknown coefficients, and inserting these expansions into extremality equations. The expansion coefficients are then determined order by order. The optimal expansions are inserted into (5.136), yielding the optimized binding energy $\varepsilon^{(1)}(B)$ as a power series

$$W_1(\mathbf{0}) = \sum_{n=0}^{\infty} \varepsilon_n B^{2n}. \tag{5.137}$$

The coefficients ε_n are listed in Table 5.3 and compared with the exact ones. Of course, the higher-order coefficients of this first-order variational approximation become rapidly inaccurate, but the results can be improved, if desired, by going to higher orders in variational perturbation theory of Section 5.13.

5.11.2 Effective Classical Hamiltonian

The quantum statistical properties of the system at an arbitrary temperature are contained in the effective classical potential $H^{\mathrm{eff\,cl}}(\mathbf{p}_0,\mathbf{x}_0)$ defined by the three-dimensional version of Eq. (3.824):

$$B(\mathbf{p}_0,\mathbf{x}_0) \equiv e^{-\beta H^{\mathrm{eff\,cl}}(\mathbf{p}_0,\mathbf{x}_0)} \equiv \oint \mathcal{D}^3x \oint \frac{\mathcal{D}^3p}{(2\pi\hbar)^3}\,\delta^{(3)}(\mathbf{x}_0-\overline{\mathbf{x}})(2\pi\hbar)^3\delta(\mathbf{p}_0-\overline{\mathbf{p}})\,e^{-\mathcal{A}[\mathbf{p},\mathbf{x}]/\hbar}, \tag{5.138}$$

Table 5.3 Perturbation coefficients up to order B^6 in weak-field expansions of variational parameters, and binding energy in comparison to exact ones (from J.E. Avron et al. and B.G. Adams et al. quoted in Notes and References).

n	0	1	2	3
η_n	1.0	$-\frac{405\pi^2}{7168} \approx -0.5576$	$\frac{16828965\pi^4}{1258815488} \approx 1.3023$	$-\frac{3886999332075\pi^6}{884272562962432} \approx -4.2260$
Ω_n	$\frac{32}{9\pi} \approx 1.1318$	$\frac{99\pi}{224} \approx 1.3885$	$-\frac{1293975\pi^3}{19668992} \approx -2.03982$	$\frac{524431667187\pi^5}{27633517592576} \approx 5.8077$
ε_n	$-\frac{4}{3\pi} \approx -0.4244$	$\frac{9\pi}{128} \approx 0.2209$	$-\frac{8019\pi^3}{1835008} \approx -0.1355$	$\frac{256449807\pi^5}{322256764928} \approx 0.2435$
$\varepsilon_n^{\rm ex}$	-0.5	0.25	$-\frac{53}{192} \approx -0.2760$	$\frac{5581}{4608} \approx 1.2112$

where $\mathcal{A}_{\rm e}[\mathbf{p},\mathbf{x}]$ is the Euclidean action

$$\mathcal{A}_{\rm e}[\mathbf{p},\mathbf{x}] = \int_0^{\hbar\beta} d\tau\,[-i\mathbf{p}(\tau)\dot{\mathbf{x}}(\tau) + H(\mathbf{p}(\tau),\mathbf{x}(\tau))], \tag{5.139}$$

and $\overline{\mathbf{x}} = \int_0^{\hbar\beta} d\tau\,\mathbf{x}(\tau)/\hbar\beta$ and $\overline{\mathbf{p}} = \int_0^{\hbar\beta} d\tau\,\mathbf{p}(\tau)/\hbar\beta$ are the temporal averages of position and momentum. Note that the deviations of $\mathbf{p}(\tau)$ from the average $\mathbf{p}_0$ share with $\mathbf{x}(\tau)-\mathbf{x}_0$ the property that the averages of the squares go to zero with increasing temperatures like $1/T$, and remains finite for $T \to 0$. while the expectation of $\mathbf{p}^2$ grows linearly with T (Dulong-Petit law). For $T \to 0$, the averages of the squares of $\mathbf{p}(\tau)$ remain finite. This property is the basis for a reliable accuracy of the variational treatment.

Thus we separate the action (5.139) (omitting the subscript e) as

$$\mathcal{A}_{\rm e}[\mathbf{p},\mathbf{x}] = \beta H(\mathbf{p}_0,\mathbf{x}_0) + \mathcal{A}_{\mathbf{\Omega}}^{\mathbf{p}_0,\mathbf{x}_0}[\mathbf{p},\mathbf{x}] + \mathcal{A}_{\rm int}[\mathbf{p},\mathbf{x}], \tag{5.140}$$

where $\mathcal{A}_{\mathbf{\Omega}}^{\mathbf{p}_0,\mathbf{x}_0}[\mathbf{p},\mathbf{x}]$ is the most general harmonic trial action containing the magnetic field. It has the form (3.828), except that we use capital frequencies to emphasize that they are now variational parameters:

$$\begin{aligned}\mathcal{A}_{\mathbf{\Omega}}^{\mathbf{p}_0,\mathbf{x}_0}[\mathbf{p},\mathbf{x}] = \int_0^{\hbar\beta} d\tau\,\Big\{ &-i[\mathbf{p}(\tau)-\mathbf{p}_0]\cdot\dot{\mathbf{x}}(\tau) + \frac{1}{2M}[\mathbf{p}(\tau)-\mathbf{p}_0]^2 \\ &+\Omega_B l_z(\mathbf{p}(\tau)-\mathbf{p}_0,\mathbf{x}(\tau)-\mathbf{x}_0) + \frac{M}{2}\Omega_\perp^2\,[\mathbf{x}_\perp(\tau)-\mathbf{x}_{0\perp}]^2 + \frac{M}{2}\Omega_\parallel^2[z(\tau)-z_0]^2\Big\}.\end{aligned} \tag{5.141}$$

The vector $\mathbf{x}^\perp = (x,y)$ is the projection of $\mathbf{x}$ orthogonal to $\mathbf{B}$.

The trial frequencies $\mathbf{\Omega} = (\Omega_B, \Omega_\perp, \Omega_\parallel)$ are arbitrary functions of $\mathbf{p}_0$, $\mathbf{x}_0$, and $\mathbf{B}$. Inserting the decomposition (5.140) into (5.138), we expand the exponential of the interaction, $\exp\{-\mathcal{A}_{\rm int}[\mathbf{p},\mathbf{x}]/\hbar\}$, and obtain a series of expectation values of powers of the interaction $\langle\,\mathcal{A}_{\rm int}^n[\mathbf{p},\mathbf{x}]\,\rangle_{\mathbf{\Omega}}^{\mathbf{p}_0,\mathbf{x}_0}$, defined in general by the path integral

$$\begin{aligned}\langle\,\mathcal{O}[\mathbf{p},\mathbf{x}]\,\rangle_{\mathbf{\Omega}}^{\mathbf{p}_0,\mathbf{x}_0} &= \frac{1}{Z_{\mathbf{\Omega}}^{\mathbf{p}_0,\mathbf{x}_0}} \oint \mathcal{D}^3x \frac{\mathcal{D}^3p}{(2\pi\hbar)^3}\,\mathcal{O}[\mathbf{p},\mathbf{x}]\,\delta^{(3)}(\mathbf{x}_0-\overline{\mathbf{x}})(2\pi\hbar)^3\delta(\mathbf{p}_0-\overline{\mathbf{p}}) \\ &\times \exp\left\{-\frac{1}{\hbar}\mathcal{A}_{\mathbf{\Omega}}^{\mathbf{p}_0,\mathbf{x}_0}[\mathbf{p},\mathbf{x}]\right\},\end{aligned} \tag{5.142}$$

where the local partition function in phase space $Z_{\mathbf{\Omega}}^{\mathbf{p}_0,\mathbf{x}_0}$ is the normalization factor which ensures that $\langle\, 1\,\rangle_{\mathbf{\Omega}}^{\mathbf{p}_0,\mathbf{x}_0} = 1$. From Eq. (3.829) we know that

$$Z_{\mathbf{\Omega}}^{\mathbf{p}_0,\mathbf{x}_0} \equiv e^{-\beta F_\Omega^{\mathbf{p}_0,\mathbf{x}_0}} = l_{\rm e}^3(\hbar\beta)\frac{\hbar\beta\Omega_+/2}{\sinh\hbar\beta\Omega_+/2}\,\frac{\hbar\beta\Omega_-/2}{\sinh\hbar\beta\Omega_-/2}\,\frac{\hbar\beta\Omega_\parallel/2}{\sinh\hbar\beta\Omega_\parallel/2}, \tag{5.143}$$

where $\Omega_\pm \equiv \Omega_B \pm \Omega_\perp$. In comparison to (3.829), the classical Boltzmann factor $e^{-\beta H(\mathbf{p}_0,\mathbf{x}_0)}$ is absent due to the shift of the integration variables in the action (5.141). Note that the fluctuations $\mathbf{p}(\tau) - \mathbf{p}_0$ decouple from $\mathbf{p}_0$ just as $\mathbf{x}(\tau) - \mathbf{x}_0$ decoupled from $\mathbf{x}_0$ due to the absence of zero frequencies in the fluctuations.

Rewriting the perturbation series as a cumulant expansion, evaluating the expectation values, and integrating out the momenta on the right-hand side of Eq. (5.138) leads to a series representation for the effective classical potential $V_{\rm eff}(\mathbf{x}_0)$. Since it is impossible to sum up the series, the perturbation expansion must be truncated, leading to an Nth-order approximation $W_{\mathbf{\Omega}}^{(N)}(\mathbf{x}_0)$ for the effective classical potential. Since the parameters $\mathbf{\Omega}$ are arbitrary, $W_{\mathbf{\Omega}}^{(N)}(\mathbf{x}_0)$ should depend *minimally* on $\mathbf{\Omega}$. This determines the optimal values of $\mathbf{\Omega}$ to be equal to $\mathbf{\Omega}^{(N)}(\mathbf{x}_0) = (\Omega_B^{(N)}(\mathbf{x}_0), \Omega_\perp^{(N)}(\mathbf{x}_0), \Omega_\parallel^{(N)}(\mathbf{x}_0))$ of Nth order. Reinserting these into $W_{\mathbf{\Omega}}^{(N)}(\mathbf{x}_0)$ yields the optimal approximation $W^{(N)}(\mathbf{x}_0) \equiv W_{\mathbf{\Omega}^{(N)}}^{(N)}(\mathbf{x}_0)$.

The first-order approximation to the effective classical potential is then, with $\omega_\parallel = 0, \omega_\perp = \omega_B$,

$$\begin{aligned} W_{\mathbf{\Omega}}^{(1)}(\mathbf{x}_0) &= F_{\mathbf{\Omega}}^{\mathbf{p}_0,\mathbf{x}_0} - \frac{M}{2}\Omega_B(\mathbf{x}_0)[\omega_B - \Omega_B(\mathbf{x}_0)]\, b_\perp^2(\mathbf{x}_0)\, a_\perp^2(\mathbf{x}_0) \\ &+ \frac{M}{2}\left[\omega_B^2 - \Omega_\perp^2(\mathbf{x}_0)\right] - \frac{1}{2}\Omega_\parallel^2 a_\parallel^2(\mathbf{x}_0) - \left\langle\, \frac{e^2}{|\mathbf{x}|}\,\right\rangle_{\mathbf{\Omega}}^{\mathbf{p}_0,\mathbf{x}_0}. \end{aligned} \tag{5.144}$$

The smearing of the Coulomb potential is performed as in Section 5.10. This yields the result (5.117). with the longitudinal width

$$a_\parallel^2(\mathbf{x}_0) = G_{zz}^{(2)\,\mathbf{x}_0}(\tau,\tau) = \frac{1}{\beta M\Omega_\parallel^2(\mathbf{x}_0)}\left[\frac{\hbar\beta\Omega_\parallel(\mathbf{x}_0)}{2}\coth\frac{\hbar\beta\Omega_\parallel(\mathbf{x}_0)}{2} - 1\right], \tag{5.145}$$

and an analog transverse width.

The quantity $b_\perp^2(\mathbf{x}_0)$ is new in this discussion based on the canonical path integral. It denotes the expectation value associated with the z-component of the angular momentum

$$b_\perp^2(\mathbf{x}_0) \equiv \frac{1}{M\Omega_B}\,\langle\, l_z\,\rangle_{\mathbf{\Omega}}^{\mathbf{p}_0,\mathbf{x}_0}, \tag{5.146}$$

which can also be written as

$$b_\perp^2(\mathbf{x}_0) = \frac{2}{M\Omega_{T1}}\,\langle\, x(\tau)p_y(\tau)\,\rangle_{\mathbf{\Omega}}^{\mathbf{p}_0,\mathbf{x}_0}. \tag{5.147}$$

According to Eq. (3.358), the correlation function $\langle\, x(\tau)p_y(\tau)\,\rangle_{\mathbf{\Omega}}^{\mathbf{p}_0,\mathbf{x}_0}$ is given by

$$\langle\, x(\tau)p_y(\tau')\,\rangle_{\mathbf{\Omega}}^{\mathbf{p}_0,\mathbf{x}_0} = iM\partial_{\tau'}G_{\omega^2,B,xx}^{(2)}(\tau,\tau') - M\omega_B G_{\omega^2,B,xy}^{(2)}(\tau,\tau'), \tag{5.148}$$

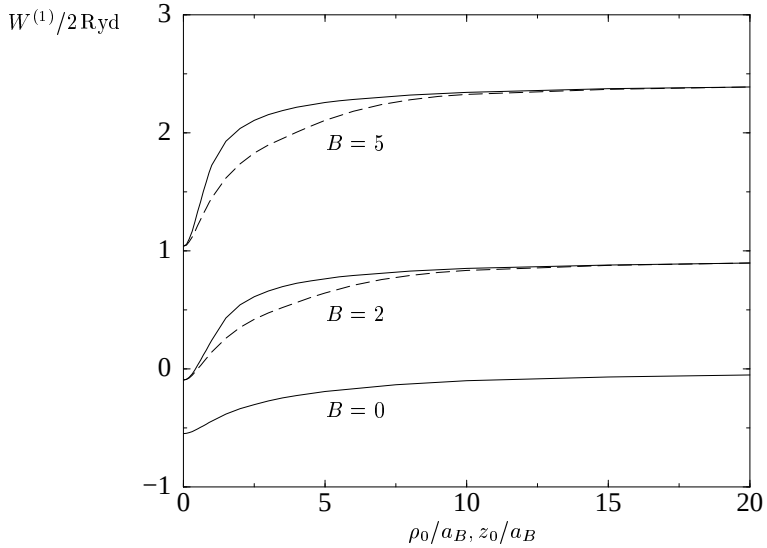

Figure 5.12 Effective classical potential of atom in strong magnetic field plotted along two directions: once as a function of the coordinate $\rho_0 = \sqrt{x_0^2 + y_0^2}$ perpendicular to the field lines at $z_0 = 0$ (solid curves), and once parallel to the magnetic field as a function of z_0 at $\rho_0 = 0$ (dashed curves). The inverse temperature is fixed at $\beta = 100$, and the strengths of the magnetic field B are varied (all in natural units).

where the expressions on the right-hand side are those of Eqs. (3.329) and (3.331), with ω replaced by Ω.

The variational energy (5.144) is minimized at each $\mathbf{x}_0$, and the resulting $W^{(N)}(\mathbf{x}_0)$ is displayed for a low temperature and different magnetic fields in Fig. 5.12. The plots show the anisotropy with respect to the magnetic field direction. The anisotropy grows when lowering the temperature and increasing the field strength. Far away from the proton at the origin, the potential becomes isotropic, due to the decreasing influence of the Coulomb interaction. Analytically, this is seen by going to the limits $\rho_0 \to \infty$ or $z_0 \to \infty$, where the expectation value of the Coulomb potential tends to zero, leaving an effective classical potential

$$W^{(1)}_{\mathbf{\Omega}}(\mathbf{x}_0) \to F^{\mathbf{p}_0,\mathbf{x}_0}_{\mathbf{\Omega}} - M\Omega_B(\omega_\perp - \Omega_B)\, b_\perp^2 + M\left(\omega_\perp^2 - \Omega_\perp^2\right) a_\perp^2 - \frac{M}{2}\Omega_\parallel^2 a_\parallel^2. \quad (5.149)$$

This is $\mathbf{x}_0$-independent, and optimization yields the constants $\Omega_B^{(1)} = \Omega_\perp^{(1)} = \omega_B$ and $\Omega_\parallel^{(1)} = 0$, with the asymptotic energy

$$W^{(1)}(\mathbf{x}_0) \to -\frac{1}{\beta}\log\frac{\beta\hbar\omega_B}{\sinh\beta\hbar\omega_B}. \quad (5.150)$$

The $B = 0$ -curves agree, of course, with those obtained from the previous variational perturbation theory of the hydrogen atom [26].

For large temperatures, the anisotropy decreases since the violent thermal fluctuations have a smaller preference of the z-direction.

5.12 Variational Approach to Excitation Energies

As explained in Section 5.4, the success of the above variational treatment is rooted in the fact that for smooth potentials, the ground state energy can be approximated quite well by the optimal expectation value of the Hamiltonian operators in a Gaussian wave packet. The question arises as to whether the energies of excited states can also be obtained by calculating an optimized expectation value between excited oscillator wave functions. If the potential shape has only a rough similarity with that of a harmonic oscillator, when there are no multiple minima, the answer is positive. Consider again the anharmonic oscillator with the action

$$\mathcal{A}[x] = \int_0^{\hbar\beta} d\tau \left[\frac{M}{2} \left(\dot{x}^2 + \omega^2 x^2 \right) + \frac{1}{4} g x^4 \right]. \tag{5.151}$$

As for the ground state, we replace the action $\mathcal{A}$ by $\mathcal{A}_\Omega^{x_0} + \mathcal{A}_{\rm int}^{x_0}$ with the trial oscillator action centered around the arbitrary point x_0

$$\mathcal{A}_\Omega^{x_0} = \int_0^{\hbar\beta} d\tau M \left[\frac{1}{2} \dot{x}^2 + \frac{\Omega^2}{2} (x - x_0)^2 \right], \tag{5.152}$$

and a remainder

$$\mathcal{A}_{\rm int}^{x_0} = \int_0^{\beta} d\tau \left[M \frac{\omega^2 - \Omega^2}{2} (x - x_0)^2 + \frac{g}{4} x^4 \right] \tag{5.153}$$

to be treated as an interaction. Let $\psi_\Omega^{(n)}(x - x_0)$ be the wave functions of the trial oscillator.[1] With these, we form the projections

$$\begin{aligned} Z_\Omega^{(n)}(x_0) &\equiv \int dx_b dx_a \psi_\Omega^{(n)*}(x_b)(x_b\tau_b|x_a\tau_a)\psi_\Omega^{(n)}(x_a) \\ &= \int dx_b dx_a \psi_\Omega^{(n)*}(x_b) \left(\int_{(x_a,0)\rightsquigarrow(x_b,\hbar\beta)} \mathcal{D}x e^{-\mathcal{A}/\hbar} \right) \psi_\Omega^{(n)}(x_a). \end{aligned} \tag{5.154}$$

If the temperature tends to zero, an optimization in the parameters x_0 and $\Omega(x_0)$ should yield information on the energy $E^{(n)}$ of this state by containing an exponentially decreasing function

$$Z^{(n)} \approx e^{-\beta E^{(n)}}. \tag{5.155}$$

Since the trial wave functions $\psi_\Omega^{(n)}(x - x_0)$ are not the true ones, the behavior (5.155) contains an admixture of Boltzmann factors $e^{-\beta E^{(n')}}$ with $n' \neq n$, which have to be eliminated. They are easily recognized by the powers of g which they carry.

The calculation of (5.154) is done in the same approximation that rendered good results for the ground state, i.e., we approximate the part of $Z^{(n)}$ behaving like (5.155) as follows:

$$Z^{(n)} \approx Z_\Omega^{(n)} e^{-\left\langle \mathcal{A}_{\rm int}^{x_0}/\hbar \right\rangle_\Omega^{(n)}}, \tag{5.156}$$

[1] In contrast to the earlier notation, we now use superscripts in parentheses to indicate the principal quantum numbers. The subscripts specify the level of approximation.

where $Z_\Omega^{(n)}$ denotes the contribution of the nth excited state to the oscillator partition function

$$Z_\Omega^{(n)} = e^{-\beta\hbar\Omega(n+1/2)}, \tag{5.157}$$

and $\langle \mathcal{A}_{\rm int}^{x_0}/\hbar \rangle_\Omega^{(n)}$ stands for the expectation of $\mathcal{A}_{\rm int}^{x_0}/\hbar$ in the state $\psi_\Omega^{(n)}(x-x_0)$. This approximation corresponds precisely to the first term in the perturbation expansion (3.509) (after continuing to imaginary times). ref(3.509)

Note that the approximation on the right-hand side of (5.156) is not necessarily smaller than the left-hand side, as in the Jensen-Peierls inequality (5.10), since the measure of integration in (5.154) is no longer positive. lab(x3.203) est(3.209)

For the action (5.151), the best value of x_0 lies at the coordinate origin. This simplifies the calculation of the expectation $\langle \mathcal{A}_{\rm int}^{x_0}/\hbar \rangle_\Omega^{(n)}$. The expectation of x^{2k} in the state $\psi_\Omega^{(n)}(x)$ is given by

$$\left\langle x^{2k} \right\rangle_\Omega^{(n)} = \frac{\hbar^k}{(M\Omega)^k} n_{2k}, \tag{5.158}$$

where

$$\begin{aligned} &n_2 = (n+1/2), \quad n_4 = \frac{3}{2}(n^2+n+1/2), \quad n_6 = \frac{5}{4}(2n^3+3n^2+4n+3/2), \\ &n_8 = \frac{1}{16}(70n^4+140n^3+344n^2+280n+105), \quad \dots \ . \end{aligned} \tag{5.159}$$

After inserting (5.153) into (5.156), the expectations (5.158) yield the approximation

$$Z^{(n)} \approx \exp\left\{ -\beta \left[\frac{1}{2}\left(\Omega^2+\omega^2\right)\frac{\hbar n_2}{\Omega} + \frac{g}{4}\frac{\hbar^2 n_4}{M^2\Omega^2} \right] \right\}. \tag{5.160}$$

With the dimensionless coupling constant $g' \equiv g\hbar/M^2\omega^3$, this corresponds to the variational energies

$$W^{(n)} = \hbar \left[\frac{1}{2}\left(\Omega + \frac{\omega^2}{\Omega}\right) n_2 + \frac{g'}{4}\frac{\omega^3}{\Omega^2} n_4 \right]. \tag{5.161}$$

They are optimized by the extremal Ω-values

$$\Omega = \Omega_1^{(n)} = \begin{cases} \frac{2}{\sqrt{3}}\omega \cosh\left[\frac{1}{3}\operatorname{arcosh}\left(g/g^{(n)}\right)\right] & \text{for} \quad g > g^{(n)}, \\ \frac{2}{\sqrt{3}}\omega \cos\left[\frac{1}{3}\arccos(g/g^{(n)})\right] & \text{for} \quad g < g^{(n)}, \end{cases} \tag{5.162}$$

where

$$g^{(n)} \equiv \frac{2}{3\sqrt{3}}\frac{n_2}{n_4}\frac{M^2\omega^3}{\hbar}. \tag{5.163}$$

The optimized $W^{(n)}$ yield the desired approximations $E_{\rm app}^{(n)}$ for the excited energies of the anharmonic oscillator.

For large g, the trial frequency grows like

$$\Omega^{(n)} \equiv 6^{1/3} \left(\frac{g\hbar}{4M^2\omega^3} \right)^{1/3} \tilde{n}, \tag{5.164}$$

where

$$\tilde{n} \equiv \frac{4n_4/3}{2n_2} = \frac{n^2+n+1/2}{n+1/2}, \tag{5.165}$$

making the energy $E^{(n)}_{\rm app}$ grow like

$$E^{(n)}_{\rm BS} \to \hbar\omega\kappa^{(n)} \left(\frac{g\hbar}{4M^2\omega^3} \right)^{1/3}, \quad \text{for large } g, \tag{5.166}$$

with

$$\kappa^{(n)} = \frac{3\cdot 6^{1/3}}{8}(2n+1)\,\tilde{n}^{1/3} \approx 0.68142 \times (2n+1)\,\tilde{n}^{1/3}. \tag{5.167}$$

For $n=0$, this is in good agreement with the precise growth behavior to be calculated in Section 5.16 where we shall find $\kappa^{(0)}_{\rm ex} = 0.667\,986\ldots$ (see Table 5.9).

In the limit of large g *and* n, this can be compared with the exact behavior obtained from the semiclassical approximation of Bohr and Sommerfeld, which gives the same leading powers in g and n as in (5.166), but a 3% larger prefactor $0.688\,253\,702 \times 2$ [recall (4.36)]. The exact values of $E^{(n)}/(g\hbar/4M^2)$ and $\frac{1}{2}\kappa^{(n)}/(n+1/2)^{4/3}$ are for $n = 0, 2, 4, 6, 8, 10$ are shown in Table 5.4.

A comparison of the approximate energies $E^{(n)}_{\rm app}$ with the precise numerical solutions of the Schrödinger equation in natural units $\hbar = 1$, $M = 1$ in Table 5.5 shows an excellent agreement for all coupling strengths.

Near the strong-coupling limit, the optimal frequencies $\Omega^{(n)}_1$ and the approximate energies $E^{(n)}_1$ behave as follows [in natural units; compare (5.76) and (5.77)]:

$$\begin{aligned} \Omega^{(n)}_1 &= 6^{1/3} \left(\frac{\tilde{n}g}{4} \right)^{1/3} \left[1 + \frac{1}{9} \left(\frac{3}{4} \right)^{1/3} \frac{1}{(\tilde{n}g/4)^{2/3}} + \ldots \right], \\ E^{(n)}_1 &= \left(\frac{3}{4} \right)^{4/3} (2n+1) \left(\frac{\tilde{n}g}{4} \right)^{1/3} \left[1 + \frac{6^{1/3}}{9} \frac{1}{(\tilde{n}g/4)^{2/3}} + \ldots \right]. \end{aligned} \tag{5.168}$$

Table 5.4 Approach of variational energies of nth excited state to Bohr-Sommerfeld approximation with increasing n. Values in the last column converge rapidly towards the Bohr-Sommerfeld value $0.688\,253\,702\ldots$ in Eq. (4.36).

n	$E^{(n)}/(g\hbar/4M^2)$	$\frac{1}{2}\kappa^{(n)}/(n+1/2)^{4/3}$
0	0.667 986 259 155 777 108 3	0.841 609 948 112 105 001
2	4.696 795 386 863 646 196 2	0.692 125 685 914 981 314
4	10.244 308 455 438 771 076 0	0.689 449 772 359 340 765
6	16.711 890 073 897 950 947 1	0.688 828 486 600 234 466
8	23.889 993 634 572 505 935 5	0.688 590 146 947 993 676
10	31.659 456 477 221 552 442 8	0.688 474 290 179 981 433

Table 5.5 Energies of the nth excited states of anharmonic oscillator $\omega^2 x^2/2 + g x^4/4$ for various coupling strengths g (in natural units). In each entry, the upper number shows the energies obtained from a numerical integration of the Schrödinger equation, whereas the lower number is our variational result.

$g/4$	$E^{(0)}$	$E^{(1)}$	$E^{(2)}$	$E^{(3)}$	$E^{(4)}$	$E^{(5)}$	$E^{(6)}$	$E^{(7)}$	$E^{(8)}$
0.1	0.559 146	1.769 50	3.138 62	4.628 88	6.220 30	7.899 77	9.657 84	11.4873	13.3790
	0.560 307	1.773 39	3.138 24	4.621 93	6.205 19	7.875 22	9.622 76	11.4407	13.3235
0.2	0.602 405	1.950 54	3.536 30	5.291 27	7.184 46	9.196 34	11.313 2	13.5249	15.8222
	0.604 901	1.958 04	3.534 89	5.278 55	7.158 70	9.156 13	11.257 3	13.4522	15.7328
0.3	0.637 992	2.094 64	3.844 78	5.796 57	7.911 75	10.1665	12.5443	15.0328	17.6224
	0.641 630	2.104 98	3.842 40	5.779 48	7.878 23	10.1151	12.4736	14.9417	17.5099
0.4	0.668 773	2.216 93	4.102 84	6.215 59	8.511 41	10.9631	13.5520	16.2642	19.0889
	0.673 394	2.229 62	4.099 59	6.194 95	8.471 69	10.9028	13.4698	16.1588	18.9591
0.5	0.696 176	2.324 41	4.327 52	6.578 40	9.028 78	11.6487	14.4177	17.3220	20.3452
	0.701 667	2.339 19	4.323 52	6.554 75	8.983 83	11.5809	14.3257	17.2029	20.2009
0.6	0.721 039	2.421 02	4.528 12	6.901 05	9.487 73	12.2557	15.1832	18.2535	21.4542
	0.727 296	2.437 50	4.523 43	6.874 77	9.438 25	12.1816	15.0828	18.1256	21.2974
0.7	0.743 904	2.509 23	4.710 33	7.193 27	9.902 61	12.8039	15.8737	19.0945	22.4530
	0.750 859	2.527 29	4.705 01	7.164 64	9.849 11	12.7240	15.7658	18.9573	22.2852
0.8	0.765 144	2.590 70	4.877 93	7.461 45	10.2828	13.3057	16.5053	19.8634	23.3658
	0.772 736	2.610 21	4.872 04	7.430 71	10.2257	13.2206	16.3907	19.7179	23.1880
0.9	0.785 032	2.666 63	5.033 60	7.710 07	10.6349	13.7700	17.0894	20.5740	24.2091
	0.793 213	2.687 45	5.027 18	7.677 39	10.5744	13.6801	16.9687	20.4209	24.0221
1	0.803 771	2.737 89	5.179 29	7.942 40	10.9636	14.2031	17.6340	21.2364	24.9950
	0.812 500	2.759 94	5.172 37	7.907 93	10.9000	14.1090	17.5076	21.0763	24.7996
10	1.504 97	5.321 61	10.3471	16.0901	22.4088	29.2115	36.4369	44.0401	51.9865
	1.531 25	5.382 13	10.3244	15.9993	22.2484	28.9793	36.1301	43.6559	51.5221
50	2.499 71	8.915 10	17.4370	27.1926	37.9385	49.5164	61.8203	74.7728	88.3143
	2.547 58	9.023 38	17.3952	27.0314	37.6562	49.1094	61.2842	74.1029	87.5059
100	3.131 38	11.1873	21.9069	34.1825	47.7072	62.2812	77.7708	94.0780	111.128
	3.192 44	11.3249	21.8535	33.9779	47.3495	61.7660	77.0924	93.2307	110.106
500	5.319 89	19.0434	37.3407	58.3016	81.4012	106.297	132.760	160.622	189.756
	5.425 76	19.2811	37.2477	57.9489	80.7856	105.411	131.595	159.167	188.001
1000	6.694 22	23.9722	47.0173	73.4191	102.516	133.877	167.212	202.311	239.012
	6.827 95	24.2721	46.9000	72.9741	101.740	132.760	165.743	200.476	236.799

The tabulated energies can be used to calculate an approximate partition function at all temperatures:

$$Z \approx \sum_{n=0}^{\infty} e^{-\beta E^{(n)}_{\mathrm{app}}}. \tag{5.169}$$

The resulting free energies $F_1' = -\log Z/\beta$ agree well with the previous variational results of the Feynman-Kleinert approximation — in the plots of Fig. 5.2, the curves are indistinguishable. This is not astonishing since both approximations are dominated near zero temperature by the same optimal energy $E^{(0)}_{\mathrm{app}}$, while approaching the semiclassical behavior at high temperatures. The previous free energy F_1 does so exactly, the free energy F_1' to a very good approximation.

By combining the Boltzmann factors with the oscillator wave functions $\psi_\Omega^{(n)}(x)$, we also calculate the density matrix $(x_b\tau_b|x_a\tau_a)$ and the distribution functions $\rho(x) = (x\,\hbar\beta|x\,0)$ in this approximation:

$$(x_b\tau_b|x_a\tau_a) \approx \sum_{n=0}^{\infty} \psi^{(n)}(x_b)\psi^{(n)*}(x_a)e^{-\beta E_{\rm app}^{(n)}}. \tag{5.170}$$

They are in general less accurate than the earlier calculated particle density $\rho_1(x_0)$ of (5.94).

5.13 Systematic Improvement of Feynman-Kleinert Approximation. Variational Perturbation Theory

A systematic improvement of the variational approach leads to a convergent *variational perturbation expansion* for the effective classical potential of a quantum-mechanical system [27]. To derive it, we expand the action in powers of the deviations of the path from its average $x_0 = \bar{x}$:

$$\delta x(\tau) \equiv x(\tau) - x_0. \tag{5.171}$$

The expansion reads

$$\mathcal{A} = V(x_0) + \mathcal{A}_\Omega^{x_0} + \mathcal{A}'^{x_0}_{\rm int}, \tag{5.172}$$

where $\mathcal{A}_\Omega^{x_0}$ is the quadratic action of the deviations $\delta x(\tau)$

$$\mathcal{A}_\Omega^{x_0} = \int_0^{\hbar/k_BT} d\tau \frac{M}{2}\left\{[\delta\dot{x}(\tau)]^2 + \Omega^2(x_0)[\delta x(\tau)]^2\right\}, \tag{5.173}$$

and $\mathcal{A}'^{x_0}_{\rm int}$ contains all higher powers in $\delta x(\tau)$:

$$\mathcal{A}'^{x_0}_{\rm int} = \int_0^{\hbar\beta} d\tau \left\{\frac{g_2}{2!}[\delta x(\tau)]^2 + \frac{g_3}{3!}[\delta x(\tau)]^3 + \frac{g_4}{4!}[\delta x(\tau)]^4 + \ldots\right\}. \tag{5.174}$$

The coupling constants are, in general, x_0-dependent:

$$g_i(x_0) = V^{(i)}(x_0) - \Omega^2\delta_{i2}, \qquad V^{(i)}(x_0) \equiv \frac{d^iV(x_0)}{dx_0^i}. \tag{5.175}$$

For the anharmonic oscillator, they take the values

$$\begin{aligned} g_2(x_0) &= M[\omega^2 - \Omega^2(x_0)] + 3gx_0^2, \\ g_3(x_0) &= 6gx_0, \\ g_4(x_0) &= 6g. \end{aligned} \tag{5.176}$$

Introducing the parameter

$$r^2 = 2M(\omega^2 - \Omega^2)/g, \tag{5.177}$$

which has the dimension length square, we write $g_2(x_0)$ as

$$g_2(x_0) = g(r^2/2 + 3x_0^2). \tag{5.178}$$

With the decomposition (5.172), the Feynman-Kleinert approximation (5.32) to the effective classical potential can be written as

$$W_1^\Omega(x_0) = V(x_0) + F_\Omega^{x_0} + \frac{1}{\hbar\beta}\,\langle \mathcal{A}_{\rm int}^{x_0}\rangle_\Omega^{x_0}\,. \tag{5.179}$$

To generalize this, we replace the local free energy $F_\Omega^{x_0}$ by $F_\Omega^{x_0} + \Delta F^{x_0}$, where ΔF^{x_0} denotes the local analog of the cumulant expansion (3.487). This leads to the variational perturbation expansion for the effective classical potential

$$\begin{aligned} V^{\rm eff\,cl}(x_0) &= V(x_0) + F_\Omega^{x_0} + \frac{1}{\hbar\beta}\,\langle \mathcal{A}_{\rm int}^{x_0}\rangle_\Omega^{x_0} \\ &\quad -\frac{1}{2!\hbar^2\beta}\left\langle \mathcal{A}_{\rm int}^{x_0\,2}\right\rangle_{\Omega,{\rm c}}^{x_0} + \frac{1}{3!\hbar^3\beta}\left\langle \mathcal{A}_{\rm int}^{x_0\,3}\right\rangle_{\Omega,{\rm c}}^{x_0} + \dots \end{aligned} \tag{5.180}$$

in terms of the connected expectation values of powers of the interaction:

$$\left\langle \mathcal{A}_{\rm int}^{x_0\,2}\right\rangle_{\Omega,{\rm c}}^{x_0} \equiv \left\langle \mathcal{A}_{\rm int}^{x_0\,2}\right\rangle_{\Omega}^{x_0} - \langle \mathcal{A}_{\rm int}^{x_0}\rangle_\Omega^{x_0\,2}, \tag{5.181}$$

$$\left\langle \mathcal{A}_{\rm int}^{x_0\,3}\right\rangle_{\Omega,{\rm c}}^{x_0} \equiv \left\langle \mathcal{A}_{\rm int}^{x_0\,3}\right\rangle_{\Omega}^{x_0} - 3\left\langle \mathcal{A}_{\rm int}^{x_0\,2}\right\rangle_{\Omega}^{x_0}\langle \mathcal{A}_{\rm int}^{x_0}\rangle_\Omega^{x_0} + 2\,\langle \mathcal{A}_{\rm int}^{x_0}\rangle_\Omega^{x_0\,3}, \tag{5.182}$$

$$\vdots \quad .$$

By construction, the infinite sum (5.180) is independent of the choice of the trial frequency $\Omega(x_0)$.

When truncating (5.180) after the Nth order, we obtain the approximation $W_N^\Omega(x_0)$ to the effective classical potential $V^{\rm eff\,cl}(x_0)$. In many applications, it is sufficient to work with the third-order approximation

$$\begin{aligned} W_3^\Omega(x_0) &= V(x_0) + F_\Omega^{x_0} + \frac{1}{\hbar\beta}\,\langle \mathcal{A}'^{x_0}_{\rm int}\rangle_\Omega^{x_0} \\ &\quad -\frac{1}{2\hbar^2\beta}\left\langle \mathcal{A}'^{x_0\,2}_{\rm int}\right\rangle_{\Omega,{\rm c}}^{x_0} + \frac{1}{6\hbar^3\beta}\left\langle \mathcal{A}'^{x_0\,3}_{\rm int}\right\rangle_{\Omega,{\rm c}}^{x_0}. \end{aligned} \tag{5.183}$$

In contrast to (5.180), the truncated sums $W_N(x_0)$ *do* depend on $\Omega(x_0)$. Since the infinite sum is $\Omega(x_0)$-independent, the best truncated sum $W_N(x_0)$ should lie at the frequency $\Omega_N(x_0)$ where $W_N^\Omega(x_0)$ depends minimally on it. The optimal $\Omega_N(x_0)$ is called the *frequency of least dependence*. Thus we require for (5.183)

$$\frac{\partial W_3^\Omega(x_0)}{\partial\Omega(x_0)} = 0. \tag{5.184}$$

At the frequency $\Omega_3(x_0)$ fixed by this condition, Eq. (5.183) yields the desired third-order approximation $W_3(x_0)$ to the effective classical potential.

The explicit calculation of the expectation values on the right-hand side of (5.183) proceeds according to the rules of Section 3.18. We have to evaluate the Feynman integrals associated with all vacuum diagrams. These are composed of p-particle vertices carrying the coupling constant $g_p/p!\hbar$, and of lines representing the correlation function of the fluctuations introduced in (5.23):

$$\begin{aligned}\langle \delta x(\tau)\delta x(\tau')\rangle_\Omega^{x_0} &= \frac{\hbar}{M} G'^{x_0}_\Omega(\tau-\tau') \\ &= a^2(\tau-\tau', x_0). \end{aligned} \tag{5.185}$$

Since this correlation function contains no zero frequency, diagrams of the type shown in Fig. 5.13 do not contribute. Their characteristic property is to fall apart when cutting a single line. They are called *one-particle reducible diagrams*. A vacuum subdiagram connected with the remainder by a single line is called a *tadpole diagram*, alluding to its biological shape. Tadpole diagrams do not contribute to the variational perturbation expansion since they vanish as a consequence of energy conservation: the connecting line ending in the vacuum, must have a vanishing frequency where the spectral representation of the correlation function $\langle \delta x(\tau)\delta x(\tau')\rangle_\Omega^{x_0}$ has no support, by construction.

The number of Feynman diagrams to be evaluated is reduced by ignoring at first all diagrams containing the vertices g_2. The omitted diagrams can be recovered from the diagrams without g_2-vertices by calculating the latter at the initial frequency ω, and by replacing ω by a modified local trial frequency,

$$\omega \to \tilde{\Omega}(x_0) \equiv \sqrt{\Omega^2(x_0) + g_2(x_0)/M}. \tag{5.186}$$

After this replacement, which will be referred to as the *square-root trick*, all diagrams are re-expanded in powers of g [remembering that $g_2(x_0)$ is by (5.178) proportional to g] up to the maximal power g^3.

5.14 Applications of Variational Perturbation Expansion

The third-order approximation $W_3(x_0)$ is far more accurate than $W_1(x_0)$. This will now be illustrated by performing the variational perturbation expansion for the an-

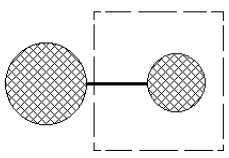

Figure 5.13 Structure of a one-particle reducible vacuum diagram. The dashed box encloses a so-called tadpole diagram. Such diagrams vanish in the present expansion since an ending line cannot carry any energy and since the correlation function $\langle \delta x(\tau)\delta x(\tau')\rangle$ contains no zero frequency.

harmonic oscillator and the double-well potential. The reason for the great increase in accuracy will become clear in Section 5.15, where we shall demonstrate that this expansion *converges* rapidly towards the exact result at *all* coupling strengths, in contrast to ordinary perturbation expansions which diverges even for arbitrarily small values of g.

5.14.1 Anharmonic Oscillator at $T = 0$

Consider first the case of zero temperature, where the calculation is simplest and the approximation should be the worst. At $T = 0$, only the point $x_0 = 0$ contributes, and $\delta x(\tau)$ coincides with the path itself $\equiv x(\tau)$. Thus we may omit the superscript x_0 in all equations, so that the interaction in (5.182) becomes writing it as

$$\mathcal{A}_{\rm int} = \frac{g}{4}\int_0^{\hbar\beta} d\tau (r^2 x^2 + x^4). \tag{5.187}$$

The effect of the r^2-term is found by replacing the frequency ω in the original perturbation expansion for the anharmonic oscillator according to the square-root trick (5.186), which for $x_0 = 0$ is simply

$$\omega \to \tilde{\Omega} \equiv \sqrt{\Omega^2 + (\omega^2 - \Omega^2)} = \sqrt{\Omega^2 + gr^2/2M}. \tag{5.188}$$

After this replacement, all terms are re-expanded in powers of g. Finally, r^2 is again replaced by

$$r^2 \to \frac{2M}{g}(\omega^2 - \Omega^2). \tag{5.189}$$

Since the interaction is even in x, the zero-temperature expansion is automatically free of tadpole diagrams.

The perturbation expansion to third order was given in Eq. (3.554). With the above replacement it leads to the free energy

ref(3.554)
lab(x3.192)
est(3.197)

$$F = \frac{\hbar\tilde{\Omega}}{2} + \frac{g}{4}\,3a^4 + \left(\frac{g}{4}\right)^2 42a^8 \frac{1}{\hbar\tilde{\Omega}} + \left(\frac{g}{4}\right)^3 4\cdot 333 a^{12}\left(\frac{1}{\hbar\tilde{\Omega}}\right)^2, \tag{5.190}$$

with

$$a^2 = \frac{\hbar}{2M\tilde{\Omega}}. \tag{5.191}$$

The higher orders can most easily be calculated with the help of the Bender-Wu recursion relations derived in Appendix 3C.[2]

By expanding F in powers of g up to g^3 we obtain

$$\begin{aligned} W_3^{\Omega} = {} & \frac{\hbar\Omega}{2} + g(3a^4 - r^2a^2)/4 - g^2(21a^8/8 + 3a^6r^2/4 + a^4r^4/16)/\hbar\Omega \\ & + g^3(333a^{12}/16 + 105a^{10}r^2/16 + 3a^8r^4/4 + a^6r^6/32)/(\hbar\Omega)^2. \end{aligned} \tag{5.192}$$

After the replacement (5.189), we minimize W_3 in Ω, and obtain the third-order

[2]The Mathematica program is available on the internet under `http://www.physik.fu-berlin.de/~kleinert/294/programs`.

Table 5.6 Second- and third-order approximations to ground state energy, in units of $\hbar\omega$, of anharmonic oscillator at various coupling constants g in comparison with exact values $E^{(0)}_{\rm ex}(g)$ and the Feynman-Kleinert approximation $E^{(0)}_1(g)$ of previous section.

$g/4$	$E^{(0)}_{\rm ex}(g)$	$E^{(0)}_1(g)$	$E^{(0)}_2(g)$	$E^{(0)}_3(g)$
0.1	0.559146	0.560307371	0.559152139	0.559154219
0.2	0.602405	0.604900748	0.602450713	0.602430621
0.3	0.637992	0.641629862	0.638088735	0.638035760
0.4	0.668773	0.673394715	0.668922455	0.668834137
0.5	0.696176	0.701661643	0.696376950	0.696253632
0.6	0.721039	0.727295668	0.721288789	0.721131776
0.7	0.743904	0.750857818	0.744199436	0.744010317
0.8	0.765144	0.772736359	0.765483301	0.765263697
0.9	0.785032	0.793213066	0.785412037	0.785163494
1	0.803771	0.812500000	0.804190095	0.803914053
10	1.50497	1.53125000	1.50674000	1.50549750
50	2.49971	2.54758040	2.50312133	2.50069963
100	3.13138	3.19244404	3.13578530	3.13265656
500	5.31989	5.42575605	5.32761969	5.32211709
1000	6.69422	6.82795331	6.70400326	6.69703286

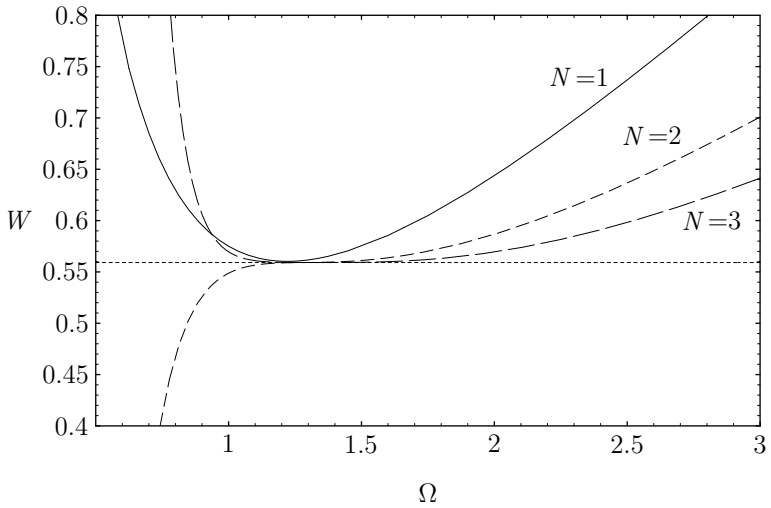

Figure 5.14 Typical Ω-dependence of approximations $W_{1,2,3}$ at $T = 0$. The coupling constant has the value $g = 0.4$. The second-order approximation W^{Ω}_2 has no extremum. Here the minimal Ω-dependence lies at the turning point, and the condition $\partial^2 W^{\Omega}_2/\partial\Omega^2$ renders the best approximation to the energy (short dashes).

approximation $E^{(0)}_3(g)$ to the ground state energy. Its accuracy at various coupling strengths is seen in Table 5.6 where it is compared with the exact values obtained from numerical solutions of the Schrödinger equation. The improvement with respect

to the earlier approximation W_1 is roughly a factor 50. The maximal error is now smaller than 0.05%.

We shall see in the last subsection that up to rather high orders N, the minimum happens to be unique.

Observe that when truncating the expansion (5.183) after the second order and working with the approximation $W_2^\Omega(x_0)$, there exists no minimum in Ω, as can be seen in Fig. 5.14. The reason for this is the alternating sign of the cumulants in (5.183). This gives an alternating sign to the highest power a and thus to the highest power of $1/\Omega$ in the g^n-terms of Eq. (5.192), causing the trial energy of order N to diverge for $\Omega \to 0$ like $(-1)^{N-1} g^N \times (1/\Omega)^{3N-1}$. Since the trial energy goes for large Ω to positive infinity, only the odd approximations are guaranteed to possess a minimum.

The second-order approximation W_2 can nevertheless be used to find an improved energy value. As shown by Fig. 5.14, the frequency of least dependence Ω_2 is well defined. It is the frequency where the Ω-dependence of W_2 has its minimal absolute value. Thus we optimize Ω with the condition

$$\frac{\partial^2 W_2^\Omega}{\partial \Omega^2} = 0. \tag{5.193}$$

This leads to the energy values $E_2^{(0)}(g)$ listed in Table 5.6. They are more accurate than the values $E_1^{(0)}(g)$ by an order of magnitude.

5.14.2 Anharmonic Oscillator for $T > 0$

Consider now the anharmonic oscillator at a finite temperature, where the expansion (5.183) consists of the sum of one-particle irreducible vacuum diagrams

$W_3^{\tilde\Omega} = \frac{1}{\beta}\Big\{ -\frac{1}{2}$ 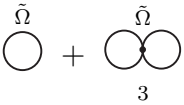 $-\frac{1}{2!}\Big($ 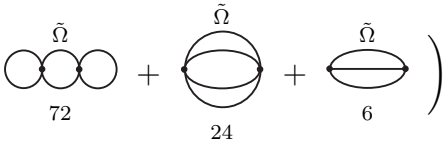 $+\frac{1}{3!}\Big($ 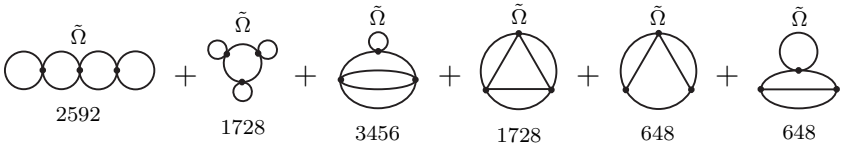 $\Big)\Big\}.$ (5.194)

The vertices represent the couplings $g_3(x_0)/3!\hbar$, $g_4(x_0)/4!\hbar$, whereas the lines stand for the correlation function $G'^{x_0}_{\tilde\Omega}(\tau,\tau')$. The numbers under each diagram are their multiplicities acting as factors.

Only the five integrals associated with the diagrams

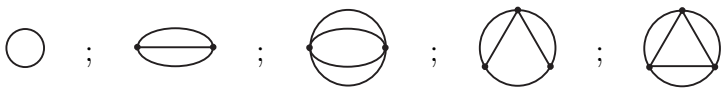

need to be evaluated explicitly; all others arise by the expansion of $\tilde{\Omega}$ or by factorization. The explicit form of three of these integrals can be found in the first, forth, and sixth of Eqs. (3.550). The results of the integrations are listed in Appendix 5A.

Only the second and fourth diagrams are new since they involve vertices with three legs. They can be found in Eqs. (3D.7) and (3D.8).

In quantum field theory one usually calculates Feynman integrals in momentum space. At finite temperatures, this requires the evaluation of multiple sums over Matsubara frequencies. The present quantum-mechanical example corresponds to a $D = 1$ -dimensional quantum field theory. Here it is more convenient to evaluate the integrals in τ-space. The diagrams

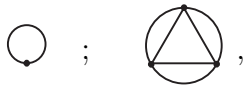

for example, are found by performing the integrals

$$\begin{aligned} \hbar\beta a^2 &\equiv \int_0^{\hbar\beta} d\tau G^2(\tau,\tau), \\ \hbar\beta\left(\frac{1}{\omega}\right)^2 a_3^{12} &\equiv \int_0^{\hbar\beta}\int_0^{\hbar\beta}\int_0^{\hbar\beta} G^2(\tau_1,\tau_2)G^2(\tau_2,\tau_3)G^2(\tau_3,\tau_1)\, d\tau_1 d\tau_2 d\tau_3. \end{aligned}$$

The factor $\hbar\beta$ on the left-hand side is due to an overall τ-integral and reflects the temporal translation symmetry of the system; the factors $1/\omega$ arise from the remaining τ-integrations whose range is limited by the correlation time $1/\omega$.

In general, the β- and x_0-dependent parameters a_V^{2L} have the dimension of a length to the nth power and the associated diagrams consist of m vertices and $n/2$ lines (defining $a_1^2 \equiv a^2$).

We now use the rule (5.188) to replace ω by $\tilde{\Omega}$ and expand everything in powers of g_2 up to the third order. The expansion can be performed diagrammatically in each Feynman diagram. Letting a dot on a line indicate the coupling $g_2/2\hbar$, the one-loop diagram is expanded as follows:

(5.195)

The other diagrams are expanded likewise:

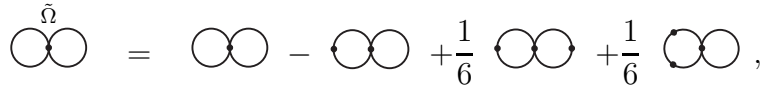

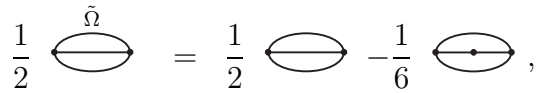

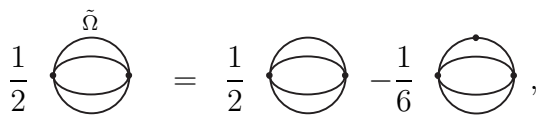

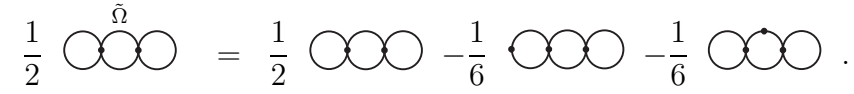

In this way, we obtain from (5.194) the complete graphical expansion for $W_3^\Omega(x_0)$ including all vertices associated with the coupling $g_2(x_0)$:

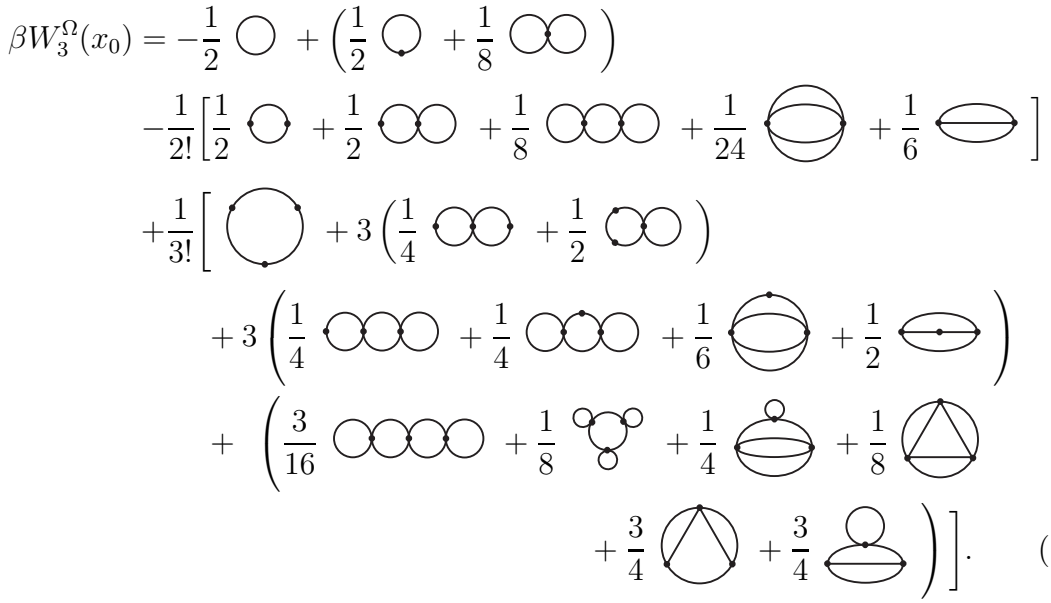

(5.196)

In the latter diagrams, the vertices represent directly the couplings $g_n/\hbar$. The denominators $n!$ of the previous vertices $g_n/n!\hbar$ have been combined with the multiplicities of the diagrams yielding the indicated prefactors. The corresponding analytic expression for $W_3^\Omega(x_0)$ is

$$\begin{aligned}
W_3^\Omega(x_0) &= V(x_0) + F_\Omega^{x_0} + \left(\frac{g_2}{2}a^2 + \frac{g_4}{8}a^4\right) \\
&\quad - \frac{1}{2!\hbar\Omega}\left[\frac{g_2^2}{2}a_2^4 + \frac{g_2 g_4}{2}a_2^4 a^2 + \frac{g_4^2}{8}a_2^4 a^4 + \frac{g_4^2}{24}a_2^8 + \frac{g_3^2}{6}a_2^6\right] \\
&\quad + \frac{1}{3!\hbar^2\Omega^2}\left[g_2^3 a_3^6 + 3\left(\frac{g_2^2 g_4}{4}(a_2^4)^2 + \frac{g_2^2 g_4}{2}a_3^6 a^2\right)\right. \\
&\quad\quad + 3\left(\frac{g_2 g_4^2}{4}(a_2^4)^2 a^2 + \frac{g_2 g_4^2}{4}a_3^6 a^4 + \frac{g_2 g_4^2}{6}a_3^{10} + \frac{g_2 g_3^2}{2}a_3^8\right) \\
&\quad \left. + \left(\frac{3g_4^3}{16}(a_2^4 a^2)^2 + \frac{g_4^3}{8}a_3^6 a^6 + \frac{g_4^3}{4}a_3^{10}a^2 + \frac{g_4^3}{8}a_3^{12} + \frac{3g_3^2 g_4}{4}a_{3'}^{10} + \frac{3g_3^2 g_4}{4}a_3^8 a^2\right)\right].
\end{aligned} \tag{5.197}$$

The quantities a_V^{2L} are ordered in the same way as the associated diagrams in (5.196). As before, we have omitted the variable x_0 in all but the first three terms, for brevity.

The optimal trial frequency $\Omega(x_0)$ is found numerically by searching, at each value of x_0, for the real roots of the first derivate of $W_3^\Omega(x_0)$ with respect to $\Omega(x_0)$. Just as for zero temperature, the solution happens to be unique.

By calculating the integral

$$Z_3 = \int_{-\infty}^{\infty} \frac{dx_0}{l_{\rm e}(\hbar\beta)} e^{-W_3(x_0)/k_B T}, \tag{5.198}$$

we obtain the approximate free energy

$$F_3 = -\frac{1}{\beta} \ln Z_3. \tag{5.199}$$

The results are listed in Table 5.7 for various coupling constants g and temperatures. They are compared with the exact free energy

$$F_{\rm ex} = -\frac{1}{\beta} \log \sum_n \exp(-\beta E_n), \tag{5.200}$$

whose energies E_n were obtained by numerically solving the Schrödinger equation.

g	β	F_1	F_3	$F_{\rm ex}$
0.002	2.0	0.427937	0.427937	0.427741
0.4	1.0	0.226084	0.226075	0.226074
	5.0	0.559155	0.558678	0.558675
2.0	1.0	0.492685	0.492578	0.492579
	5.0	0.699431	0.696180	0.696118
	10.0	0.700934	0.696285	0.696176
4.0	1.0	0.657396	0.6571051	0.6571049
	5.0	0.809835	0.803911	0.803758
20	1.0	1.18102	1.17864	1.17863
	5.0	1.24158	1.22516	1.22459
	10.0	1.24353	1.22515	1.22459
200	5.0	2.54587	2.50117	2.49971
2000	0.1	2.6997	2.69834	2.69834
	1.0	5.40827	5.32319	5.31989
	10.0	5.4525	5.3225	5.3199
80000	0.1	18.1517	18.0470	18.0451
	3.0	18.501	18.146	18.137

Table 5.7 Free energy of anharmonic oscillator with potential $V(x) = x^2/2 + gx^4/4$ for various coupling strengths g and $\beta = 1/kT$.

We see that to third order, the new approximation yields energies which are better than those of F_1 by a factor of 30 to 50. The remaining difference with respect to the exact energies lies in the fourth digit.

In the high-temperature limit, all approximations $W_N(x_0)$ tend to the classical result $V(x_0)$, as they should. Thus, for small β, the approximations $W_3(x_0)$ and $W_1(x_0)$ are practically indistinguishable.

The accuracy is worst at zero temperature. Using the $T \to 0$ -limits of the Feynman integrals a_V^{2L} given in (3.553) and (3D.14), the approximation W_3^Ω takes the simple form

$$\begin{aligned} W_3^\Omega(x_0) &= V(x_0) + \frac{\hbar\Omega(x_0)}{2} + \frac{g_2}{2}a^2 + \frac{g_4}{8}a^4 \\ &\quad - \frac{1}{2\hbar\Omega}\left[\frac{g_2^2}{2}a^4 + \frac{g_2 g_4}{2}a^6 + \frac{g_3^2}{6}\frac{2}{3}a^6 + \frac{g_4^2}{24}\frac{7}{2}a^8\right] \\ &+ \frac{1}{6\hbar^2\Omega^2}\left[g_2^3\frac{3}{2}a^6 + g_2 g_3^2\frac{4}{3}a^8 + {g_2}^2 g_4 3a^8 + g_3^2 g_4\frac{13}{3}a^{10} + g_2 g_4^2\frac{35}{16}a^{10} + g_4^3\frac{37}{64}a^{12}\right], \end{aligned} \tag{5.201}$$

where $a^2 = \hbar/2M\Omega$. As in (5.197), we have omitted the arguments x_0 in Ω and g_i, for brevity. At zero temperature, the remaining integral over x_0 in the partition function (5.198) receives its only contribution from the point $x_0 = 0$, where $W_3(0)$ is minimal. There it reduces to the energy W_3 of Eq. (5.192).

5.15 Convergence of Variational Perturbation Expansion

For a single interaction x^p, the approximation W_N at zero temperature can easily be carried to high orders [13, 14]. The perturbation coefficients are available exactly from recursion relations, which were derived for the anharmonic oscillator with $p = 4$ in Appendix 3C. The starting point is the ordinary perturbation expansion for the energy levels of the anharmonic oscillator

$$E^{(n)} = \omega \sum_{k=0}^{\infty} E_k^{(n)} \left(\frac{g}{4\omega^3}\right)^k. \tag{5.202}$$

It was remarked in (3C.27) and will be proved in Section 17.10 [see Eq. (17.323)] that the coefficients $E_k^{(n)}$ grow for large k like

$$E_k^{(n)} \longrightarrow -\frac{1}{\pi}\sqrt{\frac{6}{\pi}}\frac{12^n}{n!}(-3)^k\Gamma(k+n+1/2). \tag{5.203}$$

Using Stirling's formula[3]

$$n! \approx (2\pi)^{1/2} n^{n-1/2} e^{-n}, \tag{5.204}$$

this amounts to

$$E_k^{(n)} \longrightarrow -\frac{2\sqrt{3}}{\pi}\frac{(-4)^n}{n!}\left[\frac{-3(k+n)}{e}\right]^{n+k}. \tag{5.205}$$

Thus, $E_k^{(n)}$ grows faster than any power in k. Such a strong growth implies that the expansion has a zero radius of convergence. It is a manifestation of the fact that the energy possesses an essential singularity in the complex g-plane at the expansion point $g = 0$. The series is a so-called asymptotic series. The precise form of the

[3] M. Abramowitz and I. Stegun, op. cit., Formulas 6.1.37 and 6.1.38.

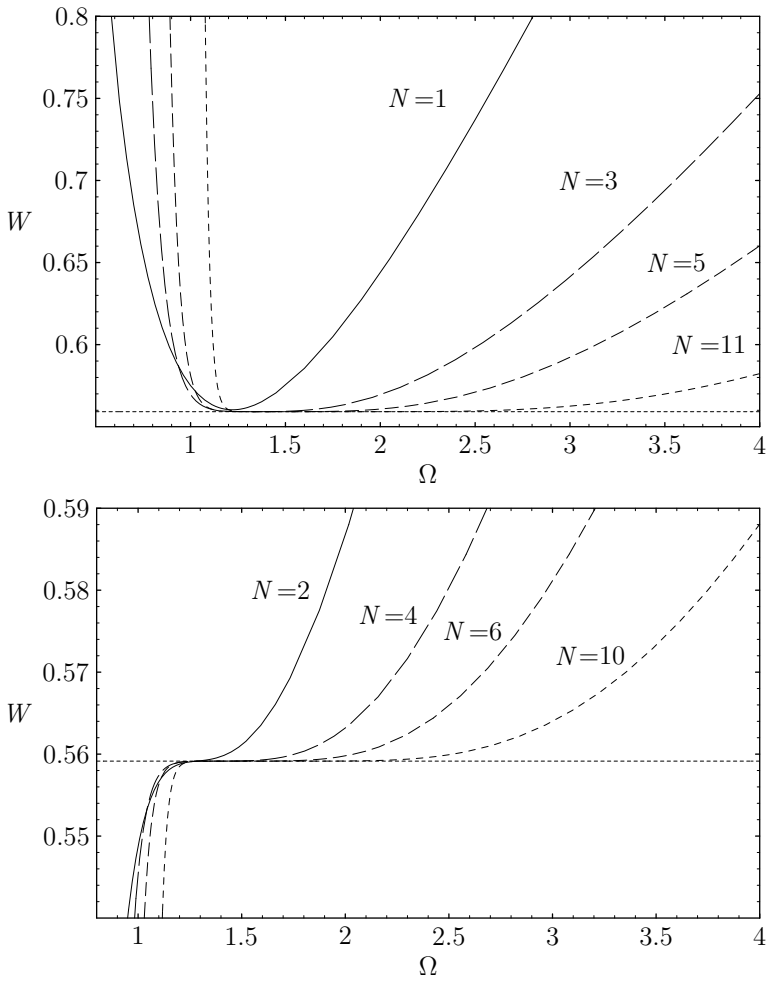

Figure 5.15 Typical Ω-dependence of Nth approximations W_N at $T = 0$ for increasing orders N. The coupling constant has the value $g/4 = 0.1$. The dashed horizontal line indicates the exact energy.

singularity will be calculated in Section 17.10 with the help of the semiclassical approximation.

If we want to extract meaningful numbers from a divergent perturbation series such as (5.202), it is necessary to find a convergent resummation procedure. Such a procedure is supplied by the variational perturbation expansion, as we now demonstrate for the ground state energy of the anharmonic oscillator.

Truncating the infinite sum (5.202) after the Nth term, the replacement (5.188) followed by a re-expansion in powers of g up to order N leads to the approximation W_N at zero temperature:

$$W_N^\Omega = \Omega \sum_{l=0}^{N} \varepsilon_l^{(0)} \left(\frac{g}{4\Omega^3} \right)^l , \tag{5.206}$$

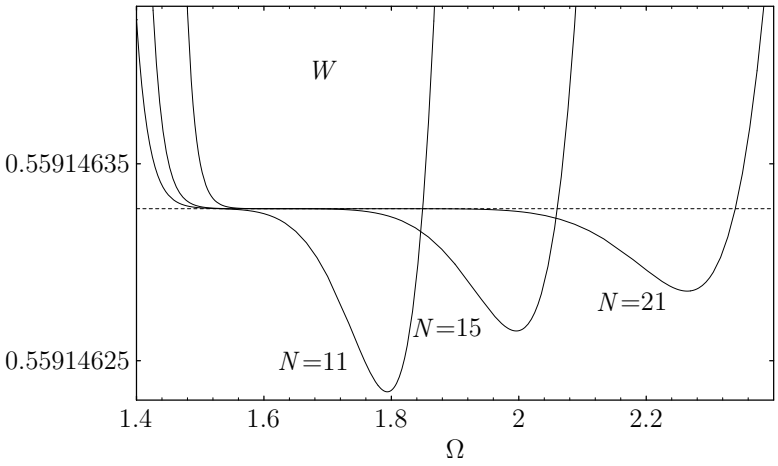

Figure 5.16 New plateaus in W_N developing for higher orders $N \geq 15$ in addition to the minimum which now gives worse results. For $N = 11$ the new plateau is not yet extremal, but it is the proper region of least Ω-dependence yielding the best approximation to the exact energy indicated by the dashed horizontal line. The minimum has fallen far below this value and is no longer useful. The figure looks similar for all couplings (in the plot, $g = 0.4$). The reason is the scaling property (5.215) proved in Appendix 5B.

with the re-expansion coefficients

$$\varepsilon_l^{(0)} = \sum_{j=0}^{l} E_j^{(0)} \begin{pmatrix} (1-3j)/2 \\ l-j \end{pmatrix} (-4\sigma)^{l-j}. \tag{5.207}$$

Here σ denotes the dimensionless function of Ω

$$\sigma \equiv -\frac{1}{2}\,\Omega r^2 = \frac{\Omega(\Omega^2-1)}{g}. \tag{5.208}$$

In Fig. 5.15 we have plotted the Ω-dependence of W_N for increasing N at the coupling constant $g/4 = 0.1$. For odd and even N, an increasingly flat plateau develops at the optimal energy.

At larger orders $N \geq 15$, the initially flat plateau is deformed into a minimum with a larger curvature and is no longer a good approximation. However, a new plateau has developed yielding the best energy. This is seen on the high-resolution plot in Fig. 5.16. At $N = 11$, the new plateau is not yet extremal but close to the correct energy.

The worsening extrema in Fig. 5.16 correspond here to points leaving the optimal dashed into the upward direction. The newly forming plateaus lie always on the dashed curve.

The set of all extremal Ω_N-values for odd N up to $N = 91$ is shown in Fig. 5.17. The optimal frequencies with smallest curvature are marked by a fat dot. In Subsection 17.10.5. we shall derive that

$$\sigma_N = \frac{\Omega_N(\Omega_N^2-1)}{g} \tag{5.209}$$

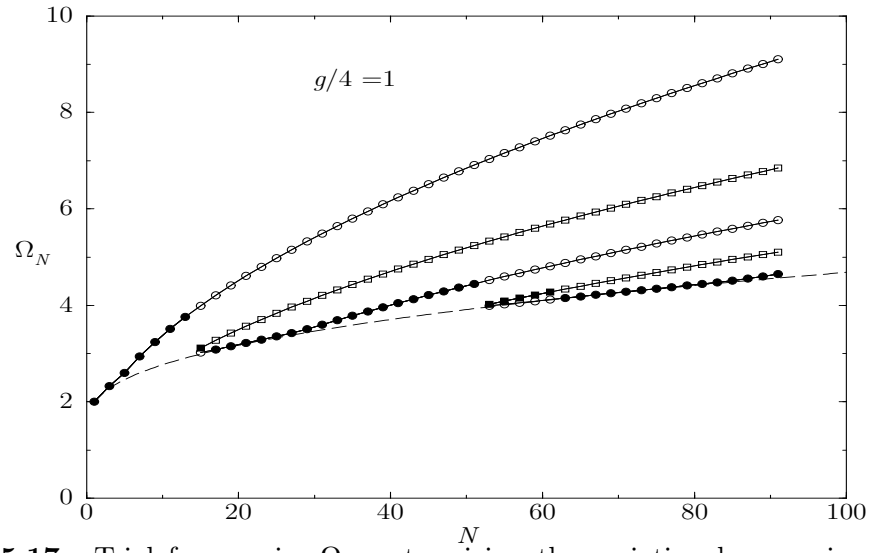

Figure 5.17 Trial frequencies Ω_N extremizing the variational approximation W_N at $T = 0$ for odd $N \leq 91$. The coupling is $g/4 = 1$. The dashed curve corresponds to the approximation (5.211) [related to Ω_N via (5.208)]. The frequencies on this curve produce the fastest convergence. The worsening extrema in Fig. 5.16 correspond here to points leaving the optimal dashed into the upward direction. The newly forming plateaus lie always on the dashed curve.

grows for large N like

$$\sigma_N \approx cN, \quad c = 0.186047\ldots\,, \tag{5.210}$$

so that Ω_N grows like $\Omega_N \approx (cNg)^{1/3}$. For smaller N, the best Ω_N-values in Fig. 5.17 can be fitted with the help of the corrected formula (5.210):

$$\sigma_N \approx cN\left(1 + \frac{6.85}{N^{2/3}}\right). \tag{5.211}$$

The associated Ω_N-curve is shown as a dashed line. It is the lower envelope of the extremal frequencies.

The set of extremal and turning point frequencies Ω_N is shown in Fig. 5.18 for even and odd N up to $N = 30$. The optimal extrema with smallest curvature are again marked by a fat dot. The theoretical curve for an optimal convergence calculated from (5.211) and (5.209) is again plotted as a dashed line.

In Table 5.8, we illustrate the precision reached for large orders N at various coupling constants g by a comparison with accurate energies derived from numerical solutions of the Schrödinger equation.

The approach to the exact energy values is illustrated in Fig. 5.19 which shows that a good convergence is achieved by using the lowest of all extremal frequencies, which lie roughly on the dashed theoretical curve in Fig. 5.17 and specify the position of the plateaus. The frequencies Ω_N on the higher branches leaving the dashed curve in that figure, on the other hand, do not yield converging energy values. The

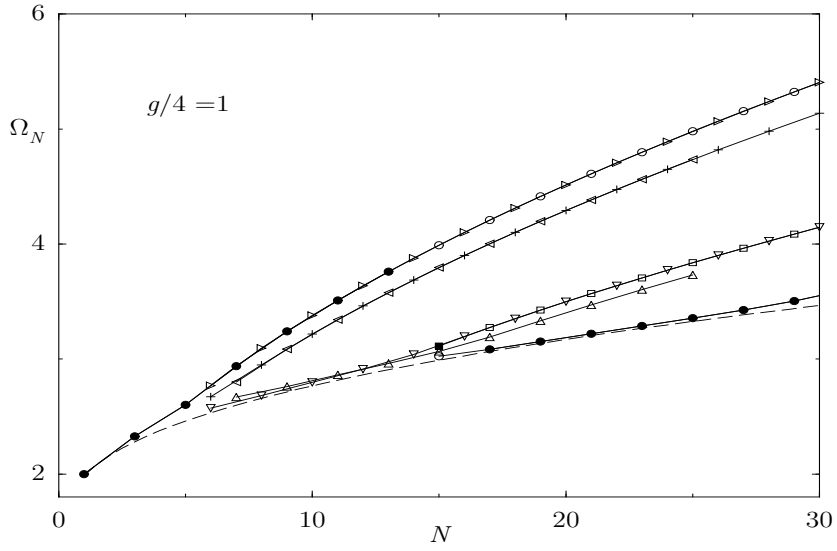

Figure 5.18 Extremal and turning point frequencies Ω_N in variational approximation W_N at $T = 0$ for even and odd $N \leq 30$. The coupling is $g/4 = 1$. The dashed curve corresponds to the approximation (5.211) [related to Ω_N via (5.208)].

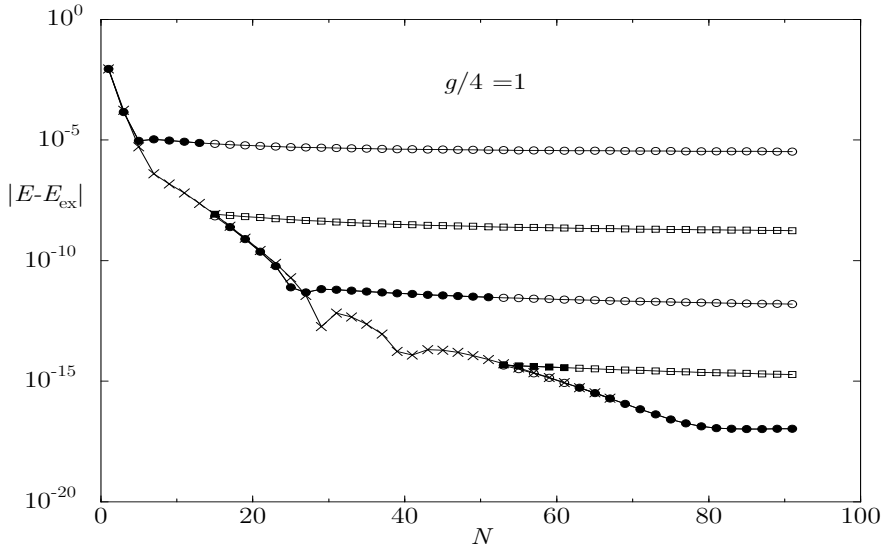

Figure 5.19 Difference between approximate ground state energies $E = W_N$ and exact energies $E_{\rm ex}$ for odd N corresponding to the Ω_N-values shown in Fig. 5.17. The coupling is $g/4 = 1$. The lower curve follows roughly the error estimate to be derived in Eq. (17.409). The extrema in Fig. (5.17) which move away from the dashed curve lie here on horizontal curves whose accuracy does not increase.

sharper minima in Fig. 5.16 correspond precisely to those branches which no longer determine the region of weakest Ω-dependence.

The anharmonic oscillator has the remarkable property that a plot of the Ω_N-values in the N, σ_N-plane is universal in the coupling strengths g; the plots do not depend on g. To see the reason for this, we reinsert explicitly the frequency ω (which

N	$g/4$ =0.1	$g/4$ = 0.3	$g/4$ =0.5	$g/4$ =1.0	$g/4$ =2.0
1	0.5603073711	0.6416298621	0.7016616429	0.8125000000	0.9644035598
2	0.5591521393	0.6380887347	0.6963769499	0.8041900946	0.9522936298
3	0.5591542188	0.6380357598	0.6962536326	0.8039140528	0.9517997694
4	0.5591457408	0.6379878713	0.6961684978	0.8037563457	0.9515444198
5	0.5591461596	0.6379899084	0.6961717475	0.8037615232	0.9515517450
10	0.5591463266	0.6379917677	0.6961757782	0.8037705329	0.9515682249
15	0.5591463272	0.6379917838	0.6961758231	0.8037706596	0.9515684933
20	0.5591463272	0.6379917836	0.6961743059	0.8037706575	0.9515684887
25	0.5591463272	0.6379917832	0.6961758208	0.8037706513	0.9515584121
exact	0.5591463272	0.6379917832	0.6961758208	0.8037706514	0.9515684727
N	$g/4$ =50	$g/4$ =200	$g/4$ =1000	$g/4$ =8000	$g/4$ =20000
1	2.5475803996	4.0084608812	6.8279533136	13.635282593	18.501658712
2	2.5031213253	3.9365586048	6.7040032606	13.386598486	18.163979967
3	2.5006996279	3.9325538203	6.6970328638	13.372561189	18.144908389
4	2.4995980125	3.9307488127	6.6939036178	13.366269038	18.136361642
5	2.4996213227	3.9307857892	6.6939667971	13.366395347	18.136533060
10	2.4997071960	3.9309286743	6.6942161680	13.366898079	18.137216200
15	2.4997089403	3.9309316283	6.6942213631	13.366908583	18.137230481
20	2.4997089079	3.9309315732	6.6942212659	13.366908387	18.137230214
25	2.4997087731	3.9309313396	6.6942208522	13.366907551	18.137230022
exact	2.4997087726	3.9309313391	6.6942208505	13.366907544	18.137229073

Table 5.8 Comparison of the variational approximations W_N at $T = 0$ for increasing N with the exact ground state energy at various coupling constants g.

was earlier set equal to unity). Then the re-expanded energy W_N in Eq. (5.206) has the general scaling form

$$W_N^\Omega = \Omega w_N(\hat{g}, \hat{\omega}^2), \tag{5.212}$$

where w_N is a dimensionless function of the reduced coupling constant and frequency

$$\hat{g} \equiv \frac{g}{\Omega^3}, \quad \hat{\omega} \equiv \frac{\omega}{\Omega}, \tag{5.213}$$

respectively. When differentiating (5.212),

$$\frac{d}{d\Omega} W_N = \left[1 - 3\hat{g}\frac{d}{d\hat{g}} - 2\hat{\omega}^2 \frac{d}{d\hat{\omega}^2}\right] w_N(\hat{g}, \hat{\omega}^2), \tag{5.214}$$

we discover that the right-hand side can be written as a product of $\hat{g}^N$ and a dimensionless polynomial of order N depending only on $\sigma = \Omega(\Omega^2 - \omega^2)/g$:

$$\frac{d}{d\Omega} W_N^\Omega = \hat{g}^N p_N(\sigma). \tag{5.215}$$

A proof of this will be given in Appendix 5B for any interaction x^p. The universal optimal σ_N-values are obtained from the zeros of $p_N(\sigma)$.

It is possible to achieve the same universality for the optimal frequencies of the even approximations W_N by determining them from the extrema of $p_N(\sigma)$ rather than from the turning points of W_N as a function of Ω.

The universal functions $p_N(\sigma)$ are found most easily by replacing the variable σ in the coefficients $\varepsilon_l^{(0)}$ of the re-expansion (5.206) by its $\omega = 0$ -limit $\sigma|_{\omega=0} = \Omega^3/g = 1/\hat{g}$. This yields the simpler expression

$$W_N^\Omega = \Omega w_N(\hat{g}, 0) = \Omega \sum_{l=0}^{N} \varepsilon_l^{(0)} \left(\frac{\hat{g}}{4}\right)^l, \tag{5.216}$$

with

$$\varepsilon_l^{(0)} = \sum_{j=0}^{l} E_j^{(0)} \begin{pmatrix} (1-3j)/2 \\ l-j \end{pmatrix} (-4/\hat{g})^{l-j}. \tag{5.217}$$

The derivative of W_N with respect to Ω yields

$$p_N(\sigma) = \hat{g}^{-N} \left[1 - 3\hat{g}\frac{d}{d\hat{g}}\right] w_N(\hat{g}, 0)\Big|_{\hat{g}=1/\sigma}. \tag{5.218}$$

In Section 17.10, we show the re-expansion coefficients $\varepsilon_k^{(0)}$ in (5.207) to be for large k proportional to $E_k^{(0)}$:

$$\varepsilon_k^{(0)} \approx e^{-2\sigma_N} E_k^{(0)}, \qquad \sigma_N = \frac{\Omega_N(\Omega_N^2 - 1)}{g} \tag{5.219}$$

[see Eq. (17.396)]. Thus, at any fixed Ω, the re-expanded series has the same asymptotic growth as the original series with the same vanishing radius of convergence. The behavior (5.219) can be seen in Fig. 5.20(a) where we have plotted the logarithm of the absolute value of the kth term

$$S_k = \varepsilon_k^{(0)} \left(\frac{\hat{g}}{4}\right)^k \tag{5.220}$$

of the re-expanded perturbation series (5.202) for various optimal values Ω_N and $g = 40$. All curves show a growth $\propto k^k$. The terms in the original series start growing immediately (precocious growth). Those in the re-expanded series, on the other hand, decrease initially and go through a minimum before they start growing (retarded growth). The dashed curves indicate the analytically calculated asymptotic behavior (5.219).

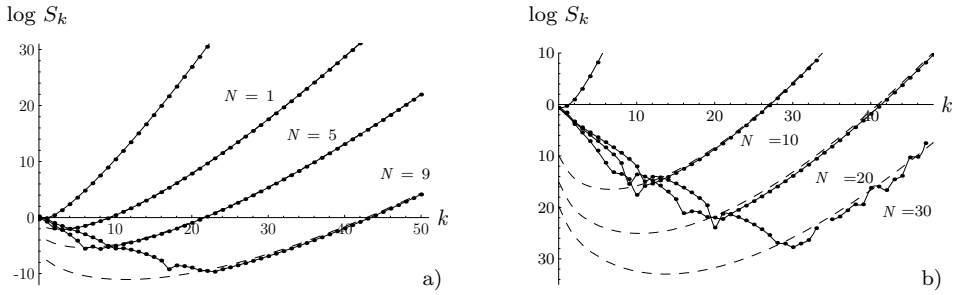

Figure 5.20 Logarithmic plot of kth terms in re-expanded perturbation series at a coupling constant $g/4 = 1$:
(a) Frequencies Ω_N extremizing the approximation W_N. The dashed curves indicate the theoretical asymptotic behavior (5.219).
(b) Frequencies Ω_N corresponding to the dashed curve in Fig. 5.17. The minima lie for each N precisely at $k = N$, producing the fastest convergence. The curves labeled $\Omega = \omega$ indicate the kth term in the original perturbation series.

The increasingly retarded growth is the reason why energies obtained from the variational expansion converge towards the exact result. Consider the terms S_k of the resummed series with frequencies Ω_N taken from the theoretical curve of optimal convergence in Fig. 5.17 (or 5.18). In Fig. 5.20(b) we see that the terms S_k are minimal at $k = N$, i.e., at the last term contained in the approximation W_N. In general, a divergent series yields an optimal result if it is truncated after the smallest term S_k. The size of the last term gives the order of magnitude of the error in the truncated evaluation. The re-expansion makes it possible to find, for every N, a frequency Ω_N which makes the truncation optimal in this sense.

5.16 Variational Perturbation Theory for Strong-Coupling Expansion

From the $\omega \to 0$ -limit of (5.206), we obtain directly the strong-coupling behavior of W_N. Since $\Omega = (g/\hat{g})^{1/3}$, we can write

$$W_N = (g/\hat{g})^{1/3} w_N(\hat{g}, 0), \tag{5.221}$$

and evaluate this at the optimal value $\hat{g} = 1/\sigma_N$. The large-g behavior of W_N is therefore

$$W_N \xrightarrow[g\to\infty]{} (g/4)^{1/3} b_0, \tag{5.222}$$

with the coefficient

$$b_0 = (4/\hat{g})^{1/3} w_N(\hat{g}, 0)|_{\hat{g}=1/\sigma_N}. \tag{5.223}$$

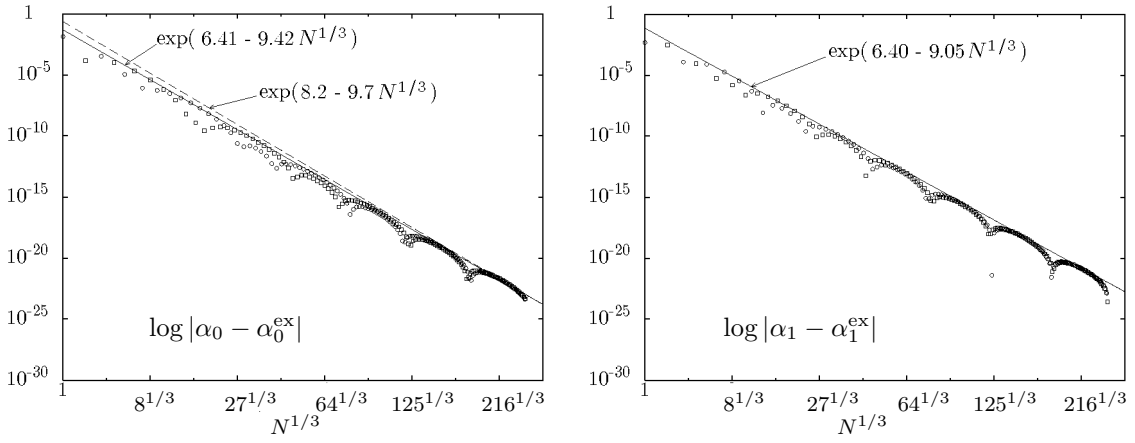

Figure 5.21 Logarithmic plot of N-behavior of strong-coupling expansion coefficients b_0 and b_1.

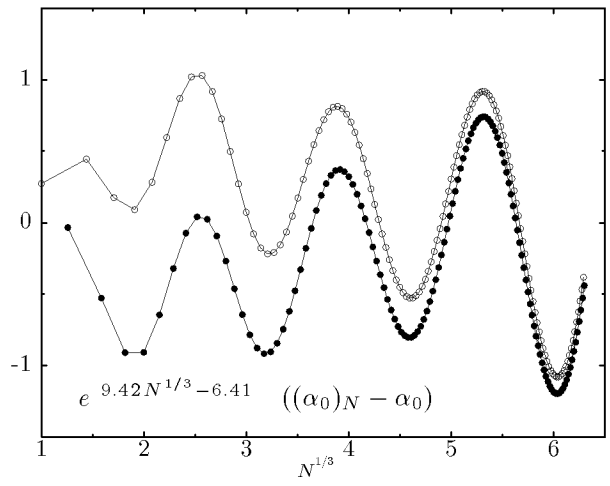

Figure 5.22 Oscillations of approximate strong-coupling expansion coefficient b_0 as a function of N when approaching exponentially fast the exact limit. The exponential behavior has been factored out. The upper and lower points show the odd-N and even-N approximations, respectively.

The higher corrections to the leading behavior (5.222) are found just as easily. By expanding $w_N(\hat{g},\hat{\omega}^2)$ in powers of $\hat{\omega}^2$,

$$W_N = \left(\frac{g}{\hat{g}}\right)^{1/3}\left[1+\hat{\omega}^2\frac{d}{d\hat{\omega}^2}+\frac{\hat{\omega}^4}{2!}\left(\frac{d}{d\hat{\omega}^2}\right)^2+\ldots\right]w_N(\hat{g},\hat{\omega}^2)\bigg|_{\hat{\omega}^2=0}, \tag{5.224}$$

and inserting

$$\hat{\omega}^2 = \frac{\hat{g}^{2/3}}{(g/\omega^3)^{2/3}}, \tag{5.225}$$

we obtain the expansion

$$W_N = \left(\frac{g}{4}\right)^{1/3}\left[b_0+b_1\left(\frac{g}{4\omega^3}\right)^{-2/3}+b_2\left(\frac{g}{4\omega^3}\right)^{-4/3}+\ldots\right], \tag{5.226}$$

with the coefficients

$$b_n = \frac{1}{n!}\left(\frac{\hat{g}}{4}\right)^{(2n-1)/3}\left(\frac{d}{d\hat{\omega}^2}\right)^n w_N(\hat{g},\hat{\omega}^2)\bigg|_{\hat{g}=1/\sigma_N,\hat{\omega}^2=0}. \tag{5.227}$$

The derivatives on the right-hand side have the expansions

$$\left(\frac{d}{d\hat{\omega}^2}\right)^n w_N(\hat{g},\hat{\omega}^2) = \sum_{l=0}^{N}\varepsilon_{nl}^{(0)}\left(\frac{\hat{g}}{4}\right)^l, \tag{5.228}$$

Table 5.9 Coefficients b_n of strong-coupling expansion of ground state energy of anharmonic oscillator obtained from a perturbation expansion of order 251. An extremely precise value for b_0 was given by F. Vinette and J. Cizek, J. Math. Phys. *32*, 3392 (1991): $b_0 = 0.667\,986\,259\,155\,777\,108\,270\,962\,016\,198\,601\,994\,304\,049\,36\ldots$.

n	b_n
0	0.667 986 259 155 777 108 270 96
1	0.143 668 783 380 864 910 020 3
2	−0.008 627 565 680 802 279 128
3	0.000 818 208 905 756 349 543
4	−0.000 082 429 217 130 077 221
5	0.000 008 069 494 235 040 966
6	−0.000 000 727 977 005 945 775
7	0.000 000 056 145 997 222 354
8	−0.000 000 002 949 562 732 712
9	−0.000 000 000 064 215 331 954
10	0.000 000 000 048 214 263 787
11	−0.000 000 000 008 940 319 867
12	0.000 000 000 001 205 637 215
13	−0.000 000 000 000 130 347 650
14	0.000 000 000 000 010 760 089
15	−0.000 000 000 000 000 445 890 1
16	−0.000 000 000 000 000 058 989 8
17	0.000 000 000 000 000 019 196 00
18	−0.000 000 000 000 000 003 288 13
19	0.000 000 000 000 000 000 429 62
20	−0.000 000 000 000 000 000 044 438
21	0.000 000 000 000 000 000 003 230 5
22	−0.000 000 000 000 000 000 000 031 4

with the re-expansion coefficients

$$\frac{1}{n!}\varepsilon^{(0)}_{n\,l} = \sum_{j=0}^{l-n} E^{(0)}_j \left(\begin{array}{c} (1-3j)/2 \\ l-j \end{array} \right) \left(\begin{array}{c} l-j \\ n \end{array} \right) (-1)^{l-j-n} (4/\hat{g})^{l-j}. \tag{5.229}$$

For increasing N, the coefficients $b_0, b_1, \ldots$ converge rapidly against the values shown in Table 5.9. From the logarithmic plot in Fig. 5.21 we extract a convergence

$$|b_0 - b_0^{\rm ex}| \sim e^{8.2-9.7N^{1/3}}, \qquad |b_1 - b_1^{\rm ex}| \sim e^{6.4-9.1N^{1/3}}. \tag{5.230}$$

This behavior will be derived in Subsection 17.10.5, where we shall find that for any $g > 0$, the error decreases at large N roughly like $e^{-[9.7+(cg)^{-2/3}]\,N^{1/3}}$ [see Eq. (17.409)].

The approach to this limiting behavior is oscillatory, as seen in Fig. 5.22 where we have removed the exponential falloff and plotted $e^{-6.5+9.42N^{1/3}}(b_0 - b_0^{\rm ex})$ against N [16].

For the proof of the convergence of the variational perturbation expansion in Subsection 17.10.5. it will be important to know that the strong-coupling expansion for the ground state energy

$$E^{(0)} = \left(\frac{g}{4}\right)^{1/3} \left[b_0 + b_1 \left(\frac{g}{4\omega^3}\right)^{-2/3} + b_2 \left(\frac{g}{4\omega^3}\right)^{-4/3} + \dots \right], \tag{5.231}$$

converges for large enough

$$g > g_{\rm s}. \tag{5.232}$$

The same is true for the excited energies.

5.17 General Strong-Coupling Expansions

The coefficients of the strong-coupling expansion can be derived for any divergent perturbation series

$$E_N(g) = \sum_{n=0}^{N} a_n g^n, \tag{5.233}$$

for which we know that it behaves at large couplings g like

$$E(g) = g^{p/q} \sum_{m=0}^{M} b_m (g^{-2/q})^m. \tag{5.234}$$

The series (5.233) can trivially be rewritten as

$$E_N(g) = \omega^p \sum_{n=0}^{N} a_n \left(\frac{g}{\omega^q}\right)^n, \tag{5.235}$$

with $\omega = 1$. We now apply the square-root trick (5.188) and replace ω by the identical expression

$$\omega \equiv \sqrt{\Omega^2 + (\omega^2 - \Omega^2)}, \tag{5.236}$$

containing a dummy scaling parameter Ω. The series (5.235) is then re-expanded in powers of g up to the order N, thereby treating $\omega^2 - \Omega^2$ as a quantity of order g. The result is most conveniently expressed in terms of dimensionless parameters $\hat{g} \equiv g/\Omega^q$ and $\sigma \equiv (1 - \hat{\omega}^2)/\hat{g}$, where $\hat{\omega} \equiv \omega/\Omega$. Then the replacement (5.236) amounts to

$$\omega \longrightarrow \Omega(1 - \sigma\hat{g})^{1/2}, \tag{5.237}$$

so that the re-expanded series reads explicitly

$$W_N(\hat{g}, \sigma) = \Omega^p \sum_{n=0}^{N} \varepsilon_n(\sigma) \, (\hat{g})^n \,, \tag{5.238}$$

with the coefficients:

$$\varepsilon_n(\sigma) = \sum_{j=0}^{n} a_j \begin{pmatrix} (p - qj)/2 \\ n - j \end{pmatrix} (-\sigma)^{n-j}. \tag{5.239}$$

For any fixed g, we form the first and second derivatives of $W_N^\Omega(g)$ with respect to Ω, calculate the Ω-values of the extrema and the turning points, and select the smallest of these as the optimal scaling parameter Ω_N. The function $W_N(g) \equiv W_N(g, \Omega_N)$ constitutes the Nth variational approximation $E_N(g)$ to the function $E(g)$.

We now take this approximation to the strong-coupling limit $g \to \infty$. For this we observe that (5.238) has the general scaling form

$$W_N^\Omega(g) = \Omega^p w_N(\hat{g}, \hat{\omega}^2). \tag{5.240}$$

For dimensional reasons, the optimal Ω_N increases with g for large g like $\Omega_N \approx g^{1/q} c_N$, so that $\hat{g} = c_N^{-q}$ and $\sigma = 1/\hat{g} = c_N^q$ remain finite in the strong-coupling limit, whereas $\hat{\omega}^2$ goes to zero like $1/[c_N(g/\omega^q)^{1/q}]^2$. Hence

$$W_N^{\Omega_N}(g) \approx g^{p/q} c_N^p w_N(c_N^{-q}, 0). \tag{5.241}$$

Here c_N plays the role of the variational parameter to be determined by the lowest extremum or turning point of $c_N^p w_N(c_N^{-q}, 0)$.

The full strong-coupling expansion is obtained by expanding $w_N(\hat{g}, \hat{\omega}^2)$ in powers of $\hat{\omega}^2 = (g/\omega^q \hat{g})^{-2/q}$ at a fixed $\hat{g}$. The result is

$$W_N(g) = g^{p/q} \left[\bar{b}_0(\hat{g}) + \bar{b}_1(\hat{g}) \left(\frac{g}{\omega^q} \right)^{-2/q} + \bar{b}_2(\hat{g}) \left(\frac{g}{\omega^q} \right)^{-4/q} + \dots \right], \tag{5.242}$$

with

$$\bar{b}_n(\hat{g}) = \frac{1}{n!} \left(\frac{d}{d\hat{\omega}^2} \right)^n w_N^{(n)}(\hat{g}, \hat{\omega}^2) \Big|_{\hat{\omega}^2 = 0} \hat{g}^{(2n-p)/q}, \tag{5.243}$$

with respect to $\hat{\omega}^2$. Explicitly:

$$\frac{1}{n!} w_N^{(n)}(\hat{g}, 0) = \sum_{l=0}^{N} (-1)^{l+n} \sum_{j=0}^{l-n} a_j \begin{pmatrix} (p-qj)/2 \\ l-j \end{pmatrix} \begin{pmatrix} l-j \\ n \end{pmatrix} (-\hat{g})^j. \tag{5.244}$$

Since $\hat{g} = c_N^{-q}$, the coefficients $\bar{b}_n(\hat{g})$ may be written as functions of the parameter c:

$$\bar{b}_n(c) = \sum_{l=0}^{N} a_l \sum_{j=0}^{N-l} \binom{(p-lq)/2}{j} \binom{j}{n} (-1)^{j-n} c^{p-lq-2n}. \tag{5.245}$$

The values of c which optimize $W_N(g)$ for fixed g yield the desired values of c_N. The optimization may be performed stepwise using directly the expansion coefficients $\bar{b}_n(c)$. First we optimize the leading coefficient $b_0(c)$ as a function of c and identifying the smallest of them as c_N. Next we have to take into account that for large but finite α, the trial frequency Ω has corrections to the behavior $\hat{g}^{1/q} c$. The coefficient c will depend on $\hat{g}$ like

$$c(\hat{g}) = c + \gamma_1 \left(\frac{\hat{g}}{\omega^q}\right)^{-2/q} + \gamma_2 \left(\frac{\hat{g}}{\omega^q}\right)^{-4/q} + \ldots, \tag{5.246}$$

requiring a re-expansion of c-dependent coefficients $\bar{b}_n$ in (5.242). The expansion coefficients c and γ_n for $n = 1, 2, \ldots$ are determined by extremizing $\bar{b}_{2n}(c)$. The final result can again be written in the form (5.242) with $\bar{b}(c)_n$ replaced by the final b_n:

$$W_N(g) = g^{p/q} \left[b_0 + b_1 \left(\frac{g}{\omega^q}\right)^{-2/q} + b_2 \left(\frac{g}{\omega^q}\right)^{-4/q} + \ldots \right]. \tag{5.247}$$

The final b_n are determined by the equations shown in Table 5.10. The two leading coefficients receive no correction and are omitted.

The extremal values of $\hat{g}$ will have a strong-coupling expansion corresponding to (5.246):

$$\hat{g} = c_N^{-q} \left[1 + \delta_1 \left(\frac{g}{\omega^q}\right)^{-2/q} + \delta_2 \left(\frac{g}{\omega^q}\right)^{-4/q} + \cdots \right]. \tag{5.248}$$

Table 5.10 Equations determining coefficients b_n in strong-coupling expansion (5.247) from the functions $\bar{b}_n(c)$ in (5.245) and their derivatives. For brevity, we have suppressed the argument c in the entries.

n	b_n	$-\gamma_{n-1}$
2	$\bar{b}_2 + \gamma_1 \bar{b}_1' + \frac{1}{2}\gamma_1^2 \bar{b}_0''$	$\bar{b}_1'/\bar{b}_0''$
3	$\bar{b}_3 + \gamma_2 \bar{b}_1' + \gamma_1 \bar{b}_2' + \gamma_1\gamma_2 \bar{b}_0'' + \frac{1}{2}\gamma_1^2 \bar{b}_1'' + \frac{1}{6}\gamma_1^3 \bar{b}_0^{(3)}$	$(\bar{b}_2' + \gamma_1 \bar{b}_1'' + \frac{1}{2}\gamma_1^2 \bar{b}_0^{(3)})/\bar{b}_0''$
4	$\bar{b}_4 + \gamma_3 \bar{b}_1' + \gamma_2 \bar{b}_2' + \gamma_1 \bar{b}_3' + (\frac{1}{2}\gamma_2^2 + \gamma_1\gamma_3)\bar{b}_0''$	$(\bar{b}_3' + \gamma_2 \bar{b}_1'' + \gamma_1 \bar{b}_2'' + \gamma_1\gamma_2 \bar{b}_0^{(3)}$
	$+\gamma_1\gamma_2 \bar{b}_1'' + \frac{1}{2}\gamma_1^2 \bar{b}_2'' + \frac{1}{2}\gamma_1^2\gamma_2 \bar{b}_0^{(3)} + \frac{1}{6}\gamma_1^3 \bar{b}_1^{(3)} + \frac{1}{24}\gamma_1^4 \bar{b}_0^{(4)}$	$+\frac{1}{2}\gamma_1^2 \bar{b}_1^{(3)} + \frac{1}{6}\gamma_1^3 \bar{b}_0^{(4)})/\bar{b}_0''$

The convergence of the general strong-coupling expansion is similar to the one observed for the anharmonic oscillator. This will be seen in Subsection 17.10.5.

The general strong-coupling expansion has important applications in the theory of critical phenomena. This theory renders expansions of the above type for the so-called critical exponents, which have to be evaluated at infinitely strong (bare) couplings of scalar field theories with $g\phi^4$ interactions. The results of these applications are better than those obtained previously with a much more involved theory based on a combination of renormalization group equations and Padé-Borel resummation techniques [28]. The critical exponents have power series expansions in powers of g/ω in the physically most interesting three-dimensional systems, where $\omega^2/2$ is the factor in front of the quadratic field term ϕ^2. The important phenomenon observed in such systems is the appearance of *anomalous dimensions*. These imply that the expansion terms $(g/\omega)^n$ cannot simply be treated with the square-root trick (5.236). The anomalous dimension requires that $(g/\omega)^n$ must be treated as if it were $(g/\omega^q)^n$

when applying the square-root trick. Thus we must use the *anomalous square-root trick*

$$\omega \to \Omega \left[1 + \left(\frac{\omega}{\Omega}\right)^{2/q}\right]^{q/2} . \tag{5.249}$$

The power $2/q$ appearing in the strong-coupling expansion (5.234) is experimentally observable since it governs the approach of the system to the scaling limit. This exponent is usually denoted by the letter ω, and is referred to as the *Wegner exponent* [29]. This exponent ω is not to be confused with the frequency ω in the present discussion. In superfluid helium, for example, this critical exponent is very close to the value $4/5$, implying $q \approx 5/2$. The Wegner exponent of fluctuating quantum fields cannot be deduced, as in quantum mechanics, from simple scaling analyses of the action. It is, however, calculable by applying variational perturbation theory to the logarithmic derivative of the power series of the other critical exponents. These are called β-functions and have to vanish for the correct ω. This procedure is referred to as *dynamical determination* of ω and has led to values in excellent agreement with experiment [17].

In the above variational procedure, the existence of anomalous dimensions is signalized by the appearance of a nonzero slope in the plateaus of Figs. 5.14. If this happens, the power q in the replacement (5.249) must be modified until the plateaus are flat. This method is a practical alternative to determining the Wegner exponent $\omega = 2/q$ via the β-function.

5.18 Variational Interpolation between Weak and Strong-Coupling Expansions

The possibility of calculating the strong-coupling coefficients from the perturbation coefficients can be used to find a *variational interpolation* of a function with known weak- and strong-coupling coefficients [18]. Such pairs of expansions are known for many other physical systems, for example most lattice models of statistical mechanics [19]. If applied to the ground state energy of the anharmonic oscillator, this method converges exponentially fast [15]. The weak-coupling expansion of the ground state energy of the anharmonic oscillator has the form (5.233). In natural units with $\hbar = M = \omega = 1$, the lowest coefficient a_0 is trivially determined to be $a_0 = 1/2$ by the ground state energy of the harmonic oscillator. If we identify $\alpha = g/4$ with the coupling constant in (5.233), to save factors $1/4$, the first coefficient is $a_1 = 3/4$ [see (5.190)]. We have seen before in Section 5.12 that even the lowest order variational perturbation theory yields leading strong-coupling coefficient in excellent agreement with the exact one [with a maximal error of $\approx 2\%$, see Eq. (5.167)]. In Fig. 5.23 we have plotted the relative deviation of the variational approximation from the exact one in percent.

The strong-coupling behavior is known from (5.226). It starts out like $g^{1/3}$, followed by powers of $g^{-1/3}, g^{-1}, g^{-5/3}$. Comparison with (5.234) shows that this

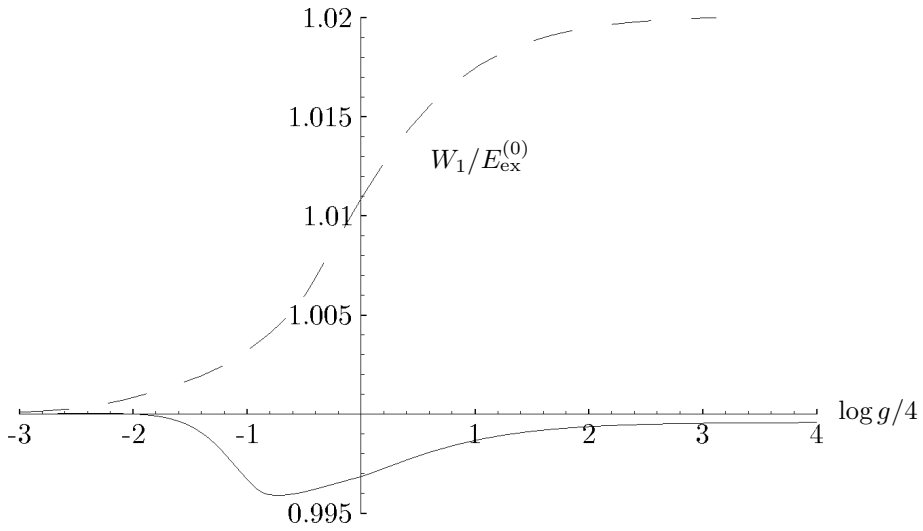

Figure 5.23 Ratio of approximate and exact ground state energy of anharmonic oscillator from lowest-order variational interpolation. Dashed curve shows first-order Feynman-Kleinert approximation $W_1(g)$. The accuracy is everywhere better than 99.5 %. For comparison, we also display the much worse (although quite good) variational perturbation result using the exact $a_1^{\rm ex} = 3/4$.

corresponds to $p = 1$ and $q = 3$. The leading coefficient is given in Table 5.9 with extreme accuracy: $b_0 = 0.667\,986\,259\,155\,777\,108\,270\,962\,016\,919\,860\ldots$.

In a variational interpolation, this value is used to determine an approximate a_1 (forgetting that we know the exact value $a_1^{\rm ex} = 3/4$). The energy (5.238) reads for $N = 1$ (with $\alpha = g/4$ instead of g):

$$W_1(\alpha,\Omega) = \left(\frac{\Omega}{2} + \frac{1}{2\Omega}\right) a_0 + \frac{a_1}{\Omega^2}\alpha. \tag{5.250}$$

Equation (5.245) yields, for $n = 0$:

$$b_0 = \frac{c}{2}a_0 + \frac{a_1}{c^2}. \tag{5.251}$$

Minimizing b_0 with respect to c we find $c = c_1 \equiv 2(a_1/2a_0)^{1/3}$ with $b_0 = 3a_0c_1/4 = 3(a_0^2a_1/2)^{1/3}/2$. Inserting this into (5.251) fixes $a_1 = 2(2/3b_0)^3/a_0^2 = 0.773\,970\ldots$, quite close to the exact value 3/4. With our approximate a_1 we calculate $W_1(\alpha,\Omega)$ at its minimum, where

$$\Omega_1 = \begin{cases} \frac{2}{\sqrt{3}}\omega\cosh\left[\frac{1}{3}\text{acosh}(g/g^{(0)})\right] \\ \frac{2}{\sqrt{3}}\omega\cos\left[\frac{1}{3}\arccos(g/g^{(0)})\right] \end{cases} \quad \text{for} \quad \begin{matrix} g > g^{(0)}, \\ g < g^{(0)}, \end{matrix} \tag{5.252}$$

with $g^{(0)} \equiv 2\omega^3 a_0/3\sqrt{3}a_1$. The result is shown in Fig. 5.23. Since the difference with respect to the exact solution would be too small to be visible on a direct plot of the energy, we display the ratio with respect to the exact energy $W_1(g)/E_{\rm ex}^0$. The accuracy is everywhere better than 99.5 %.

5.19 Systematic Improvement of Excited Energies

The variational method for the energies of excited states developed in Section 5.12 can also be improved systematically. Recall the n-dependent level shift formulas (3.518) and (3.519), according to which

$$\begin{aligned}\Delta E^{(n)} &= \Delta_1 E^{(n)} + \Delta_2 E^{(n)} + \Delta_3 E^{(n)} = \Delta V_{nn} - \sum_{k\neq n} \frac{\Delta V_{nk}\Delta V_{kn}}{E_k - E_n} \\ &+ \sum_{k\neq n}\sum_{l\neq n} \frac{\Delta V_{nk}\Delta V_{kl}\Delta V_{ln}}{(E_k - E_n)(E_l - E_n)} - \Delta V_{nn}\sum_{k\neq n}\frac{\Delta V_{nk}\Delta V_{kn}}{(E_k - E_n)^2}. \end{aligned} \tag{5.253}$$

By applying the substitution rule (5.188) to the total energies

$$E^{(n)} = \hbar\Omega(n + 1/2) + \Delta E^{(n)},$$

and expanding each term in powers of g up to g^3, we find the contributions to the level shift

$$\begin{aligned}\Delta_1 E^{(n)} &= \frac{g}{4}\,[3(2n^2+2n+1)a^4 + (2n+1)a^2r^2], \\ \Delta_2 E^{(n)} &= -\left(\frac{g}{4}\right)^2 [2(34n^3+51n^2+59n+21)a^8 \\ &\quad +4\cdot 3(2n^2+2n+1)a^6r^2 + (2n+1)a^4r^4]\frac{1}{\hbar\Omega}, \\ \Delta_3 E^{(n)} &= \left(\frac{g}{4}\right)^3 [4\cdot 3(125n^4+250n^3+472n^2+347n+111)a^{12} \\ &\quad +4\cdot 5(34n^3+51n^2+59n+21)a^{10}r^2 \\ &\quad +16\cdot 3(2n^2+2n+1)a^8r^4 + 2\cdot(2n+1)a^6r^6]\frac{1}{\hbar^2\Omega^2}, \end{aligned} \tag{5.254}$$

which for $n = 0$ reduce to the corresponding terms in (5.192). The extremization in Ω leads to energies which lie only very little above the exact values for all n. This is illustrated in Table 5.11 for $n = 8$ (compare with the energies in Table 5.5). A sum over the Boltzmann factors $e^{-\beta E_3^{(n)}}$ produces an approximate partition function Z_3 which deviates from the exact one by less than 50.1%.

It will be interesting to use the improved variational approach for the calculation of density matrices, particle distributions, and magnetization curves.

Table 5.11 Higher approximations to excited energy with $n = 8$ of anharmonic oscillator at various coupling constants g. The third-order approximation $E_3^{(8)}(g)$ is compared with the exact values $E_{\rm ex}^{(8)}(g)$, with the approximation $E_1^{(8)}(g)$ of the last section, and with the lower approximation of even order $E_2^{(8)}(g)$ (all in units of $\hbar\omega$).

$g/4$	$E_{\rm ex}^{(8)}(g)$	$E_1^{(8)}(g)$	$E_2^{(8)}(g)$	$E_3^{(8)}(g)$
0.1	13.3790	13.3235257	13.3766211	13.3847643
0.2	15.8222	15.7327929	15.8135994	15.8275802
0.3	17.6224	17.5099190	17.6099785	17.6281810
0.4	19.0889	18.9591071	19.0742800	19.0958388
0.5	20.3452	20.2009502	20.3287326	20.3531080
0.6	21.4542	21.2974258	21.4361207	21.4629384
0.7	22.4530	22.2851972	22.4335694	22.4625543
0.8	23.3658	23.1879959	23.3451009	23.3760415
0.9	24.2091	24.0221820	24.1872711	24.2199988
1	24.9950	24.7995745	24.9720376	25.0064145
10	51.9865	51.5221384	51.9301030	51.9986710
50	88.3143	87.5058600	88.2154879	88.3500454
100	111.128	110.105819	111.002842	111.173183
500	189.756	188.001018	189.540577	189.833415
1000	239.012	236.799221	238.740320	239.109584

5.20 Variational Treatment of Double-Well Potential

Let us also calculate the approximate effective classical potential of third order $W_3(x_0)$ for the double-well potential

$$V(x) = M\frac{\omega^2}{2}x^2 + \frac{g}{4}x^4 + \frac{M^2\omega^4}{4g}, \qquad \omega^2 = -1. \tag{5.255}$$

In the expression (5.197), the sign change of ω^2 affects only the coupling $g_2(x_0)$, which becomes

$$g_2(x_0) = M[-1 - \Omega^2(x_0)] + 3gx_0^2 = gr^2/2 + 3gx_0^2 \tag{5.256}$$

[recall (5.176)]. Note the constant energy $M^2\omega^4/4g$ in $V(x)$ which shifts the minima of the potential to zero [compare (5.78)].

To see the improved accuracy of W_3 with respect to the first approximation $W_1(x_0)$ discussed in Section 5.7 [corresponding to the first line of (5.197)], we study the limit of zero temperature where the accuracy is expected to be the worst. In this limit, $W_3(x_0)$ reduces to (5.201) and is easily minimized in x_0 and Ω.

At larger coupling constants $g > g_c \approx 0.3$, the energy has a minimum at $x_0 = 0$. For $g \leq g_c$, there is an additional symmetric pair of minima at $x_0 = \pm x_m \neq 0$ (recall Figs. 5.5 and 5.6). The resulting $W_3(0)$ is plotted in Fig. 5.24 together with $W_1(0)$. The figure also contains the first excited energy which is obtained by setting $\omega^2 = -1$ in $r^2 = 2M(\omega^2 - \Omega^2)/g$ of Eqs. (5.253)–(5.255).

For small couplings g, the energies $W_1(0)$, $W_3(0)$, ... diverge and the minima at $x = \pm x_m$ of Eq. (5.82) become relevant. Moreover, there is quantum tunneling across the central barrier from one minimum to the other which takes place for $g \leq g_c \approx 0.3$ and is unaccounted for by $W_3(0)$ and $W_3(x_m)$. Tunneling leads to a level splitting to be calculated in Chapter 17. In this chapter, we test the accuracy of $W_1(x_m)$ and $W_3(x_m)$ by comparing them with the averages of the two lowest energies. Figure 5.24 shows that the accuracy of the approximation $W_3(x_m)$ is quite good.

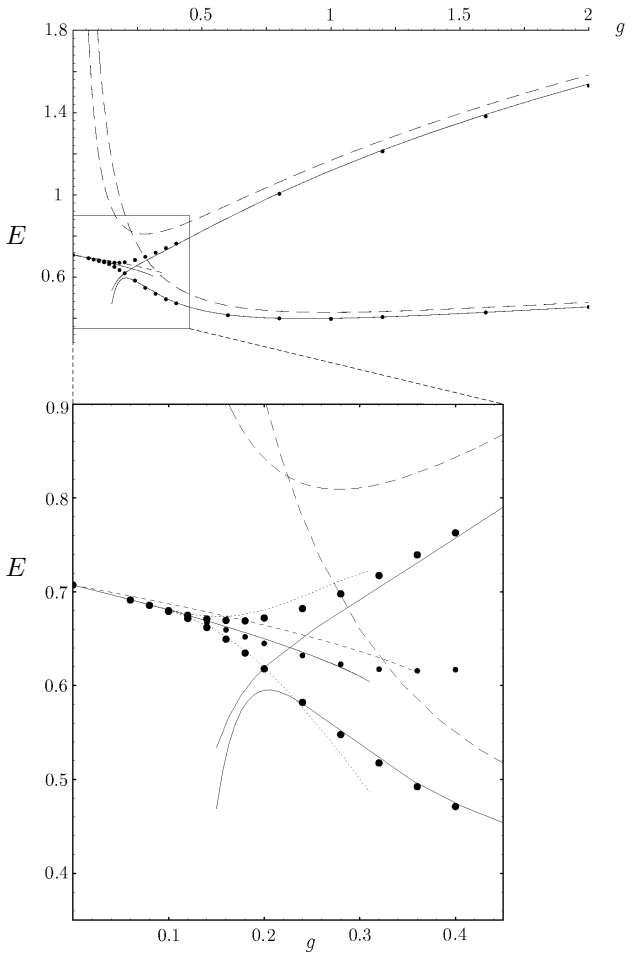

Figure 5.24 Lowest two energies in double-well potential as function of coupling strength g. The approximations are $W_1(0)$ (dashed line) and $W_3(0)$ (solid line). The dots indicate numeric results of the Schrödinger equation. The lower part of the figure shows $W_1(x_m)$ and $W_3(0)$ in comparison with the average of the Schrödinger energies (small dots). Note that W_1 misses the slope by 25%. Tunneling causes a level splitting to be calculated in Chapter 17 (dotted curves).

Note that the approximation $W_1(x_m)$ does not possess the correct slope in g, which is missed by 25%. In fact, a Taylor expansion of $W_1(x_m)$ reads

$$W_1(x_m) = \frac{\sqrt{2}}{2} - \frac{3}{16}g - \frac{9\sqrt{2}}{128}g^2 - \frac{27}{256}g^3 + \dots \ , \tag{5.257}$$

whereas the true expansion starts out with

$$E^{(0)} = \frac{\sqrt{2}}{2} - \frac{1}{4}g + \dots \ . \tag{5.258}$$

The optimal frequency associated with (5.257) has the expansion

$$\Omega_1(x_m) = \sqrt{2} - \frac{3}{4}g - \frac{27\sqrt{2}}{64}g^2 - \frac{27}{32}g^3 + \dots \ .$$

Let us also compare the x_0-behavior of $W_3(x_0)$ with that of the true effective classical potential calculated numerically by Monte Carlo simulations. The curves are plotted in Fig. 5.5, and the

agreement is seen to be excellent. There are significant deviations only for low temperatures with $\beta \gtrsim 20$.

At zero temperature, there exists a simple way of recovering the effective classical potential from the classical potential calculated up to two loops in Eq. (3.770). As we learned in Eq. (3.833), x_0 coincides at zero temperature. with X in Eq. (3.770) Thus we merely have to employ the square-root trick (5.186) to the effective potential (3.770) and interchange X by x_0 to obtain the variational approximation $W_1(x_0)$ to the effective classical potantial to be varied. Explicitly, we replace, as in (5.188), the one-loop contribtions, ground state energies $\hbar\omega_{T,L}$ in (3.770) by $\sqrt{\Omega_{T,L}^2+(\omega_{T,L}^2(X)-\Omega_{T,L}^2)} \approx \Omega_{T,L}+(\omega_{T,L}^2(X)-\Omega_{T,L}^2)/2\Omega_{T,L}$, and exchange $\omega_{L,T}(X)$ of the remaining two-loop terms by $\Omega_{T,L}$. This yields for the D-dimensional rotated double-well potential (the Mexical hat potential in Fig. 3.13]:

$$
\begin{aligned}
W(x_0) \underset{T\to 0}{=} \Bigg\{ & v(X)+\hbar\left[\frac{\Omega_L}{4}+\frac{\omega_L^2(X)}{4\Omega_L}\right]+(D-1)\hbar\left[\frac{\Omega_T}{4}+\frac{\omega_T^2(X)}{4\Omega_T}\right]+\frac{\hbar^2}{8(2M)^2}\Bigg\{\frac{1}{\Omega_L^2}v^{(4)}(X) \\
& +\frac{D^2-1}{\Omega_T^2}\left[\frac{v''(X)}{X^2}-\frac{v'(X)}{X^3}\right]+\frac{2(D-1)}{\Omega_L\Omega_T}\left[\frac{v'''(X)}{X}-\frac{2v''(X)}{X^2}+\frac{2v'(X)}{X^3}\right]\Bigg\} \\
& -\frac{\hbar^2}{6(2M)^3}\Bigg\{\frac{1}{3\Omega_L^4}[v'''(X)]^2+\frac{3(D-1)}{2\Omega_T+\Omega_L}\frac{1}{\Omega_L\Omega_T^2}\left[\frac{v''(X)}{X}-\frac{v'(X)}{X^2}\right]^2\Bigg\}+\mathcal{O}(\hbar^3)\Bigg\}_{X\to x_0}. \qquad (5.259)
\end{aligned}
$$

This has to be extremized in $\Omega_{T,L}$ at fixed x_0.

5.21 Higher-Order Effective Classical Potential for Nonpolynomial Interactions

The systematic improvement of the Feynman-Kleinert approximation in Section 5.13 was based on Feynman diagrams and therefore applicable only to polynomial potentials. If we want to calculate higher-order effective classical potentials for nonpolynomial interactions such as the Coulomb interaction, we need a generalization of the smearing rule (5.30) to the correlation functions of interaction potentials which occur in the expansion (5.180). The second-order term, for example, requires the calculation of

$$
\left\langle \mathcal{A}_{\rm int}^{x_0\,2}\right\rangle_{\Omega,{\rm c}}^{x_0}=\int_0^{\hbar\beta}d\tau\int_0^{\hbar\beta}d\tau'\,\langle V_{\rm int}^{x_0}(x(\tau))V_{\rm int}^{x_0}(x(\tau'))\rangle_{\Omega,{\rm c}}^{x_0}, \qquad (5.260)
$$

where

$$
V_{\rm int}^{x_0}(x)=V(x)-\frac{1}{2}M\Omega^2(x_0)(x-x_0)^2. \qquad (5.261)
$$

Thus we need an efficient smearing formula for local expectations of the form

$$
\begin{aligned}
\langle F_1(x(\tau_1))\dots F_n(x(\tau_n))\rangle_\Omega^{x_0} &= \frac{1}{Z_\Omega^{x_0}} \\
&\times \oint \mathcal{D}x(\tau)F_1(x(\tau_1))\cdots F_n(x(\tau_n))\delta(\overline{x}-x_0)\exp\left\{-\frac{1}{\hbar}\mathcal{A}_\Omega^{x_0}[x(\tau)]\right\}, \qquad (5.262)
\end{aligned}
$$

where $\mathcal{A}_\Omega^{x_0}[x(\tau)]$ and $Z_\Omega^{x_0}$ are the local action and partition function of Eqs. (5.3) and (5.4). After rearranging the correlation functions to connected ones according to Eqs. (5.182) we find the cumulant expansion for the effective classical potential [see (5.180)]

$$
V^{\rm eff,cl}(x_0)=F_\Omega^{x_0}+\frac{1}{\hbar\beta}\int_0^{\hbar\beta}d\tau_1\,\langle V_{\rm int}^{x_0}(x(\tau_1))\rangle_{\Omega,c}^{x_0}
$$

$$- \frac{1}{2\hbar^2\beta}\int_0^{\hbar\beta} d\tau_1 \int_0^{\hbar\beta} d\tau_2 \, \langle V_{\rm int}^{x_0}(x(\tau_1)) V_{\rm int}^{x_0}(x(\tau_2))\rangle_{\Omega,c}^{x_0} \tag{5.263}$$
$$+ \frac{1}{6\hbar^3\beta}\int_0^{\hbar\beta} d\tau_1 \int_0^{\hbar\beta} d\tau_2 \int_0^{\hbar\beta} d\tau_3 \, \langle V_{\rm int}^{x_0}(x(\tau_1)) V_{\rm int}^{x_0}(x(\tau_2)) V_{\rm int}^{x_0}(x(\tau_3))\rangle_{\Omega,c}^{x_0} + \dots .$$

It differs from the previous expansion (5.180) for polynomial interactions by the potential $V(x)$ not being expanded around x_0. The first term on the right-hand side is the local free energy (5.6).

5.21.1 Evaluation of Path Integrals

The local pair correlation function was given in Eq. (5.19):

$$\langle \delta x(\tau)\delta x(\tau')\rangle_\Omega^{x_0} \equiv \langle [x(\tau)-x_0][x(\tau')-x_0]\rangle_\Omega^{x_0} = \frac{\hbar}{M} G_\Omega^{(2)x_0}(\tau,\tau') = a_{\tau\tau'}^2(x_0), \tag{5.264}$$

with [recall (5.19)–(5.24)]

$$a_{\tau\tau'}^2(x_0) = \frac{\hbar}{2M\Omega(x_0)} \frac{\cosh[\Omega(x_0)(\tau-\tau'-\hbar\beta/2)]}{\sinh[\Omega(x_0)\hbar\beta/2]} - \frac{1}{M\beta\Omega^2(x_0)}, \quad \tau\in(0,\hbar\beta). \tag{5.265}$$

Higher correlation functions are expanded in products of these according to Wick's rule (3.305). For an even number of $\delta x(\tau)$'s one has

$$\langle \delta x(\tau_1)\delta x(\tau_2)\cdots\delta x(\tau_n)\rangle_\Omega^{x_0} = \sum_{\rm pairs} a^2_{\tau_{p(1)}\tau_{p(2)}}(x_0)\cdots a^2_{\tau_{p(n-1)}\tau_{p(n)}}(x_0)\,, \tag{5.266}$$

where the sum runs over all $(n-1)!!$ pair contractions. For an exponential, Wick's rule implies

$$\left\langle \exp\left[i\int_0^{\hbar\beta} d\tau j(\tau)\,\delta x(\tau)\right]\right\rangle_\Omega^{x_0} = \exp\left[-\frac{1}{2}\int_0^{\hbar\beta} d\tau \int_0^{\hbar\beta} d\tau' j(\tau) a^2_{\tau\tau'}(x_0) j(\tau')\right]. \tag{5.267}$$

Inserting $j(\tau)=\sum_{i=1}^n k_i\delta(\tau-\tau_i)$, this gives for the expectation value of a sum of exponentials

$$\left\langle \exp\left[i\sum_{i=1}^n k_i\,\delta x(\tau_i)\right]\right\rangle_\Omega^{x_0} = \exp\left[-\frac{1}{2}\sum_{i=1}^n\sum_{j=1}^n a^2_{\tau_i\tau_j}(x_0)k_ik_j\right]. \tag{5.268}$$

By Fourier-decomposing the functions $F(x(\tau)) = \int (dk/2\pi) F(k)\exp ik\,[x_0+\delta x(\tau)]$ in (5.262), we obtain from (5.268) the new smearing formula

$$\langle F_1(x(\tau_1))\cdots F_n(x(\tau_n))\rangle_\Omega^{x_0} = \left\{\prod_{k=1}^n \int_{-\infty}^{+\infty} d\,\delta x_k F_k(x_0+\delta x_k)\right\}$$
$$\times \frac{1}{\sqrt{(2\pi)^n {\rm Det}\left[a^2_{\tau_k\tau_{k'}}(x_0)\right]}} \exp\left\{-\frac{1}{2}\sum_{k=1}^n\sum_{k'=1}^n \delta x_k\, a^{-2}_{\tau_k\tau_{k'}}(x_0)\,\delta x_{k'}\right\}, \tag{5.269}$$

where $a^{-2}_{\tau_i\tau_j}(x_0)$ is the inverse of the $n\times n$ -matrix $a^2_{\tau_i\tau_j}(x_0)$. This smearing formula determines the harmonic expectation values in the variational perturbation expansion (5.263) as convolutions with Gaussian functions.

For $n=1$ and only the diagonal elements $a^2(x_0)=a^2_{\tau\tau}(x_0)$ appear in the smearing formula (5.269), which reduces to the previous one in Eq. (5.30) [$F(x(\tau))=V(x(\tau))$].

For polynomials $F(x(\tau))$, we set $x(\tau) = x_0 + \delta x(\tau)$ and expand in powers of $\delta x(\tau)$, and see that the smearing formula (5.269) reproduces the Wick expansion (5.266).

For two functions, the smearing formula (5.269) reads explicitly

$$\langle F_1(x(\tau_1))F_2(x(\tau_2))\rangle_\Omega^{x_0} = \int_{-\infty}^{+\infty} dx_1 \int_{-\infty}^{+\infty} dx_2\, F_1(x_1)F_2(x_2)\, \frac{1}{\sqrt{(2\pi)^2[a^4(x_0) - a^4_{\tau_1\tau_2}(x_0)]}}$$
$$\times \exp\left\{-\frac{a^2(x_0)(x_1-x_0)^2 - 2a^2_{\tau_1\tau_2}(x_0)(x_1-x_0)(x_2-x_0) + a^2(x_0)(x_2-x_0)^2}{2[a^4(x_0) - a^4_{\tau_1\tau_2}(x_0)]}\right\}. \tag{5.270}$$

Specializing $F_2(x(\tau_2))$ to quadratic functions in $x(\tau)$, we obtain from this

$$\left\langle F_1(x(\tau_1))\,[x(\tau_2)-x_0]^2\right\rangle_\Omega^{x_0} = \langle F_1(x(\tau_1))\rangle_\Omega^{x_0}\, a^2(x_0)\left[1 - \frac{a^4_{\tau_1\tau_2}(x_0)}{a^4(x_0)}\right]$$
$$+ \left\langle F_1(x(\tau_1))\,[x(\tau_1)-x_0]^2\right\rangle_\Omega^{x_0} \frac{a^4_{\tau_1\tau_2}(x_0)}{a^4(x_0)}\,, \tag{5.271}$$

and

$$\left\langle [x(\tau_1)-x_0]^2\,[x(\tau_2)-x_0]^2\right\rangle_\Omega^{x_0} = a^4(x_0) + 2a^4_{\tau_1\tau_2}(x_0)\,. \tag{5.272}$$

5.21.2 Higher-Order Smearing Formula in D Dimensions

The smearing formula can easily be generalized to D-dimensional systems, where the local pair correlation function (5.264) becomes a $D \times D$ -dimensional matrix:

$$\langle \delta x_i(\tau)\delta x_j(\tau')\rangle_\Omega^{x_0} = a^2_{ij;\tau\tau'}(\mathbf{x}_0). \tag{5.273}$$

For rotationally-invariant systems, the matrix can be decomposed in the same way as the trial frequency $\Omega^2_{ij}(\mathbf{x}_0)$ in (5.95) into longitudinal and transversal components with respect to $\mathbf{x}_0$:

$$a^2_{ij;\tau\tau'}(\mathbf{x}_0) = a^2_{L;\tau\tau'}(r_0)P_{L;ij}(\hat{\mathbf{x}}_0) + a^2_{T;\tau\tau'}(r_0)P_{T;ij}(\hat{\mathbf{x}}_0), \tag{5.274}$$

where $P_{L;ij}(\hat{\mathbf{x}}_0)$ and $P_{T;ij}(\hat{\mathbf{x}}_0)$ are longitudinal and transversal projection matrices introduced in (5.96). Denoting the matrix (5.274) by $\mathbf{a}^2_{\tau,\tau'}(\mathbf{x}_0)$, we can write the D-dimensional generalization of the smearing formula (5.275) as

$$\langle F_1(\mathbf{x}(\tau_1))\cdots F_n(\mathbf{x}(\tau_n))\rangle_\Omega^{\mathbf{x}_0} = \left\{\prod_{k=1}^{n}\int_{-\infty}^{+\infty} d\,\delta x_k F_k(\mathbf{x}_0 + \delta\mathbf{x}_k)\right\}$$
$$\times\, \frac{1}{\sqrt{(2\pi)^n \mathrm{Det}\left[\mathbf{a}^2_{\tau_k\tau_{k'}}(\mathbf{x}_0)\right]}} \exp\left\{-\frac{1}{2}\sum_{k=1}^{n}\sum_{k'=1}^{n}\delta\mathbf{x}_k\, \mathbf{a}^{-2}_{\tau_k\tau_{k'}}(x_0)\,\delta\mathbf{x}_{k'}\right\}. \tag{5.275}$$

The inverse $D \times D$ -matrix $\mathbf{a}^{-2}_{\tau_k\tau_{k'}}(\mathbf{x}_0)$ is formed by simply inverting the $n \times n$ -matrices $\mathbf{a}^{-2}_{L;\tau_k\tau_{k'}}(r_0), \mathbf{a}^{-2}_{T;\tau_k\tau_{k'}}(r_0)$ in the projection formula (5.274) with projection matrices $\mathbf{P}_L(\hat{\mathbf{x}}_0)$ and $\mathbf{P}_T(\hat{\mathbf{x}}_0)$:

$$\mathbf{a}^{-2}_{\tau_k\tau_{k'}}(\mathbf{x}_0) = \mathbf{a}^{-2}_{L;\tau_k\tau_{k'}}(r_0)\mathbf{P}_L(\hat{\mathbf{x}}_0) + \mathbf{a}^{-2}_{T;\tau_k\tau_{k'}}(r_0)\mathbf{P}_T(\hat{\mathbf{x}}_0). \tag{5.276}$$

In D dimensions, the trial potential contains a $D \times D$ frequency matrix and reads

$$\frac{M}{2}\Omega^2_{ij}(\mathbf{x}_0)(x_i - x_{0i})(x_j - x_{0j})\,,$$

with the analogous decomposition

$$\Omega_{ij}^2(\mathbf{x}_0) = \Omega_L^2(\mathbf{x}_0)\,\frac{x_{0i}x_{0j}}{r_0^2} + \Omega_T^2(\mathbf{x}_0)\,\left(\delta_{ij} - \frac{x_{0i}x_{0j}}{r_0^2}\right). \tag{5.277}$$

The interaction potential (5.261) becomes

$$V_{\rm int}^{\mathbf{x}_0}(\mathbf{x}) = V(\mathbf{x}) - \frac{M}{2}\Omega_{ij}^2(\mathbf{x}_0)(x_i - x_{0i})(x_j - x_{0j})\,. \tag{5.278}$$

To first order, the anisotropic smearing formula (5.275) reads

$$\langle F_1(\mathbf{x}(\tau_1)\rangle_{\Omega_T,\Omega_L}^{r_0} = \int_{-\infty}^{+\infty} d^3x_1 F_1(\mathbf{x}_1)\,\frac{1}{\sqrt{(2\pi)^3 a_T^4 a_L^2}}\exp\left\{-\frac{(x_{1L}-r_0)^2}{2a_L^2} - \frac{\mathbf{x}_{1T}^2}{2a_T^2}\right\}, \tag{5.279}$$

with the special cases

$$\left\langle [\delta\mathbf{x}(\tau_1)]_T^2\right\rangle_{\Omega_T,\Omega_L}^{r_0} = 2a_T^2\,, \qquad \left\langle [\delta\mathbf{x}(\tau_1)]_L^2\right\rangle_{\Omega_T,\Omega_L}^{r_0} = a_L^2\,. \tag{5.280}$$

Inserting this into formula (5.263) we obtain the first-order approximation for the effective classical potential

$$W_1(\mathbf{x}_0) = F_\Omega^{\mathbf{x}_0} + \frac{1}{\hbar\beta}\int_0^{\hbar\beta} d\tau_1\,\langle V_{\rm int}^{\mathbf{x}_0}(\mathbf{x}(\tau_1))\rangle_{\Omega,c}^{\mathbf{x}_0}\,, \tag{5.281}$$

in agreement with the earlier result (5.97).

To second-order, the smearing formula (5.275) yields [33]

$$\begin{aligned}\langle F_1(\mathbf{x}(\tau_1)F_2(\mathbf{x}(\tau_2))\rangle_{\Omega_T,\Omega_L}^{r_0} &= \int_{-\infty}^{+\infty} d^3x_1 \int_{-\infty}^{+\infty} d^3x_2\, F_1(\mathbf{x}_1)F_2(\mathbf{x}_2)\\ &\times \frac{1}{(2\pi)^3(a_T^4 - a_{T\tau_1\tau_2}^4)\sqrt{a_L^4 - a_{L\tau_1\tau_2}^4}}\exp\left\{-\frac{a_T^2\mathbf{x}_{1T}^2 - 2a_{T\tau_1\tau_2}^2\mathbf{x}_{1T}\mathbf{x}_{2T} + a_T^2\mathbf{x}_{2T}^2}{2(a_T^4 - a_{T\tau_1\tau_2}^4)}\right\}\\ &\times \exp\left\{-\frac{a_L^2(x_{1L}-r_0)^2 - 2a_{L\tau_1\tau_2}^2(x_{1L}-r_0)(x_{2L}-r_0) + a_L^2(x_{2L}-r_0)^2}{2(a_L^4 - a_{L\tau_1\tau_2}^4)}\right\},\end{aligned} \tag{5.282}$$

so that rule (5.271) for expectation values generalizes to

$$\begin{aligned}\left\langle F_1(\mathbf{x}(\tau_1)\,[\delta\mathbf{x}(\tau_2)]_T^2\right\rangle_{\Omega_T,\Omega_L}^{r_0} &= 2a_T^2\left[1 - \frac{a_{T\tau_1\tau_2}^4}{a_T^4}\right]\langle F_1(\mathbf{x}(\tau_1))\rangle_{\Omega_T,\Omega_L}^{r_0}\\ &\quad + \frac{a_{T\tau_1\tau_2}^4}{a_T^4}\left\langle F_1(\mathbf{x}(\tau_1))\,[\delta\mathbf{x}(\tau_1)]_T^2\right\rangle_{\Omega_T,\Omega_L}^{r_0},\end{aligned} \tag{5.283}$$

$$\begin{aligned}\left\langle F_1(\mathbf{x}(\tau_1)\,[\delta\mathbf{x}(\tau_2)]_L^2\right\rangle_{\Omega_T,\Omega_L}^{r_0} &= a_L^2\left[1 - \frac{a_{L\tau_1\tau_2}^4}{a_L^4}\right]\langle F_1(\mathbf{x}(\tau_1))\rangle_{\Omega_T,\Omega_L}^{r_0}\\ &\quad + \frac{a_{L\tau_1\tau_2}^4}{a_L^4}\left\langle F_1(\mathbf{x}(\tau_1)[\delta\mathbf{x}(\tau_1)]_L^2\right\rangle_{\Omega_T,\Omega_L}^{r_0}.\end{aligned} \tag{5.284}$$

Specializing $F(\mathbf{x})$ to quadratic function, we obtain the generalizations of (5.272)

$$\left\langle [\delta\mathbf{x}(\tau_1)]_T^2\,[\delta\mathbf{x}(\tau_2)]_T^2\right\rangle_{\Omega_T,\Omega_L}^{r_0} = 4a_T^4 + 4a_{T\tau_1\tau_2}^4\,, \tag{5.285}$$

$$\left\langle [\delta\mathbf{x}(\tau_1)]_T^2\,[\delta\mathbf{x}(\tau_2)]_L^2\right\rangle_{\Omega_T,\Omega_L}^{r_0} = 2a_T^2a_L^2\,, \tag{5.286}$$

$$\left\langle [\delta\mathbf{x}(\tau_1)]_L^2\,[\delta\mathbf{x}(\tau_2)]_L^2\right\rangle_{\Omega_T,\Omega_L}^{r_0} = a_L^4 + 2a_{L\tau_1\tau_2}^4\,. \tag{5.287}$$

5.21.3 Isotropic Second-Order Approximation to Coulomb Problem

To demonstrate the use of the higher-order smearing formula (5.275), we calculate the effective classical potential of the three-dimensional Coulomb potential

$$V(\mathbf{x}) = -\frac{e^2}{|\mathbf{x}|} \tag{5.288}$$

to second order in variational perturbation theory, thus going beyond the earlier results in Eq. (5.53) and Section 5.10. The interaction potential corresponding to (5.278) is

$$V_{\rm int}^{\mathbf{x}_0}(\mathbf{x}) = -\frac{e^2}{|\mathbf{x}|} - \frac{M}{2}\Omega^2(\mathbf{x}_0)(\mathbf{x}-\mathbf{x}_0)^2\,. \tag{5.289}$$

For simplicity, we consider only the isotropic approximation with only a single trial frequency. Then all formulas derived in the beginning of this section have a trivial extension to three dimensions. Better results will, of course be obtained with two trial frequencies $\Omega_L^2(r_0)$ and $\Omega_T^2(r_0)$ of Section 5.9.

The Fourier transform $4\pi e^2/|\mathbf{k}|^2$ of the Coulomb potential $e^2/|\mathbf{x}|$ is most conveniently written in a proper-time type of representation as

$$V(\mathbf{k}) = \frac{4\pi e^2}{2}\int_0^\infty d\sigma e^{-\sigma\mathbf{k}^2/2 - i\mathbf{k}\mathbf{x}}, \tag{5.290}$$

where σ has the dimension length square. The lowest-order smeared potentials were calculated before in Section 5.10. For brevity, we consider here only the isotropic approximation in which longitudinal and transverse trial frequencies are identified [compare (5.112)]:

$$\left\langle [\mathbf{x}(\tau_1)-\mathbf{x}_0]^2\right\rangle_\Omega^{\mathbf{x}_0} = 3a^2(\mathbf{x}_0)\,, \quad \left\langle \frac{1}{|\mathbf{x}(\tau_1)|}\right\rangle_\Omega^{\mathbf{x}_0} = \frac{1}{|\mathbf{x}_0|}\,{\rm erf}\left[\frac{|\mathbf{x}_0|}{\sqrt{2a^2(\mathbf{x}_0)}}\right]. \tag{5.291}$$

The first-order variational approximation to the effective classical potential (5.281) is then given by the earlier-calculated expression (5.115).

To second order in variational perturbation theory we calculate expectation values

$$\left\langle [\mathbf{x}(\tau_1)-\mathbf{x}_0]^2\,[\mathbf{x}(\tau_2)-\mathbf{x}_0]^2\right\rangle_\Omega^{\mathbf{x}_0} = 9a^4(\mathbf{x}_0) + 6a^4_{\tau_1\tau_2}(\mathbf{x}_0)\,, \tag{5.292}$$

$$\left\langle [\mathbf{x}(\tau_1)-\mathbf{x}_0]^2\,\frac{1}{|\mathbf{x}(\tau_2)|}\right\rangle_\Omega^{\mathbf{x}_0} = \frac{2[3a^4(\mathbf{x}_0) - a^4_{\tau_1\tau_2}(\mathbf{x}_0)]}{\sqrt{\pi a^6(\mathbf{x}_0)}}\,, \tag{5.293}$$

which follow from the obvious generalization of (5.271), (5.272) to three dimensions. More involved is the Coulomb-Coulomb correlation function

$$\begin{aligned}\left\langle \frac{1}{|\mathbf{x}(\tau_1)|}\frac{1}{|\mathbf{x}(\tau_2)|}\right\rangle_\Omega^{\mathbf{x}_0} &= \frac{1}{2\pi}\int_0^{+\infty} d\sigma_1 \int_0^{+\infty} d\sigma_2\, \frac{1}{\sqrt{[a^2(\mathbf{x}_0)+\sigma_1][a^2(\mathbf{x}_0)+\sigma_2] - a^4_{\tau_1\tau_2}(\mathbf{x}_0)^3}} \\ &\quad\times \exp\left\{-\mathbf{x}_0^2\frac{a^2(\mathbf{x}_0)+\sigma_1/2+\sigma_2/2 - a^2_{\tau_1\tau_2}(\mathbf{x}_0)}{[a^2(\mathbf{x}_0)+\sigma_1][a^2(\mathbf{x}_0)+\sigma_2] - a^4_{\tau_1\tau_2}(\mathbf{x}_0)}\right\}.\end{aligned} \tag{5.294}$$

Using these smearing results we calculate the second connected correlation functions of the interaction potential (5.289) appearing in (5.263) and find the effective classical potential to second order in variational perturbation theory

$$\begin{aligned}W_2(\mathbf{x}_0) &= W_1(\mathbf{x}_0) + \left[\frac{Me^2\Omega(\mathbf{x}_0)}{\hbar\sqrt{2\pi a^6(\mathbf{x}_0)}} - \frac{3M^2\Omega^3(\mathbf{x}_0)}{4\hbar}\right] l^4(\mathbf{x}_0) \\ &\quad - \frac{e^4}{2\hbar}\int_0^{\hbar\beta} d\tau \left\langle \frac{1}{|\mathbf{x}(\tau)|}\frac{1}{|\mathbf{x}(0)|}\right\rangle_\Omega^{\mathbf{x}_0},\end{aligned} \tag{5.295}$$

with the abbreviation

$$l^4(\mathbf{x}_0) \equiv \frac{\hbar\left[4+\hbar^2\beta^2\Omega^2(\mathbf{x}_0)-4\cosh\hbar\beta\Omega(\mathbf{x}_0)+\hbar\beta\Omega(\mathbf{x}_0)\sinh\hbar\beta\Omega(\mathbf{x}_0)\right]}{8\beta M^2\Omega^3(\mathbf{x}_0)\sinh[\hbar\beta\Omega(\mathbf{x}_0)/2]}\,, \tag{5.296}$$

the symbol indicating that this is a quantity of dimension length to the forth power. After an extremization of (5.295) with respect to the trial frequency $\Omega(\mathbf{x}_0)$, which has to be done numerically, we obtain the second-order approximation for the effective classical potential of the Coulomb system plotted in Fig. 5.25 for various temperatures. The curves lie all below the first-order ones, and the difference between the two decreases with increasing temperature and increasing distance from the origin.

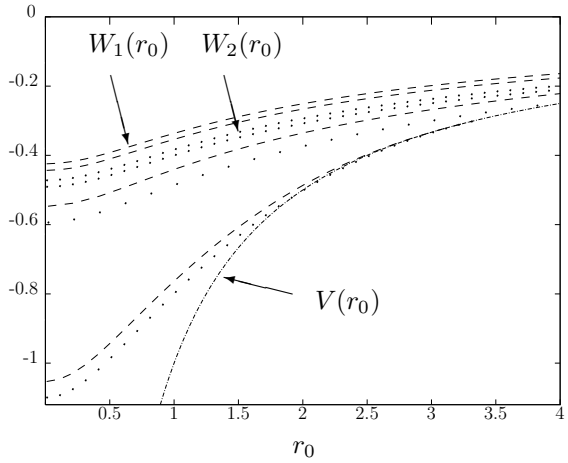

Figure 5.25 Isotropic approximation to effective classical potential of Coulomb system in the first (lines) and second order (dots). The temperatures are $10^{-4}, 10^{-3}, 10^{-2}, 10^{-1}$, and ∞ from top to bottom in atomic units. Compare also Fig. 5.9.

5.21.4 Anisotropic Second-Order Approximation to Coulomb Problem

The first-order effective classical potential $W_1(\mathbf{x}_0)$ was derived in Eqs. (5.97) and (5.117)–(5.121). To obtain the second-order approximation $W_2(\mathbf{x}_0)$, we insert the Coulomb potential in the representation (5.290) into the second-order smearing formula (5.282), and find

$$\left\langle \frac{1}{|\mathbf{x}(\tau_1)|}\,[\delta\mathbf{x}(\tau_2)]_T^2 \right\rangle_{\Omega_T,\Omega_L}^{r_0} = \sqrt{\frac{2a_L^2}{\pi}}\int_0^1 d\lambda\, e^{-\frac{r_0^2}{2a_L^2}\lambda^2}\left\{\frac{2a_T^2}{(a_T^2-a_L^2)\lambda^2+a_L^2}-\frac{2a_{T\tau_1\tau_2}^4\lambda^2}{[(a_T^2-a_L^2)\lambda^2+a_L^2]^2}\right\},$$

$$\left\langle \frac{1}{|\mathbf{x}(\tau_1)|}\,[\delta\mathbf{x}(\tau_2)]_L^2 \right\rangle_{\Omega_T,\Omega_L}^{r_0} = \sqrt{\frac{2a_L^2}{\pi}}\int_0^1 d\lambda\, e^{-\frac{r_0^2}{2a_L^2}\lambda^2}\,\frac{a_L^6+a_{L\tau_1\tau_2}^4[r_0^2\lambda^4-a_L^2\lambda^2]}{a_L^4[(a_T^2-a_L^2)\lambda^2+a_L^2]}\,. \tag{5.297}$$

These are special cases of the more general expectation value

$$\left\langle \frac{1}{|\mathbf{x}(\tau_1)|}F(\mathbf{x}(\tau_2)) \right\rangle_{\Omega_T,\Omega_L}^{r_0} = \frac{1}{2\pi^2}\int_0^{+\infty} d\sigma\,\frac{\exp\left\{-\dfrac{a_L^2r_0^2}{2[a_L^4-a_{L\tau_1\tau_2}^4+2a_L^2\sigma]}\right\}}{[a_T^4-a_{T\tau_1\tau_2}^4+2a_T^2\sigma]\sqrt{a_L^4-a_{L\tau_1\tau_2}^4+2a_L^2\sigma}}$$
$$\times\int d^3x F(\mathbf{x})\exp\left\{-\frac{(a_T^2+2\sigma)\mathbf{x}_T^2}{2[a_T^4-a_{T\tau_1\tau_2}^4+2a_T^2\sigma]}-\frac{(a_L^2+2\sigma)(x_L-r_0)^2+2a_{L\tau_1\tau_2}^2r_0(x_L-r_0)}{2[a_L^4-a_{L\tau_1\tau_2}^4+2a_L^2\sigma]}\right\}, \tag{5.298}$$

which furthermore leads to

$$\left\langle \frac{1}{|\mathbf{x}(\tau_1)|}\frac{1}{|\mathbf{x}(\tau_2)|}\right\rangle^{r_0}_{\Omega_T,\Omega_L} = \frac{2}{\pi}\int_0^{+\infty} d\sigma_1 \int_0^{+\infty} d\sigma_2 \, \frac{1}{[a_T^2+2\sigma_1][a_T^2+2\sigma_2]-a_{T\tau_1\tau_2}^4}$$
$$\times \frac{1}{\sqrt{[a_L^2+2\sigma_1][a_L^2+2\sigma_2]-a_{L\tau_1\tau_2}^4}} \exp\left\{-\frac{r_0^2[a_L^2+\sigma_1+\sigma_2-a_{L\tau_1\tau_2}^2]}{[a_L^2+2\sigma_1][a_L^2+2\sigma_2]-a_{L\tau_1\tau_2}^4}\right\}. \quad (5.299)$$

From these smearing results we calculate the second-order approximation to the effective classical potential

$$W_2(\mathbf{x}_0) = F_\Omega^{\mathbf{x}_0} + \frac{1}{\hbar\beta}\int_0^{\hbar\beta} d\tau_1 \, \langle V_{\rm int}^{\mathbf{x}_0}(\mathbf{x}(\tau_1))\rangle_{\Omega,c}^{\mathbf{x}_0} - \frac{1}{2\hbar^2\beta}\int_0^{\hbar\beta} d\tau_1 \int_0^{\hbar\beta} d\tau_2 \, \langle V_{\rm int}^{\mathbf{x}_0}(\mathbf{x}(\tau_1)) V_{\rm int}^{\mathbf{x}_0}(\mathbf{x}(\tau_2))\rangle_{\Omega,c}^{\mathbf{x}_0}. \quad (5.300)$$

The result is

$$\begin{aligned} W_2^{\Omega_T,\Omega_L}(r_0) \;=\; & W_1^{\Omega_T,\Omega_L}(r_0) \\ & + \frac{e^2M}{2\hbar}\sqrt{\frac{2a_L^2}{\pi}}\int_0^1 d\lambda \left\{\frac{2\Omega_T l_T^4\lambda^2}{[(a_T^2-a_L^2)\lambda^2+a_L^2]^2} - \frac{\Omega_L l_L^4[r_0^2\lambda^4-a_L^2\lambda^2]}{a_L^4[(a_T^2-a_L^2)\lambda^2+a_L^2]}\right\} e^{-r_0^2\lambda^2/2a_L^2} \\ & - \frac{M^2[2\Omega_T^3 l_T^4+\Omega_L^3 l_L^4]}{4\hbar} - \frac{e^4}{2\hbar^2\beta}\int_0^{\hbar\beta} d\tau_1 \int_0^{\hbar\beta} d\tau_2 \left\langle \frac{1}{|\mathbf{x}(\tau_1)|}\frac{1}{|\mathbf{x}(\tau_2)|}\right\rangle^{r_0}_{\Omega_T,\Omega_L,c}, \end{aligned} \quad (5.301)$$

with the abbreviation

$$l_{T,L}^4 = \frac{\hbar\left[4+\hbar^2\beta^2\Omega_{T,L}^2 - 4\cosh\hbar\beta\Omega_{T,L} + \hbar\beta\Omega_{T,L}\sinh\hbar\beta\Omega_{T,L}\right]}{8\beta M^2\Omega_{T,L}^3\sinh[\hbar\beta\Omega_{T,L}/2]}, \quad (5.302)$$

which is a quantity of dimension (length)^4. After an extremization of (5.115) and (5.301) with respect to the trial frequencies Ω_T, Ω_L which has to be done numerically, we obtain the second-order approximation for the effective classical potential of the Coulomb system plotted in Fig. 5.26 for various temperatures. The second order curves lie all below the first-order ones, and the difference between the two decreases with increasing temperature and increasing distance from the origin.

5.21.5 Zero-Temperature Limit

As a cross check of our result we take (5.301) to the limit $T \to 0$. Just as in the lowest-order discussion in Sect. (5.4), the x_0-integral can be evaluated in the saddle-point approximation which becomes exact in this limit, so that the minimum of $W_N(\mathbf{x}_0)$ in x_0 yields the nth approximation to the free energy at $T = 0$ and thus the nth approximations $E_N^{(0)}$ the ground state energy $E^{(0)}$ of the Coulomb system. In this limit, the results should coincide with those derived from a direct variational treatment of the Rayleigh-Schrödinger perturbation expansion in Section 3.18. With the help of such a treatment, we shall also carry the approximation to the next order, thereby illustrating the convergence of the variational perturbation expansions. For symmetry reasons, the minimum of the effective classical potential occurs for all temperatures at the origin, such that we may restrict (5.115) and (5.301) to this point. Recalling the zero-temperature limit of the two-point correlations (5.19) from (3.249),

$$\lim_{\beta\to\infty} a_{\tau\tau'}^2(\mathbf{x}_0) = \frac{\hbar}{2M\Omega(\mathbf{x}_0)}\exp\left\{-\Omega(\mathbf{x}_0)\,|\tau-\tau'|\right\}, \quad (5.303)$$

we immediately deduce for the first order approximation (5.115) with $\Omega = \Omega(\mathbf{0})$ the limit

$$E_1^{(0)}(\Omega) = \lim_{\beta\to\infty} W_1^{\Omega}(\mathbf{0}) = \frac{3}{4}\hbar\Omega - \frac{2}{\sqrt{\pi}}\sqrt{\frac{M\Omega}{\hbar}}e^2\,. \tag{5.304}$$

In the second-order expression (5.301), the zero-temperature limit is more tedious to take. Performing the integrals over σ_1 and σ_2, we obtain the connected correlation function

$$\left\langle \frac{1}{|\mathbf{x}(\tau_1)|}\frac{1}{|\mathbf{x}(\tau_2)|}\right\rangle_{\Omega,c}^{\mathbf{x}_0} = \frac{1}{a^4_{\tau_1\tau_2}(\mathbf{0})} - \frac{2}{\pi a^4_{\tau_1\tau_2}(\mathbf{0})}\arctan\sqrt{\frac{a^2_{\tau_1\tau_2}(\mathbf{0})}{a_{\tau_1\tau_2}(\mathbf{0})}-1} - \frac{2}{\pi a^2_{\tau_1\tau_2}(\mathbf{0})}\,. \tag{5.305}$$

Inserting (5.303), setting $\tau_1 = 0$ and integrating over the imaginary times $\tau = \tau_2 \in [0, \hbar\beta]$, we find

$$\begin{aligned}\int_0^{\hbar\beta} d\tau \left\langle \frac{1}{|\mathbf{x}(\tau)|}\frac{1}{|\mathbf{x}(0)|}\right\rangle_{\Omega,c}^{\mathbf{x}_0} &\underset{\beta\to\infty}{\approx} \frac{4M}{\hbar^2\beta\Omega}\left\{e^{\hbar\beta\Omega} - 1 - \hbar\beta\Omega - \frac{\hbar^2\beta^2\Omega^2}{\pi} - \frac{2}{\pi}\right.\\ &\times\left.\left[e^{\hbar\beta\Omega}\arcsin\sqrt{1-e^{-2\hbar\beta\Omega}} + \frac{1}{2}\ln\alpha(\beta) - \frac{1}{8}\left[\ln\alpha(\beta)\right]^2 - \frac{1}{2}\int_{\alpha(\beta)}^{1} du\,\frac{\ln u}{1+u}\right]\right\},\end{aligned} \tag{5.306}$$

with the abbreviation

$$\alpha(\beta) = \frac{1-\sqrt{1-e^{-2\hbar\beta\Omega}}}{1+\sqrt{1-e^{-2\hbar\beta\Omega}}}\,. \tag{5.307}$$

Inserting this into (5.301) and going to the limit $\beta\to\infty$ we obtain

$$E_2^{(0)}(\Omega) = \lim_{\beta\to\infty} W_2^{\Omega}(\mathbf{0}) = \frac{9}{16}\hbar\Omega - \frac{3}{2\sqrt{\pi}}\sqrt{\frac{M\Omega}{\hbar}}e^2 - \frac{4}{\pi}\left(1+\ln 2-\frac{\pi}{2}\right)\frac{M}{\hbar^2}e^4. \tag{5.308}$$

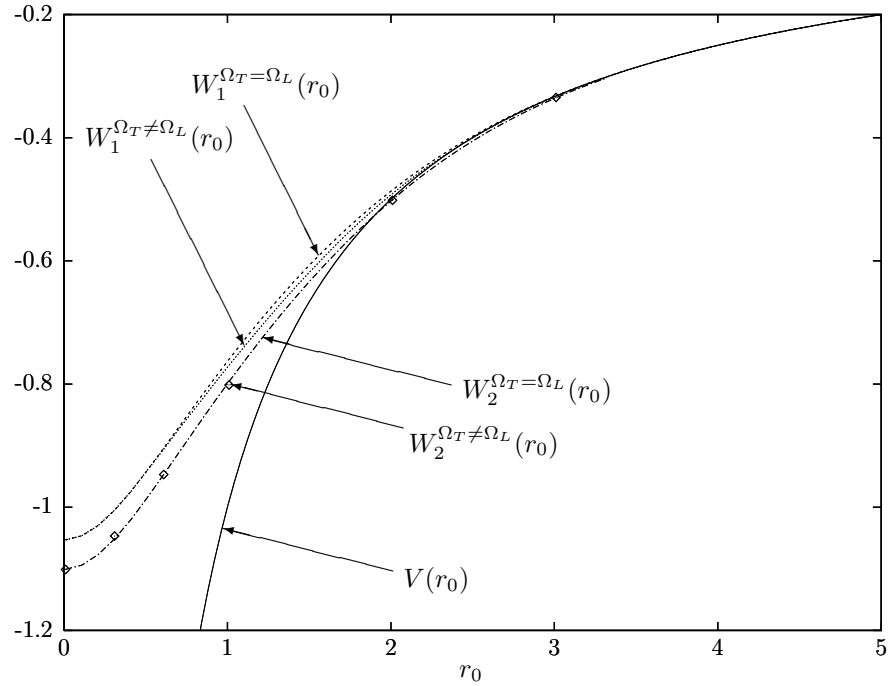

Figure 5.26 Isotropic and anisotropic approximations to effective classical potential of Coulomb system in first and second order at temperature 0.1 in atomic units. The lowest line represents the high temperature limit in which all isotropic and anisotropic approximations coincide.

Postponing for a moment the extremization of (5.304) and (5.308) with respect to the trial frequency Ω, let us first rederive this result from a variational treatment of the ordinary Rayleigh-Schrödinger perturbation expansion for the ground state energy in Section 3.18. According to the replacement rule (5.186), we must first calculate the ground state energy for a Coulomb potential in the presence of a harmonic potential of frequency ω:

$$V(\mathbf{x}) = \frac{M}{2}\omega^2\mathbf{x}^2 - \frac{e^2}{|\mathbf{x}|}. \tag{5.309}$$

After this, we make the trivial replacement $\omega \to \sqrt{\Omega^2 + \omega^2 - \Omega^2}$ and re-expand the energy in powers of $\omega^2 - \Omega^2$, considering this quantity as being of the order e^2 and truncating the re-expansion accordingly. At the end we go to $\omega = 0$, since the original Coulomb system contains no oscillator potential. The result of this treatment will be precisely the expansions (5.304) and (5.308).

The Rayleigh-Schrödinger perturbation expansion of the ground state energy $E_N^{(0)}(\omega)$ for the potential (5.309) in Section 3.18 requires knowledge of the matrix elements of the Coulomb potential (5.288) with respect to the eigenfunctions of the harmonic oscillator with the frequency ω:

$$V_{n,l,m;n',l',m'} = \int_0^{2\pi} d\varphi \int_0^{\pi} d\vartheta \sin\vartheta \int_0^{\infty} dr\, r^2\, \psi^*_{n,l,m}(r,\vartheta,\varphi)\frac{-e^2}{r}\psi_{n',l',m'}(r,\vartheta,\varphi), \tag{5.310}$$

where [see (9.67), (9.68), and (9.53)]

$$\begin{aligned}\psi_{n,l,m}(r,\vartheta,\varphi) &= \sqrt{\frac{2n!}{\Gamma(n+l+3/2)}}\sqrt[4]{\frac{M\omega}{\hbar}}\left(\frac{M\omega}{\hbar}r^2\right)^{(l+1)/2} \\ &\quad \times L_n^{l+1/2}\left(\frac{M\omega}{\hbar}r^2\right)\exp\left\{-\frac{M\omega}{2\hbar}r^2\right\}Y_{l,m}(\vartheta,\varphi)\,.\end{aligned} \tag{5.311}$$

Here n denotes the radial quantum number, $L_n^{\alpha}(x)$ the Laguerre polynomials and $Y_{l,m}(\vartheta,\varphi)$ the spherical harmonics obeying the orthonormality relation

$$\int_0^{2\pi} d\varphi \int_0^{\pi} d\vartheta \sin\vartheta\, Y^*_{l,m}(\vartheta,\varphi)Y_{l',m'}(\vartheta,\varphi) = \delta_{l,l'}\delta_{m,m'}\,. \tag{5.312}$$

Inserting (5.311) into (5.310), and evaluating the integrals, we find

$$\begin{aligned}V_{n,l,m;n',l',m'} &= -e^2\sqrt{\frac{M\omega}{\pi\hbar}}\,\frac{\Gamma(l+1)\Gamma(n+1/2)}{\Gamma(l+3/2)}\sqrt{\frac{\Gamma(n'+l+3/2)}{n!n'!\Gamma(n+l+3/2)}} \\ &\quad \times {}_3F_2\left(-n', l+1, \frac{1}{2}; l+\frac{3}{2}, \frac{1}{2}-n; 1\right)\delta_{l,l'}\,\delta_{m,m'}\,,\end{aligned} \tag{5.313}$$

with the generalized hypergeometric series [compare (1.453)]

$${}_3F_2(\alpha_1,\alpha_2,\alpha_3;\beta_1,\beta_2;x) = \sum_{k=0}^{\infty}\frac{(\alpha_1)_k(\alpha_2)_k(\alpha_3)_k}{(\beta_1)_k(\beta_2)_k}\,\frac{x^k}{k!} \tag{5.314}$$

and the Pochhammer symbol $(\alpha)_k = \Gamma(\alpha+k)/\Gamma(\alpha)$.
These matrix elements are now inserted into the Rayleigh-Schrödinger perturbation expansion for the ground state energy

$$E^{(0)}(\omega) = E_{0,0,0} + V_{0,0,0;0,0,0} + {\sum_{n,l,m}}' \frac{V_{0,0,0;n,l,m}V_{n,l,m;0,0,0}}{E_{0,0,0} - E_{n,l,m}}$$

$$- \sum_{n,l,m}{}' V_{0,0,0;0,0,0} \frac{V_{0,0,0;n,l,m} V_{n,l,m;0,0,0}}{\left[E_{0,0,0} - E_{n,l,m}\right]^2}$$
$$+ \sum_{n,l,m}{}' \sum_{n',l',m'}{}' \frac{V_{0,0,0;n,l,m} V_{n,l,m;n',l',m'} V_{n',l',m';0,0,0}}{\left[E_{0,0,0} - E_{n,l,m}\right]\left[E_{0,0,0} - E_{n',l',m'}\right]} + \dots \,, \tag{5.315}$$

the denominators containing the energy eigenvalues of the harmonic oscillator

$$E_{n,l,m} = \hbar\omega \left(2n + l + \frac{3}{2}\right) . \tag{5.316}$$

The primed sums in (5.315) run over all values of the quantum numbers $n, l = -\infty, \dots, +\infty$ and $m = -l, \dots, +l$, excluding those for which the denominators vanish. For the first three orders we obtain from (5.313)–(5.316)

$$E^{(0)}(\omega) = \frac{3}{2}\hbar\omega - \frac{2}{\sqrt{\pi}} \sqrt{\frac{M\omega}{\hbar}} e^2 - \frac{4}{\pi}\left(1 + \ln 2 - \frac{\pi}{2}\right) \frac{M}{\hbar^2} e^4 - c \sqrt{\frac{M^3}{\hbar^7 \omega}} e^6 + \dots \,, \tag{5.317}$$

with the constant

$$c = \frac{1}{\pi^{3/2}} \left\{ \sum_{n=1}^{\infty} \frac{1 \cdot 3 \cdot \dots \cdot (2n-1)}{2 \cdot 4 \cdots 2n} \frac{1}{n^2\,(n+1/2)} - \sum_{n=1}^{\infty} \sum_{n'=1}^{\infty} \frac{1 \cdot 3 \cdots (2n-1)}{2 \cdot 4 \cdots 2n} \right.$$
$$\left. \times \frac{1 \cdot 3 \cdots (2n'-1)}{2 \cdot 4 \cdots 2n'} \frac{{}_3F_2\left(-n', l+1, \frac{1}{2}; l+\frac{3}{2}, \frac{1}{2} - n; 1\right)}{n\,n'\,(n+1/2)} \right\} \approx 0.031801 \,. \tag{5.318}$$

Since we are interested only in the energies in the pure Coulomb system with $\omega = 0$, the variational re-expansion procedure described after (5.309) becomes particularly simple: We simply have to replace ω by $\sqrt{\Omega^2 - \Omega^2}$ which is appropriately re-expanded in the second Ω^2, thereby considering Ω^2 as a quantity of order e^2. For the first term in the energy (5.317) which is proportional to Ω itself this amounts to a multiplication by a factor $(1-1)^{1/2}$ which is re-expanded in the second "1" up to the third order as $1 - \frac{1}{2} - \frac{1}{8} - \frac{1}{16} = \frac{5}{16}$. The term $3\omega/2$ in (5.317) becomes therefore $15/32\omega$. By the same rule, the factor $\omega^{1/2}$ in the second term of the energy (5.317) goes over into $\Omega^{1/2}(1-1)^{1/4}$, re-expanded to second order in the second "1", i.e., into $\Omega^{1/4}(1 - \frac{1}{4} - \frac{3}{32}) = \frac{21}{32}$. The next term in (5.317) happens to be independent of ω and needs no re-expansion, whereas the last term remains unchanged since it is already of highest order in e^2. In this way we obtain from (5.317) the third-order variational perturbation expansion

$$E_3^{(0)}(\Omega) = \frac{15}{32}\hbar\Omega - \frac{21}{16\sqrt{\pi}} \sqrt{\frac{M\Omega}{\hbar}} e^2 - \frac{4}{\pi}\left(1 + \ln 2 - \frac{\pi}{2}\right) \frac{M}{\hbar^2} e^4 - c \sqrt{\frac{M^3}{\hbar^7 \Omega}} e^6 \,. \tag{5.319}$$

Extremizing (5.304), (5.308), and (5.317) successively with respect to the trial frequency Ω we find to orders $1, 2$, and 3 the optimal values

$$\Omega_1 = \Omega_2 = \frac{16}{9\pi} \frac{Me^4}{\hbar^3} \,, \qquad \Omega_3 = c' \, \frac{Me^4}{\hbar^3} , \tag{5.320}$$

with $c' \approx 0.52621$. The corresponding approximations to the ground state energy are

$$E_N^{(0)}(\Omega^N) = -\gamma_N \frac{Me^4}{\hbar^2} \,, \tag{5.321}$$

with the constants

$$\gamma_1 = \frac{4}{3\pi} \approx 0.42441 \,, \quad \gamma_2 = \frac{5 + 4\ln 2}{\pi} - 2 \approx 0.47409 \,, \quad \gamma_3 \approx 0.49012 \,, \tag{5.322}$$

approaching exponentially fast the exact value $\gamma = 0.5$, as shown in Fig. 5.27.

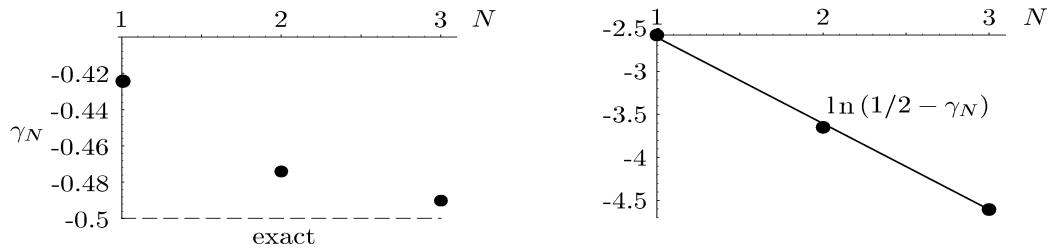

Figure 5.27 Approach of the variational approximations of first, second, and third order to the correct ground state energy -0.5, in atomic units.

5.22 Polarons

An important role in the development of variational methods for the approximate solution of path integrals was played by the *polaron* problem [34]. Polarons arise when electrons travel through ionic crystals thereby producing an electrostatic deformation in their neighborhood. If $\mathbf{P}^{\mathrm{i}}(\mathbf{x},t)$ denotes electric polarization density caused by the displacement of the positive against the negative ions, an electron sees a local ionic charge distribution

$$\rho^{\mathrm{i}}(\mathbf{x},t) = \boldsymbol{\nabla}\cdot\mathbf{P}^{\mathrm{i}}(\mathbf{x},t), \tag{5.323}$$

which gives rise to an electric potential satisfying

$$\boldsymbol{\nabla}^2 A^0(\mathbf{x},t) = 4\pi\,\boldsymbol{\nabla}\cdot\mathbf{P}^{\mathrm{i}}(\mathbf{x},t). \tag{5.324}$$

The Fourier transform of this,

$$A^0_{\mathbf{k}}(t) \equiv \int_{-\infty}^{\infty} d^3x\, A^0(\mathbf{x},t)e^{-i\mathbf{kp}}, \tag{5.325}$$

and that of $\mathbf{P}^{\mathrm{i}}(\mathbf{x},t)$,

$$\mathbf{P}^{\mathrm{i}}_{\mathbf{k}}(t) = \int_{-\infty}^{\infty} d^3x\, \mathbf{P}^{\mathrm{i}}(\mathbf{x},t)e^{-i\mathbf{kx}}, \tag{5.326}$$

are related by

$$A^0_{\mathbf{k}}(t) = -\frac{4\pi}{\mathbf{k}^2}\, i\mathbf{k}\cdot\mathbf{P}^{\mathrm{i}}_{\mathbf{k}}(t). \tag{5.327}$$

Only longitudinal phonons which have $\mathbf{P}^{\mathrm{i}}_{\mathbf{k}}(t) \propto \mathbf{k}$ and correspond to density fluctuations in the crystal contribute. For these, an electron at position $\mathbf{x}(t)$ experiences an electric potential

$$A^0(\mathbf{x},t) = -\sum_{\mathbf{k}} A^0_{\mathbf{k}}(t)\frac{e^{i\mathbf{kx}}}{\sqrt{V}} = i\sum_{\mathbf{k}}\frac{4\pi}{|\mathbf{k}|}\mathbf{P}_{\mathbf{k}}(\tau)\frac{e^{i\mathbf{kx}}}{\sqrt{V}}. \tag{5.328}$$

In the regime of optical phonons, each Fourier component oscillates with approximately the same frequency ω, the frequency of longitudinal optical phonons. The variables $\mathbf{P}^{\mathrm{i}}_{\mathbf{k}}(t)$ have therefore a Lagrangian

$$L(t) = \frac{1}{2\mu}\sum_{\mathbf{k}}\left[\dot{\mathbf{P}}^{\mathrm{i}}_{-\mathbf{k}}(t)\dot{\mathbf{P}}^{\mathrm{i}}_{\mathbf{k}}(t) - \omega^2\mathbf{P}^{\mathrm{i}}_{-\mathbf{k}}(t)\mathbf{P}^{\mathrm{i}}_{\mathbf{k}}(t)\right], \tag{5.329}$$

with some material constant μ and $\mathbf{P}^{\mathrm{i}}_{-\mathbf{k}}(t) = \mathbf{P}^{\mathrm{i}\,*}_{\mathbf{k}}(t)$, since the polarization is a real field. This can be expressed in terms of measurable properties of the crystal. For this we note that the interaction of the polarization field with a given total charge distribution $\rho(\mathbf{x}, t)$ is described by a Lagrangian

$$L_{\mathrm{int}}(t) = -\int d^3x\, \rho(\mathbf{x}, t) V(\mathbf{x}, t). \tag{5.330}$$

Inserting (5.325) and performing a partial

$$L_{\mathrm{int}}(t) = 4\pi \int d^3x\, \frac{1}{\boldsymbol{\nabla}^2}\, \boldsymbol{\nabla}\rho(\mathbf{x}, t) \cdot \mathbf{P}^{\mathrm{i}}(\mathbf{x}', t). \tag{5.331}$$

Recalling the Gauss law $\boldsymbol{\nabla} \cdot \mathbf{D}(\mathbf{x}, t) = 4\pi\rho(\mathbf{x}, t)$ we identify the factor of $\mathbf{P}^{\mathrm{i}}(\mathbf{x}, t)$ with the total electric displacement field and write

$$L_{\mathrm{int}}(t) = 4\pi \int d^3x\, \mathbf{D}(\mathbf{x}, t) \cdot \mathbf{P}^{\mathrm{i}}(\mathbf{x}, t). \tag{5.332}$$

In combination with (5.329) this leads to an equation of motion

$$\frac{1}{\mu}\left[\ddot{\mathbf{P}}^{\mathrm{i}}_{\mathbf{k}}(t) + \omega^2 \mathbf{P}^{\mathrm{i}}_{\mathbf{k}}(t)\right] = \mathbf{D}_{\mathbf{k}}(t). \tag{5.333}$$

If we go over to the temporal Fourier components $\mathbf{P}^{\mathrm{i}}_{\omega',\mathbf{k}}$ of the ionic polarization, we find the relation

$$\frac{1}{\mu}\left(\omega^2 - \omega'^2\right) \mathbf{P}^{\mathrm{i}}_{\omega',\mathbf{k}} = \mathbf{D}_{\omega',\mathbf{k}}. \tag{5.334}$$

For very slow deformations, this becomes

$$\frac{\omega^2}{\mu} \mathbf{P}^{\mathrm{i}}_{\omega',\mathbf{k}} \approx \mathbf{D}_{0,\mathbf{k}}. \tag{5.335}$$

Using the general relation

$$\mathbf{D}_{\omega',\mathbf{k}} = \mathbf{E}_{\omega',\mathbf{k}} + 4\pi \mathbf{P}_{\omega',\mathbf{k}}, \tag{5.336}$$

where $4\pi\mathbf{P}_{\omega',\mathbf{k}}$ contains both ionic *and* electronic polarizations, we obtain

$$4\pi \mathbf{P}_{\omega',\mathbf{k}} = \left(1 - \frac{1}{\epsilon_{\omega'}}\right) \mathbf{D}_{\omega',\mathbf{k}}, \tag{5.337}$$

with $\epsilon_{\omega'}$ being the dielectric constant at frequency ω'. For a slowly moving electron, the lattice deformations have small frequencies, and we can write the time-dependent equation

$$4\pi \mathbf{P}_{\mathbf{k}}(t) \approx \left(1 - \frac{1}{\epsilon_0}\right) \mathbf{D}_{\mathbf{k}}(t). \tag{5.338}$$

By comparison with Eq. (5.335) we determine the parameter μ. Before we can do so, however, we must subtract from (5.338) the contribution of the electrons. These fulfill the approximate time-dependent equation

$$4\pi \mathbf{P}^{\mathrm{el}}_{\mathbf{k}}(t) \approx \left(1 - \frac{1}{\epsilon_\infty}\right) \mathbf{D}_{\mathbf{k}}(t), \tag{5.339}$$

where ϵ_∞ is the dielectric constant at high frequency where only electrons can follow the field oscillations. The purely ionic polarization field is therefore given by

$$4\pi \mathbf{P}^{\mathrm{i}}_{\mathbf{k}}(t) \approx \left(\frac{1}{\epsilon_\infty} - \frac{1}{\epsilon_0}\right) \mathbf{D}_{\mathbf{k}}(t). \tag{5.340}$$

By comparison with (5.334) we identify

$$\mu \approx \frac{\omega^2}{4\pi}\left(\frac{1}{\epsilon_\infty} - \frac{1}{\epsilon_0}\right). \tag{5.341}$$

5.22.1 Partition Function

The partition function of the combined system of an electron and the oscillating polarization is therefore described by the imaginary-time path integral

$$\begin{aligned} Z = \int \mathcal{D}^3 x \prod_{\mathbf{k}} \int \mathcal{D}^3 \mathbf{P}_{\mathbf{k}} \exp\Bigg(-\frac{1}{\hbar}\int_0^{\hbar\beta} d\tau \Bigg\{ \frac{M}{2}\dot{\mathbf{x}}^2(\tau) \\ + \sum_{\mathbf{k}} \frac{1}{2\mu}\left[\dot{\mathbf{P}}^{\mathrm{i}}_{-\mathbf{k}}(t)\dot{\mathbf{P}}^{\mathrm{i}}_{\mathbf{k}}(t) - \omega^2 \mathbf{P}^{\mathrm{i}}_{-\mathbf{k}}(t)\mathbf{P}^{\mathrm{i}}_{\mathbf{k}}(t)\right] + ie\sum_{\mathbf{k}} \frac{4\pi}{|\mathbf{k}|}\mathbf{P}_{\mathbf{k}}(\tau)\frac{e^{i\mathbf{k}\mathbf{x}(\tau)}}{\sqrt{V}} \Bigg\}\Bigg), \end{aligned} \tag{5.342}$$

where V is the volume of the system. The path integral is Gaussian in the Fourier components $\mathbf{P}_{\mathbf{k}}(\tau)$. These can therefore be integrated out with the rules of Subsection 3.8.2. For the correlation function of the polarizations we shall use the representation of the Green function (3.251) as a sum of periodic repetitions of the zero-temperature Green function

$$\langle \mathbf{P}_{\mathbf{k}}(\tau)\mathbf{P}_{-\mathbf{k}}(\tau')\rangle = \frac{\hbar}{2\omega}\sum_{n=-\infty}^{\infty} e^{-\omega|\tau-\tau'+n\hbar\beta|}. \tag{5.343}$$

Abbreviating

$$\sum_{n=-\infty}^{\infty} e^{-\omega|\tau-\tau'+n\hbar\beta|} \equiv e^{-\omega|\tau-\tau'|}_{\mathrm{per}} = \frac{1}{2\omega}\left(e^{-\omega|\tau-\tau'|} - e^{-\omega(\hbar\beta-|\tau-\tau'|)}\right)\frac{1}{1-e^{-\hbar\beta\omega}}, \tag{5.344}$$

the right-hand side being valid for $\hbar\beta > \tau, \tau' > 0$, we find

$$\begin{aligned} Z = \int \mathcal{D}^3 x \exp\Bigg\{ -\frac{1}{\hbar}\int_0^{\hbar\beta} d\tau \frac{M}{2}\dot{\mathbf{x}}^2(\tau) \\ + \frac{\mu}{2\hbar^2}\,4\pi e^2 \frac{\hbar}{2\omega}\frac{1}{V}\sum_{\mathbf{k}}\frac{4\pi}{\mathbf{k}^2}\int_0^{\hbar\beta} d\tau \int_0^{\hbar\beta} d\tau' e^{i\mathbf{k}[\mathbf{x}(\tau)-\mathbf{x}(\tau')]} e^{-\omega|\tau-\tau'|}_{\mathrm{per}} \Bigg\}. \end{aligned} \tag{5.345}$$

Performing the sum over all wave vectors $\mathbf{k}$ using the formula

$$\frac{1}{V}\sum_{\mathbf{k}}\frac{4\pi}{\mathbf{k}^2}e^{i\mathbf{k}\mathbf{x}}=\frac{1}{|\mathbf{x}|}, \tag{5.346}$$

we obtain the path integral

$$Z=\int\mathcal{D}^3x\,\exp\left\{-\frac{1}{\hbar}\left[\int_0^{\hbar\beta}d\tau\frac{M}{2}\dot{\mathbf{x}}^2(\tau)-\frac{a}{2\sqrt{2}}\int_0^{\hbar\beta}d\tau\int_0^{\hbar\beta}d\tau'\frac{e_{\rm per}^{-\omega|\tau-\tau'|}}{|\mathbf{x}(\tau)-\mathbf{x}(\tau')|}\right]\right\}, \tag{5.347}$$

where

$$a\equiv\frac{\mu}{\hbar}\,4\pi e^2\frac{\hbar}{2\omega}\sqrt{2}. \tag{5.348}$$

The factor $\sqrt{2}$ is a matter of historic convention. Staying with this convention, we use the characteristic length scale (9.73) associated with the mass M and the frequency ω:

$$\lambda_\omega\equiv\sqrt{\frac{\hbar}{M\omega}}. \tag{5.349}$$

This length scale will appear in the wave functions of the harmonic oscillator in Eq. (9.73). Using this we introduce a dimensionless coupling constant α defined by

$$\alpha\equiv\frac{1}{\sqrt{2}}\left(\frac{1}{\epsilon_\omega}-\frac{1}{\epsilon_0}\right)\frac{e^2}{\hbar\omega\lambda_\omega}. \tag{5.350}$$

A typical value of α is 5 for sodium chloride. In different crystals it varies between 1 and 20, thus requiring a strong-coupling treatment. In terms of α, one has

$$a=\hbar\omega^2\lambda_\omega\alpha. \tag{5.351}$$

The expression (5.348) is the famous path integral of the polaron problem written down in 1955 by Feynman [20] and solved approximately by a variational perturbation approach.

In order to allow for later calculations of a particle density in an external potential, we decompose the paths in a Fourier series with fixed endpoints $\mathbf{x}(\beta)\equiv\mathbf{x}_b=\mathbf{x}_a$:

$$\mathbf{x}(\tau)=\mathbf{x}_a+\sum_{n=1}^{\infty}\mathbf{x}_n\sin\nu_n\tau,\quad \nu_n\equiv n\pi/\hbar\beta. \tag{5.352}$$

The path integral is then the limit $N\to\infty$ of the product of integrals

$$\int\mathcal{D}^3x\equiv\int\frac{d^2x_a}{\sqrt{2\pi\hbar^2\beta/M}^3}\prod_{n=1}^{\infty}\left[\int\frac{d^3x_n}{\sqrt{4\pi/M\nu_n^2\beta}^3}\right]. \tag{5.353}$$

The correctness of this measure is verified by considering the free particle in which case the action is

$$\mathcal{A}_0=\frac{1}{2}\sum_{n=1}^{\infty}A_n^0\mathbf{x}_n^2,\quad\text{with}\quad A_n^0\equiv\frac{M}{2}\hbar\beta\,\nu_n^2. \tag{5.354}$$

The Fourier components $\mathbf{x}_n$ can be integrated leaving a final integral

$$Z = \int \frac{d^2 x_a}{\sqrt{2\pi\hbar^2\beta/M}^3}, \tag{5.355}$$

which is the correct partition function of a free particle [compare with the one-dimensional expression (3.811)].

The endpoints $\mathbf{x}_b = \mathbf{x}_a$ do not appear in the integrand of (5.347) as a manifestation of translational invariance. The integral over the endpoints produces therefore a total volume factor V. We may imagine performing the path integral with fixed endpoints which produces the particle density.

5.22.2 Harmonic Trial System

The harmonic trial system used by Feynman as a starting point of his variational treatment has the generating functional

$$Z^{\Omega,C}[\,\mathbf{j}\,] = \int \mathcal{D}^3 x \, \exp\Bigg\{ -\frac{1}{\hbar}\int_0^{\hbar\beta} d\tau \left[\frac{M}{2}\dot{\mathbf{x}}^2(\tau) - \mathbf{j}(\tau)\mathbf{x}(\tau)\right] - \frac{C}{2}\frac{M}{\hbar}\int_0^{\hbar\beta} d\tau \int_0^{\hbar\beta} d\tau' \left[\mathbf{x}(\tau) - \mathbf{x}(\tau')\right]^2 e_{\rm per}^{-\Omega|\tau-\tau'|} \Bigg\}. \tag{5.356}$$

The external current is Fourier-decomposed in the same way as $\mathbf{x}(\tau)$ in (5.352). To preserve translational invariance, we assume the current to vanish at the endpoints: $\mathbf{j}_a = 0$. Then the first two terms in the action in (5.356) are

$$\mathcal{A}[\,\mathbf{j}\,] = \frac{1}{2}\sum_{n=1}^{\infty}\left(A_n^0 \mathbf{x}_n^2 - \beta\,\mathbf{j}_n\mathbf{x}_n\right). \tag{5.357}$$

The Fourier decomposition of the double integral in (5.356) reads

$$\int_0^{\hbar\beta} d\tau \int_0^{\hbar\beta} d\tau' \left[\sum_{n=1}^{\infty}\left(\sin\nu_n\tau - \sin\nu_n\tau'\right)\mathbf{x}_n\right]^2 e_{\rm per}^{-\Omega|\tau-\tau'|}. \tag{5.358}$$

With the help of trigonometric identities and a change of variables to $\sigma = (\tau+\tau')/2$ and $\Delta\tau = (\tau-\tau')/2$, this becomes

$$2\int_0^{\hbar\beta} d\sigma \int_0^{2\hbar\beta} d\Delta\tau \left[\sum_{n=1}^{\infty}\cos\nu_n\sigma\,\sin(\nu_n\Delta\tau/2)\,\mathbf{x}_n\right]^2 e_{\rm per}^{-\Omega|\Delta\tau|}. \tag{5.359}$$

Integrating out σ leaves

$$\hbar\beta\int_0^{2\hbar\beta} d\Delta\tau \sum_{n=1}^{\infty}\sin^2(\nu_n\Delta\tau/2)\,\mathbf{x}_n^2\, e_{\rm per}^{-\Omega|\Delta\tau|}, \tag{5.360}$$

and performing the integral over $\delta\tau$ gives for (5.358) the result

$$\frac{\hbar\beta}{2}\left(1-e^{-2\hbar\beta\Omega}\right)\left(1+2\sum_{n'=1}^{\infty}e^{-n'\hbar\beta\Omega}\right)\sum_{n=1}^{\infty}\mathbf{x}_n^2\,\frac{\nu_n^2}{\nu_n^2+\Omega^2}. \tag{5.361}$$

Hence we can write the interaction term in (5.356) as

$$-\frac{C_\beta M\beta}{4\Omega}\sum_{n=1}^{\infty}\mathbf{x}_n^2\,\frac{\nu_n^2}{\nu_n^2+\Omega^2},\qquad C_\beta\equiv C\left(1-e^{-2\hbar\beta\Omega}\right)\coth\frac{\hbar\beta\Omega}{2}. \tag{5.362}$$

This changes A_n^0 in (5.357) into

$$A_n\equiv\frac{M\hbar\beta\nu_n^2}{2}\left(1+\frac{C_\beta}{\Omega}\frac{1}{\nu_n^2+\Omega^2}\right)=A_n^0\left(1+\frac{C_\beta}{\Omega}\frac{1}{\nu_n^2+\Omega^2}\right). \tag{5.363}$$

The trial partition function without external source is then approximately equal to

$$Z^{\Omega,C}\underset{T\approx0}{\equiv}\int\mathcal{D}^3x\int\frac{d^2x_a}{\sqrt{2\pi\hbar^2\beta/M}^3}\prod_{n=1}^{\infty}\sqrt{\frac{A_n^0}{A_n}}^3. \tag{5.364}$$

The product is calculated as follows:

$$\prod_{n=1}^{\infty}\sqrt{\frac{A_n^0}{A_n}}^3=\prod_{n=1}^{\infty}\sqrt{1+\frac{C_\beta}{\Omega}\frac{1}{\nu_n^2+\Omega^2}}^{-3}=e^{-\beta F^{\Omega,C}}, \tag{5.365}$$

resulting in the approximate free energy

$$F^{\Omega,C}\underset{T\approx0}{=}\frac{1}{\beta}\sum_{n=1}^{\infty}\log\frac{\nu_n^2+\Gamma_\beta^2}{\nu_n^2+\Omega^2}, \tag{5.366}$$

where we have introduced the function of the trial frequency Ω:

$$\Gamma_\beta^2(\Omega)\equiv\Omega^2+C_\beta/\Omega. \tag{5.367}$$

With the help of formula (2.173) we find therefore

$$F^{\Omega,C}=\frac{3}{2\beta}\log\frac{\sinh\hbar\beta\Gamma_\beta}{\sinh\hbar\beta\Omega}. \tag{5.368}$$

For simplicity, we shall from now on consider only the low-temperature regime where $C_\beta->C$, $\Gamma_\beta\to\Omega^2+C/\Omega$, and the free energy (5.368) becomes approximately

$$F^{\Omega,C}\underset{T\approx0}{=}\frac{3\hbar}{2}\left(\Gamma-\Omega\right)\equiv E_0^{\Omega,C}. \tag{5.369}$$

The right-hand side is the ground state energy of the harmonic trial system (5.356).

In Feynman's variational approach, the ground state energy of the polaron is smaller than this given by the minimum of [compare (5.18), (5.32) and (5.45)]

$$E_0 \leq E_0^{\Omega,C} + \Delta E_{\rm int}^{\Omega,C} - \Delta E_{\rm int,harm}^{\Omega,C}, \tag{5.370}$$

where the two additional terms are the limits $\beta \to \infty$ of the harmonic expectation values

$$\Delta E_{\rm int}^{\Omega,C} = -\frac{1}{\hbar\beta}\left\langle \mathcal{A}_{\rm int}\right\rangle^{\Omega,C} \equiv \frac{1}{\hbar\beta}\left\langle -\frac{a}{2\sqrt{2}}\int_0^{\hbar\beta} d\tau \int_0^{\hbar\beta} d\tau' \frac{e^{-\omega|\tau-\tau'|}}{|\mathbf{x}(\tau)-\mathbf{x}(\tau')|}\right\rangle^{\Omega,C}, \tag{5.371}$$

and

$$\Delta E_{\rm int,harm}^{\Omega,C} = -\frac{1}{\hbar\beta}\left\langle \mathcal{A}_{\rm int,harm}\right\rangle^{\Omega,C} \equiv \frac{1}{\hbar\beta}\left\langle \frac{C}{2}\int_0^{\hbar\beta} d\tau \int_0^{\hbar\beta} d\tau' \left[\mathbf{x}(\tau)-\mathbf{x}(\tau')\right]^2 e^{-\Omega|\tau-\tau'|}\right\rangle^{\Omega,C}. \tag{5.372}$$

The calculation of the first expectation value is most easily done using the Fourier decomposition (5.345), where we must find the expectation value

$$\left\langle e^{i\mathbf{k}[\mathbf{x}(\tau)-\mathbf{x}(\tau')]}\right\rangle^{\Omega,C}. \tag{5.373}$$

In the trial path integral (5.356), the exponential corresponds to a source

$$\mathbf{j}(\tau'') = \hbar\mathbf{k}\left[\delta^{(3)}(\tau-\tau'') - \delta^{(3)}(\tau'-\tau'')\right], \tag{5.374}$$

in terms of which (5.373) reads

$$\left\langle e^{i\int d\tau \mathbf{j}(\tau)\mathbf{x}(\tau)/\hbar}\right\rangle^{\Omega,C}. \tag{5.375}$$

Introducing the correlation function

$$\left\langle x_i(\tau)x_j(\tau')\right\rangle^{\Omega,C} \equiv \delta_{ij}G^{\Omega,\Gamma}(\tau,\tau'), \tag{5.376}$$

and using Wick's rule (3.309) for harmonically fluctuating paths, the expectation value (5.375) is equal to

$$\left\langle e^{i\int d\tau \mathbf{j}(\tau)\mathbf{x}(\tau)/\hbar}\right\rangle^{\Omega,C} = \exp\left\{-\frac{1}{2\hbar^2}\int_0^{\hbar\beta} d\tau \int_0^{\hbar\beta} d\tau'\, \mathbf{j}(\tau)\, G^{\Omega,\Gamma}(\tau,\tau')\, \mathbf{j}(\tau')\right\}. \tag{5.377}$$

Inserting the special source (5.373), we obtain

$$\left\langle e^{i\mathbf{k}[\mathbf{x}(\tau)-\mathbf{x}(\tau')]}\right\rangle^{\Omega,C} = I^{\Omega,C}(\mathbf{k},\tau,\tau') \equiv \exp\left[\mathbf{k}^2\, \bar{G}^{\Omega,\Gamma}(\tau,\tau')\right], \tag{5.378}$$

where the exponent contains the subtracted Green function

$$\bar{G}^{\Omega,\Gamma}(\tau,\tau') \equiv G^{\Omega,\Gamma}(\tau,\tau') - \frac{1}{2}G^{\Omega,\Gamma}(\tau,\tau) - \frac{1}{2}G^{\Omega,\Gamma}(\tau',\tau'). \tag{5.379}$$

The Green function $G^{\Omega,\Gamma}(\tau,\tau')$ itself has the Fourier expansion

$$G^{\Omega,\Gamma}(\tau,\tau') = \hbar \sum_{n=1}^{\infty} \frac{\sin\nu_n\tau\,\sin\nu_n\tau'}{2A_n/\hbar\beta} = \frac{\hbar}{M}\sum_{n=1}^{\infty}\frac{\nu_n^2+\Omega^2}{\nu_n^2(\nu_n^2+\Gamma_\beta^2)}\sin\nu_n\tau\,\sin\nu_n\tau'. \quad (5.380)$$

It solves the Euler-Lagrange equation which extremizes the action in (5.356) for a source $\mathbf{j}(\tau) = M\delta(\tau-\tau')$:

$$\left\{-\partial_\tau^2 + 2C\int_0^{\hbar\beta} d\tau'\,[x_i(\tau)-x_i(\tau')]\,e^{-\Omega|\tau-\tau'|}_{\rm per}\right\} G^{\Omega,\Gamma}(\tau,\tau') = \delta(\tau-\tau'). \quad (5.381)$$

Decomposing

$$\frac{\nu_n^2+\Omega^2}{\nu_n^2(\nu_n^2+\Gamma_\beta^2)} = \frac{\Omega^2}{\Gamma_\beta^2}\times\frac{1}{\nu_n^2} + \frac{\Gamma_\beta^2-\Omega^2}{\Gamma_\beta^2}\times\frac{1}{\nu_n^2+\Gamma_\beta^2}, \quad (5.382)$$

we obtain a combination of ordinary Green functions of the second-order operator differential equation (3.239), but with Dirichlet boundary conditions. For such Green functions, the spectral sum over n was calculated in Section 3.4 for real time [see (3.36) and (3.145)]. The imaginary-time result is

$$G_{\omega^2}(\tau,\tau') = \sum_{n=1}^{\infty}\frac{\sin\nu_n\tau\,\sin\nu_n\tau'}{\nu_n^2+\omega^2} = \frac{\sinh\omega(\hbar\beta-\tau)\,\sinh\omega\tau'}{\omega\sinh\omega\hbar\beta}, \text{ for } \tau>\tau'>0. \quad (5.383)$$

In the low-temperature limit, this becomes

$$G_{\omega^2}(\tau,\tau') = \frac{1}{2\omega}\left(e^{-\omega(\tau-\tau')} - e^{-\omega(\tau+\tau')}\right), \quad \text{for } \tau>\tau'>0, \quad (5.384)$$

such that

$$\bar{G}_{\Gamma^2}(\tau,\tau') = \frac{1}{2\Gamma}\left(e^{-\Gamma(\tau-\tau')} - 1 - e^{-\Gamma(\tau+\tau')} + \frac{1}{2}e^{-2\Gamma\tau} + \frac{1}{2}e^{-2\Gamma\tau'}\right), \quad \text{for } \tau>\tau'>0. \quad (5.385)$$

In the limit $\Gamma\to 0$, this becomes $-\frac{1}{2}|\tau-\tau'|$. We therefore obtain at zero temperature

$$\bar{G}^{\Omega,\Gamma}(\tau,\tau') \underset{T=0}{=} \frac{\hbar}{2M}\left[\frac{\Omega^2}{\Gamma^2}\bar{G}_0(\tau,\tau') + \frac{\Gamma^2-\Omega^2}{\Gamma^2}\bar{G}_0(\tau,\tau')\right] \quad (5.386)$$

$$= -\frac{\hbar}{2M}\left\{\frac{\Omega^2}{\Gamma^2}|\tau-\tau'| + \frac{\Gamma^2-\Omega^2}{\Gamma^3}\left(1 - e^{-\Gamma|\tau-\tau'|} + e^{-\Gamma(\tau+\tau')} - \frac{1}{2}e^{-2\Gamma\tau} - \frac{1}{2}e^{-2\Gamma\tau'}\right)\right\},$$

to be inserted into (5.378) to get the expectation value $\left\langle e^{i\mathbf{k}[\mathbf{x}(\tau)-\mathbf{x}(\tau')]}\right\rangle$. The last three terms can be avoided by shifting the time interval under consideration and thus the Fourier expansion (5.352) from $(0,\hbar\beta)$ to $(-\hbar\beta/2,\hbar\beta/2)$, which changes Green function (5.387) to

$$\begin{aligned} G_{\omega^2}(\tau,\tau') &= \sum_{n=1}^{\infty}\frac{\sin\nu_n(\tau+\hbar\beta/2)\,\sin\nu_n(\tau'+\hbar\beta/2)}{\nu_n^2+\omega^2} \\ &= \frac{\sinh\omega(\hbar\beta/2-\tau)\,\sinh\omega(\tau'+\hbar\beta/2)}{\omega\sinh\omega\hbar\beta}, \text{ for } \tau>\tau'>0. \end{aligned} \quad (5.387)$$

We have seen before at the end of Section 3.20 that such a shift is important when discussing the limit $T \to 0$ which we want to do in the sequel. With the symmetric limits of integration, the Green function (5.384) loses its last term [compare with (3.147) for real times] and (5.386) simplifies to

$$\bar{G}^{\Omega,\Gamma}(\tau,\tau') \underset{T=0}{\approx} -\frac{\hbar}{2M}\left\{\frac{\Omega^2}{\Gamma^2}|\tau-\tau'| + \frac{\Gamma^2-\Omega^2}{\Gamma^3}\left(1-e^{-\Gamma|\tau-\tau'|}\right)\right\}. \quad (5.388)$$

At any temperature, we have the complicated expression for $\tau > \tau'$:

$$\bar{G}^{\Omega,\Gamma}(\tau,\tau') = -\frac{\hbar}{2M}\left\{\frac{\Omega^2}{\Gamma_\beta^2}\left[\tau-\tau'-\frac{1}{\hbar\beta}(\tau-\tau')^2\right]\right. \quad (5.389)$$
$$\left. -\frac{\Gamma_\beta^2-\Omega^2}{\Gamma_\beta^2\sinh\hbar\beta\Gamma_\beta}\left[\sinh\Gamma_\beta(\hbar\beta/2-\tau)\,\sinh\Gamma_\beta(\tau'+\hbar\beta/2)-(\tau'\to\tau)-(\tau\to\tau')\right]\right\}.$$

With the help of the Fourier integral (5.346) we find from this the expectation value of the interaction in (5.347):

$$\left\langle\frac{1}{|\mathbf{x}(\tau)-\mathbf{x}(\tau')|}\right\rangle = \int\frac{d^3k}{(2\pi)^3}\frac{4\pi}{\mathbf{k}^2}\left\langle e^{i\mathbf{k}[\mathbf{x}(\tau)-\mathbf{x}(\tau')]}\right\rangle = \int\frac{d^3k}{(2\pi)^3}\frac{4\pi}{\mathbf{k}^2}I^{\Omega,C}(\mathbf{k},\tau,\tau'). \quad (5.390)$$

For zero temperature, this leads directly to the expectation value of the interaction in (5.347):

$$\int_0^{\hbar\beta}d\tau\int_0^{\hbar\beta}d\tau'\left\langle\frac{e^{-\omega|\tau-\tau'|}}{|\mathbf{x}(\tau)-\mathbf{x}(\tau')|}\right\rangle \approx 2\hbar\beta\int_0^{\hbar\beta/2}d\Delta\tau\,e^{-\omega\Delta\tau}\int\frac{d^3k}{(2\pi)^3}\frac{4\pi}{\mathbf{k}^2}e^{\mathbf{k}^2\bar{G}^{\Omega,\Gamma}(\Delta\tau,0)}$$
$$\approx 4\frac{\hbar\beta}{\sqrt{2\pi\omega}\lambda_\omega}\int_0^\infty d\Delta\tau\frac{e^{-\omega\Delta\tau}}{\sqrt{-2\bar{G}^{\Omega,\Gamma}(\Delta\tau,0)}}. \quad (5.391)$$

The expectation value of the harmonic trial interaction in (5.356), on the other hand, is simply found from the correlation function (5.376) [or equivalently from the second derivative of $I^{\Omega,C}(\mathbf{k},\tau,\tau')$ with respect to the momenta]:

$$\left\langle[\mathbf{x}(\tau)-\mathbf{x}(\tau')]^2\right\rangle^{\Omega,C} = -6\bar{G}^{\Omega,\Gamma}(\tau,\tau'). \quad (5.392)$$

At low temperatures, this leads to an integral

$$\frac{CM}{2\hbar}\int_0^{\hbar\beta}d\tau\int_0^{\hbar\beta}d\tau'\left\langle[\mathbf{x}(\tau)-\mathbf{x}(\tau')]^2\right\rangle^{\Omega,C}e^{-\Omega|\tau-\tau'|}_{\rm per} \underset{T=0}{=} \hbar\beta\frac{3C}{4\Omega\Gamma}. \quad (5.393)$$

This expectation value contributes to the ground state energy a term

$$\Delta E^{\Omega,C}_{\rm int,\,var} = \frac{3\hbar C}{4\Omega\Gamma}. \quad (5.394)$$

Note that this term can be derived from the derivative of the ground state energy (5.368) as $C\partial_C E_0^{\Omega,C}$. Together with $-a/2\sqrt{2}$ times the result of (5.391), the inequality (5.370) for the ground state energy becomes

$$E_0 \leq \frac{3\hbar}{4\Gamma}(\Gamma-\Omega)^2 - \hbar\omega\frac{\alpha\,\omega}{\sqrt{\pi\omega}}\int_0^\infty d\Delta\tau\frac{e^{-\omega\Delta\tau}}{\sqrt{-2\bar{G}^{\Omega,\Gamma}(\Delta\tau,0)}}. \tag{5.395}$$

This has to be minimized in Ω and C, or equivalently, in Ω and Γ. Considering the low-temperature limit, we have taken the upper limit of integration to infinity (the frequency ω corresponds usually to temperatures of the order of 1000 K).

For small α, the optimal parameters Ω and Γ differ by terms of order α. We can therefore expand the integral in (5.395) and find that the minimum lies, in natural units with $\hbar=\omega=1$, at $\Omega=3$ and $\Gamma=3[1+2\alpha(1-P)/3\Gamma$, where $P=2[(1-\Gamma)^{1/2}-1]$. From this we obtain the upper bound

$$E_0 \leq -\alpha - \frac{\alpha^2}{81} + \ldots \approx -\alpha - 0.0123\alpha^2 + \ldots\ . \tag{5.396}$$

This agrees well with the perturbative result [21]

$$E_{\rm w}^{\rm ex} = -\alpha - 0.0159196220\alpha^2 - 0.000806070048\alpha^3 - O(\alpha^4). \tag{5.397}$$

The second term has the exact value

$$\left[\frac{1}{\sqrt{2}} - \log\left(1+3\sqrt{2}/4\right)\right]\alpha^2. \tag{5.398}$$

In the strong-coupling region, the best parameters are $\Omega=1$, $\Gamma=4\alpha^2/9\pi-[4(\log 2+\gamma/2)-1]$, where $\gamma\approx 0.5773156649$ is the Euler-Mascheroni constant (2.469). At these values, we obtain the upper bound

$$E_0 \leq -\frac{\alpha^2}{3\pi} - 3\left(\frac{1}{4}+\log 2\right) + \mathcal{O}(\alpha^{-2}) \approx -0.1061\alpha - 2.8294 + \mathcal{O}(\alpha^{-2}). \tag{5.399}$$

This agrees reasonably well with the precise strong-coupling expansion [23].

$$E_{\rm s}^{\rm ex} = -0.108513\alpha^2 - 2.836 - O(\alpha^{-2}). \tag{5.400}$$

The numerical results for variational parameters and energy are shown in Table 5.12.

5.22.3 Effective Mass

By performing a shift in the velocity of the path integral (5.347), Feynman calculated also an effective mass for the polaron. The result is

$$M^{\rm eff} = M\left[1+\frac{\alpha}{3}\frac{\omega}{\sqrt{\pi\omega}}\Gamma^2\int_0^\infty d\Delta\tau\frac{(\Delta\tau)^2 e^{-\omega\Delta\tau}}{\sqrt{-2\bar{G}^{\Omega,\Gamma}(\Delta\tau,0)}}\right]. \tag{5.401}$$

Table 5.12 Numerical results for variational parameters and energy.

α	Γ	Ω	E_0	$\Delta E_0^{(2)}$	$E_{\rm tot}$	correction
1	3.110	2.871	-1.01	-0.0035	-1.02	0.35 %
3	3.421	2.560	-3.13	-0.031	-3.16	1.0 %
5	4.034	2.140	-5.44	-0.083	-5.52	1.5 %
7	5.810	1.604	-8.11	-0.13	-8.24	1.6 %
9	9.850	1.282	-11.5	-0.17	-11.7	1.4 %
11	15.41	1.162	-15.7	-0.22	-15.9	1.4 %
15	30.08	1.076	-26.7	-0.39	-27.1	1.5 %

The reduced effective mass $m \equiv M^{\rm eff}/M$ has the weak-coupling expansion

$$m_{\rm w} = 1 + \frac{\alpha}{6} + 2.469136 \times 10^{-2}\alpha^2 + 3.566719 \times 10^{-3}\alpha^3 + \ldots \quad (5.402)$$

and behaves for strong couplings like

$$\begin{aligned} m_{\rm s} &\approx \frac{16}{81\pi^2}\alpha^4 - \frac{4}{3\pi}\left(1+\log 4\right)\alpha^2 + 11.85579 + \ldots \\ &\approx 0.020141\alpha^4 - 1.012775\alpha^2 + 11.85579 + \ldots . \end{aligned} \quad (5.403)$$

The exact expansions are [31]

$$m_{\rm w}^{\rm ex} = 1 + \frac{\alpha}{6} + 2.362763 \times 10^{-2}\alpha^2 + O(\alpha^4), \quad (5.404)$$

$$m_{\rm s}^{\rm ex} = 0.0227019\alpha^4 + O(\alpha^2). \quad (5.405)$$

5.22.4 Second-Order Correction

With some effort, also the second-order contribution to the variational energy has been calculated at zero temperature [32]. It gives a contribution to the ground state energy

$$\Delta E_0^{(2)} = -\frac{1}{2\hbar\beta}\frac{1}{\hbar^2}\left\langle \left(\mathcal{A}_{\rm int} - \mathcal{A}_{\rm int,harm}\right)^2 \right\rangle_c^{\Omega,C}. \quad (5.406)$$

Recall the definitions of the interactions in Eqs. (5.371) and (5.372). There are three terms

$$\Delta E_0^{(2,1)} = -\frac{1}{2\hbar\beta}\frac{1}{\hbar^2}\left\{ \left\langle \mathcal{A}_{\rm int}^2 \right\rangle^{\Omega,C} - \left[\langle \mathcal{A}_{\rm int} \rangle^{\Omega,C} \right]^2 \right\}, \quad (5.407)$$

$$\Delta E_0^{(2,2)} = 2\frac{1}{2\hbar\beta}\frac{1}{\hbar^2}\left\{ \langle \mathcal{A}_{\rm int}\mathcal{A}_{\rm int,harm} \rangle^{\Omega,C} - \langle \mathcal{A}_{\rm int} \rangle^{\Omega,C} \langle \mathcal{A}_{\rm int,harm} \rangle^{\Omega,C} \right\}, \quad (5.408)$$

and

$$\Delta E_0^{(2,3)} = -\frac{1}{2\hbar\beta}\frac{1}{\hbar^2}\left\{\left\langle \mathcal{A}^2_{\rm int,harm}\right\rangle^{\Omega,C} - \left[\left\langle \mathcal{A}_{\rm int,harm}\right\rangle^{\Omega,C}\right]^2\right\}. \tag{5.409}$$

The second term can be written as

$$\Delta E_0^{(2,2)} = -\frac{1}{2\hbar\beta}\frac{1}{\hbar^2}\left\{-2C\partial_C \left\langle \mathcal{A}_{\rm int}\right\rangle^{\Omega,C}\right\}, \tag{5.410}$$

the third as

$$\Delta E_0^{(2,3)} = -\frac{1}{2\hbar\beta}\frac{1}{\hbar^2}\left\{\{1-C\partial_C\left\langle \mathcal{A}_{\rm int,harm}\right\rangle^{\Omega,C}\right\}. \tag{5.411}$$

The final expression is rather involved and given in Appendix 5C. The second-order correction leads to the second term (5.398) found in perturbation theory. In the strong coupling limit, it changes the leading term $-\alpha^2/3\pi \approx -0.1061$ in (5.399) into

$$-\frac{1}{4\pi}-\frac{2}{\pi}\sum_{n=1}^{\infty}\frac{(2n)!}{2^{4n}(n!)^2 n(2n+1)} = \frac{-17+64\arcsin(\frac{\sqrt{2-\sqrt{3}}}{2})-32\log(4\frac{\sqrt{2-\sqrt{3}}}{2})}{4\,\pi}, \tag{5.412}$$

which is approximately equal to -0.1078. The corrections are shown numerically in the previous Table 5.12.

5.22.5 Polaron in Magnetic Field, Bipolarons, Small Polarons, Polaronic Excitons, and More

Feynman's solution of the polaron problem has instigated a great deal of research on this subject [34]. There are many publications dealing with a polaron in a magnetic field. In particular, there was considerable discussion on the validity of the Jensen-Peierls inequality (5.10) in the presence of a magnetic field until it was shown by Larsen in 1985 that the variational energy does indeed lie below the exact energy for sufficiently strong magnetic fields. On the basis of this result he criticized the entire approach. The problem was, however, solved by Devreese and collaborators who determined the range of variational parameters for which the inequality remained valid.

In the light of the systematic higher-order variational perturbation theory developed in this chapter we do not consider problems with the inequality any more as an obstacle to variational procedures. The optimization procedure introduced in Section 5.13 for even and odd approximations does not require an inequality. We have seen that for higher orders, the exact result will be approached rapidly with exponential convergence. The inequality is useful only in Feynman's original lowest-order variational approach where it is important to know the direction of the error. For higher orders, the importance of this information decreases rapidly since the convergence behavior allows us to estimate the limiting value quantitatively, whereas the inequality tells us merely the sign of the error which is often quite large in the lowest-order variational approach, for instance in the Coulomb system.

There is also considerable interest in bound states of two polarons called bipolarons. Such investigations have become popular since the discovery of high-temperature superconductivity.[3]

5.22.6 Variational Interpolation for Polaron Energy and Mass

Let us apply the method of variational interpolation developed in Section 5.18 to the polaron. Starting from the presently known weak-coupling expansions (5.397) and (5.404) we fix a few more expansion coefficients such that the curves fit also the strong-coupling expansions (5.400) and (5.405). We find it convenient to make the series start out with α^0 by removing an overall factor $-\alpha$ from E and deal with the quantity $-E_{\rm w}^{\rm ex}/\alpha$. Then we see from (5.400) that the correct leading power in the strong-coupling expansion requires taking $p = 1, q = 1$. The knowledge of b_0 and b_1 allows us to extend the known weak coupling expansion (5.397) by two further expansion terms. Their coefficients a_3, a_4 are solutions of the equations [recall (5.245)]

$$b_0 = \frac{35}{128}a_0 c + a_1 + \frac{15}{8}\frac{a_2}{c} + \frac{2a_3}{c^2} + \frac{a_4}{c^3}, \tag{5.413}$$

$$b_1 = \frac{35}{32}\frac{a_0}{c} - \frac{5}{4}\frac{a_2}{c^3} - \frac{a_3}{c^3}. \tag{5.414}$$

The constant c governing the growth of Ω_N for $\alpha \to \infty$ is obtained by extremizing b_0 in c, which yields the equation

$$\frac{35}{128}a_0 - \frac{15}{8}\frac{a_2}{c^2} - \frac{4a_3}{c^3} - \frac{4a_4}{c^5} = 0. \tag{5.415}$$

The simultaneous solution of (5.413)–(5.415) renders

$$\begin{aligned} c_4 &= 0.09819868, \\ a_3 &= 6.43047343 \times 10^{-4}, \\ a_4 &= -8.4505836 \times 10^{-5}. \end{aligned} \tag{5.416}$$

The re-expanded energy (5.238) reads explicitly as a function of α and Ω (for E including the earlier-removed factor $-\alpha$)

$$\begin{aligned} W_4(\alpha,\Omega) &= a_0\alpha\left(-\frac{35}{128}\Omega - \frac{35}{32\Omega} + \frac{35}{64\Omega^3} - \frac{7}{32\Omega^5} + \frac{5}{128\Omega^7}\right) - a_1\alpha^2 \\ &+ a_2\alpha^3\left(-\frac{15}{8\Omega} + \frac{5}{4\Omega^3} - \frac{3}{8\Omega^5}\right) + a_3\alpha^4\left(-\frac{2}{\Omega^2} + \frac{1}{\Omega^4}\right) - a_4\alpha^5\frac{1}{\Omega^3}. \end{aligned} \tag{5.417}$$

Extremizing this we find Ω_4 as a function of α [it turns out to be quite well approximated by the simple function $\Omega_4 \approx c_4\alpha + 1/(1+0.07\alpha)$]. This is to be compared with the optimal frequency obtained from minimizing the lower approximation $W_2(\alpha,\Omega)$:

$$\Omega_2^2 = 1 + \frac{4a_2}{3a_0}x^2 + \sqrt{\left(1 + \frac{4a_2}{3a_0}x^2\right)^2 - 1}, \tag{5.418}$$

which behaves like $c_2\alpha+1+\ldots$ with $c_2=\sqrt{8a_2/3a_0}\approx 0.120154$. The resulting energy is shown in Fig. 5.28, where it is compared with the Feynman variational energy. For completeness, we have also plotted the weak-coupling expansion, the strong-coupling expansion, the lower approximation $W_2(\alpha)$, and two Padé approximants given in Ref. [22] as upper and lower bounds to the energy.

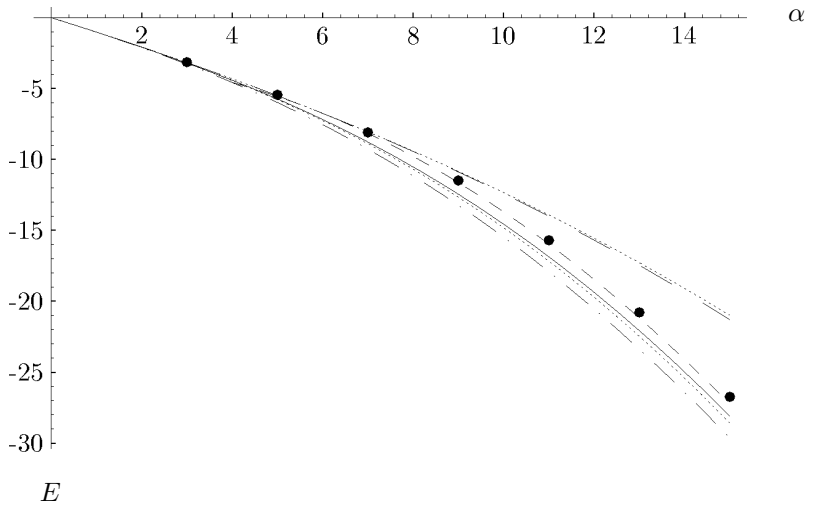

Figure 5.28 Variational interpolation of polaron energy (solid line) between the weak-coupling expansion (dashed) and the strong-coupling expansion (short-dashed) shown in comparison with Feynman's variational approximation (fat dots), which is an upper bound to the energy. The dotted curves are upper and lower bounds coming from Padé approximants [22]. The dot-dashed curve shows the variational perturbation theory $W_2(\alpha)$ which does not make use of the strong-coupling information.

Consider now the effective mass of the polaron, where the strong-coupling behavior (5.405) fixes $p=4, q=1$. The coefficient b_0 allows us to determine an approximate coefficient a_3 and to calculate the variational perturbation expansion $W_3(\alpha)$. From (5.245) we find the equation

$$b_0=-a_1c^3/8+a_3c, \tag{5.419}$$

whose minimum lies at $c_3=\sqrt{8a_2/3a_0}$ where $b_0=\sqrt{32a_3^3/27a_1}$. Equating b_0 of Eq. (5.419) with the leading coefficient in the strong-coupling expansion (5.405), we obtain $a_3=[27a_1b_0^2/32]^{1/3}\approx 0.0416929$.

The variational expression for the polaron mass is from (5.238)

$$W_3(\alpha,\omega)=a_0+a_1\alpha\left(-\frac{\Omega^3}{8}+\frac{3\Omega}{4}+\frac{3}{8\Omega}\right)+a_2\alpha^2+a_3\alpha^3\Omega. \tag{5.420}$$

This is extremal at

$$\Omega_3^2=1+\frac{4a_3}{3a_1}x^2+\sqrt{\left(1+\frac{4a_3}{3a_1}x^2\right)^2-1}. \tag{5.421}$$

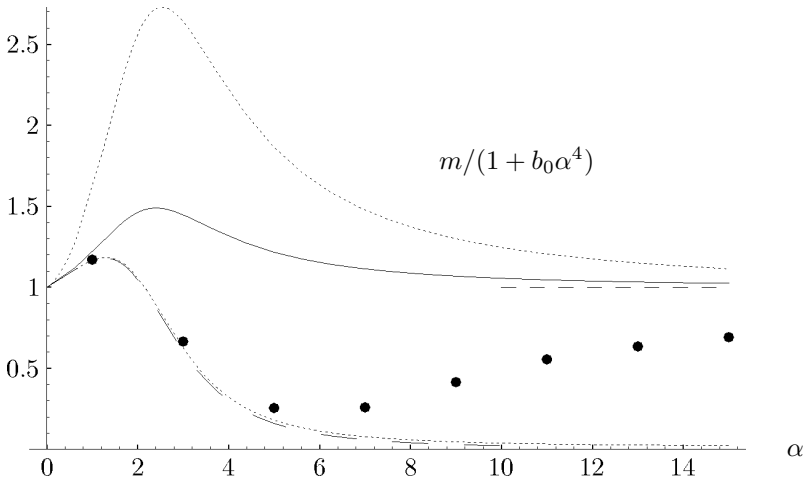

Figure 5.29 Variational interpolation of polaron effective mass between the weak- (dashed) and strong-coupling expansions (short-dashed). To see better the differences between the strongly rising functions, we have divided out the asymptotic behavior $m_{\rm as} = 1 + b_0\alpha^4$ before plotting the curves. The fat dots show Feynman's variational approximation. The dotted curves are upper and lower bounds coming from Padé approximants [22].

From this we may find once more $c_3 = \sqrt{8a_2/3a_0}$. The approximation $W_3(\alpha) = W_3(\alpha, \Omega_3)$ for the polaron mass is shown in Fig. 5.29, where it is compared with the weak and strong-coupling expansions and with Feynman's variational result. To see better the differences between the curves which all grow fast with α, we have divided out the asymptotic behavior $m_{\rm as} = 1 + b_0\alpha^4$ before plotting the data. As for the energy, we have again displayed two Padé approximants given in Ref. [22] as upper and lower bounds to the energy. Note that our interpolation differs considerably from Feynman's and higher order expansion coefficients in the weak- or the strong-coupling expansions will be necessary to find out which is the true behavior of the model.

Our curve has, incidentally, the strong-coupling expansion

$$m^{\rm s} = 0.0227019\alpha^4 + 0.125722\alpha^2 + 1.15304 + O(\alpha^{-2}), \tag{5.422}$$

the second term $\propto \alpha^2$-term being in sharp contrast with Feynman's expression (5.403). On the weak-coupling side, a comparison of our expansion with Feynman's in Eq. (5.402) shows that our coefficient $a_3 \approx 0.0416929$ is about 10 times larger than his.

Both differences are the reason for our curve forming a positive arch in Fig. 2, whereas Feynman's has a valley. It will be interesting to find out how the polaron mass really behaves. This would be possible by calculating a few more terms in either the weak- or the strong-coupling expansion.

Note that our interpolation algorithm is much more powerful than Padé's. First, we can account for an arbitrary fractional leading power behavior α^p as $\alpha \to \infty$. Second, the successive lower powers in the strong-coupling expansion can be spaced by an arbitrary $2/q$. Third, our functions have in general a cut in the complex α-plane approximating the cuts in the function to be interpolated (see the discussion in Subsection 17.10.4). Padé approximants, in contrast, have always an integer power behavior in the strong-coupling limit, a unit spacing in the strong-coupling expansion, and poles to approximate cuts.

5.23 Density Matrices

In path integrals with fixed end points, the separate treatment of the path average $x_0 \equiv (1/\hbar\beta)\int_0^{\hbar\beta} d\tau\, x(\tau)$ loses its special virtues. Recall that the success of this separation in the variational approach was based on the fact that for fixed x_0, the fluctuation square width $a^2(x_0)$ shrinks to zero for large temperatures like $\hbar^2/12Mk_BT$ [recall (5.25)]. A similar shrinking occurs for paths whose endpoints held fixed, which is the case in path integrals for the density. Thus there is no need for a separate treatment of x_0, and one may develop a variational perturbation theory for fixed endpoints instead. These may, moreover, be taken to be different from one another $x_b \neq x_a$, thus allowing us to calculate directly density matrices.[4]

The density matrix is defined by the normalized expression

$$\rho(x_b, x_a) = \frac{1}{Z}\tilde{\rho}(x_b, x_a)\,, \tag{5.423}$$

where $\tilde{\rho}(x_b, x_a)$ is the unnormalized transition amplitude given by the path integral

$$\tilde{\rho}(x_b, x_a) = (x_b\, \hbar\beta | x_a 0) = \int\limits_{(x_a,0)\rightsquigarrow(x_b,\hbar/k_BT)} \mathcal{D}x\, \exp\left\{-\mathcal{A}[x]/\hbar\right\}, \tag{5.424}$$

summing all paths with the fixed endpoints $x(0) = x_a$ and $x(\hbar/k_BT) = x_b$. The diagonal matrix elements of the density matrix in the integrand yield, of course, the particle density (5.90). The diagonal elements coincide with the partition function density $z(x)$ introduced in Eq. (2.333).

The partition function divided out in (5.423) is found from the trace

$$Z = \int\limits_{-\infty}^{\infty} dx\, \tilde{\rho}(x, x). \tag{5.425}$$

5.23.1 Harmonic Oscillator

As usual in the variational approach, we shall base the approximations to be developed on the exactly solvable density matrix of the harmonic oscillator. For the sake of generality, this will be assumed to be centered around x_m, with an action

$$\mathcal{A}_{\Omega,x_m}[x] = \int_0^{\hbar/k_BT} d\tau\, \left\{\frac{1}{2}M\dot{x}^2(\tau) + \frac{1}{2}M\Omega^2[x(\tau) - x_m]^2\right\}. \tag{5.426}$$

[4] H. Kleinert, M. Bachmann, and A. Pelster, Phys. Rev. A *60* , 3429 (1999) (quant-ph/9812063).

Its unnormalized density matrix is [see (2.411)]

$$\tilde{\rho}_0^{\,\Omega,x_m}(x_b,x_a)=\sqrt{\frac{M\Omega}{2\pi\hbar\sinh\hbar\Omega/k_BT}} \times\exp\left\{-\frac{M\Omega}{2\hbar\sinh\hbar\Omega/k_BT}\left[(\tilde{x}_b^2+\tilde{x}_a^2)\cosh\hbar\Omega/k_BT-2\tilde{x}_b\tilde{x}_a\right]\right\}, \quad (5.427)$$

with the abbreviation

$$\tilde{x}(\tau)\equiv x(\tau)-x_m. \quad (5.428)$$

At fixed endpoints x_b, x_a and oscillation center x_m, the quantum-mechanical correlation functions are given by the path integral

$$\langle\, O_1(x(\tau_1))\, O_2(x(\tau_2))\cdots\rangle_{x_b,x_a}^{\Omega,x_m}=\frac{1}{\tilde{\rho}_0^{\,\Omega,x_m}(x_b,x_a)} \times\int\limits_{(x_a,0)\rightsquigarrow(x_b,\hbar/k_BT)}\mathcal{D}x\, O_1(x(\tau_1))\, O_2(x(\tau_2))\cdots\exp\left\{-\mathcal{A}_{\Omega,x_m}[x]/\hbar\right\}. \quad (5.429)$$

The path $x(\tau)$ at a fixed imaginary time τ has a distribution

$$p(x,\tau)\equiv\langle\,\delta(x-x(\tau))\,\rangle_{x_b,x_a}^{\Omega,x_m}=\frac{1}{\sqrt{2\pi b^2(\tau)}}\exp\left[-\frac{(\tilde{x}-x_{\rm cl}(\tau))^2}{2b^2(\tau)}\right], \quad (5.430)$$

where $x_{\rm cl}(\tau)$ is the classical path of a particle in the harmonic potential

$$x_{\rm cl}(\tau)=\frac{\tilde{x}_b\sinh\Omega\tau+\tilde{x}_a\sinh\Omega(\hbar/k_BT-\tau)}{\sinh\hbar\Omega/k_BT}, \quad (5.431)$$

and $b^2(\tau)$ is the square width

$$b^2(\tau)=\frac{\hbar}{2M\Omega}\left\{\coth\frac{\hbar\Omega}{k_BT}-\frac{\cosh[\Omega(2\tau-\hbar/k_BT)]}{\sinh\hbar\Omega/k_BT}\right\}. \quad (5.432)$$

In contrast to the square width $a^2(x_0)$ in Eq. (5.24) this depends on the Euclidean time τ, which makes calculations more cumbersome than before. Since the τ lies in the interval $0\le\tau\le\hbar/k_BT$, the width (5.432) is bounded by

$$b^2(\tau)\le\frac{\hbar}{2M\Omega}\tanh\frac{\hbar\Omega}{2k_BT}, \quad (5.433)$$

thus sharing with $a^2(x_0)$ the property of remaining finite at all temperatures. The temporal average of (5.432) is

$$\overline{b^2}=\frac{k_BT}{\hbar}\int_0^{\hbar/k_BT}d\tau\, b^2(\tau)=\frac{\hbar}{2M\Omega}\left(\coth\frac{\hbar\Omega}{k_BT}-\frac{k_BT}{\hbar\Omega}\right). \quad (5.434)$$

Just as $a^2(x_0)$, this goes to zero for $T\to\infty$. Note however, that the asymptotic behavior is

$$\overline{b^2}\underset{T\to\infty}{\longrightarrow}\hbar\Omega/6k_BT, \quad (5.435)$$

which is twice as big as that of $a^2(x_0)$ in Eq. (5.25) (see Fig. 5.30).

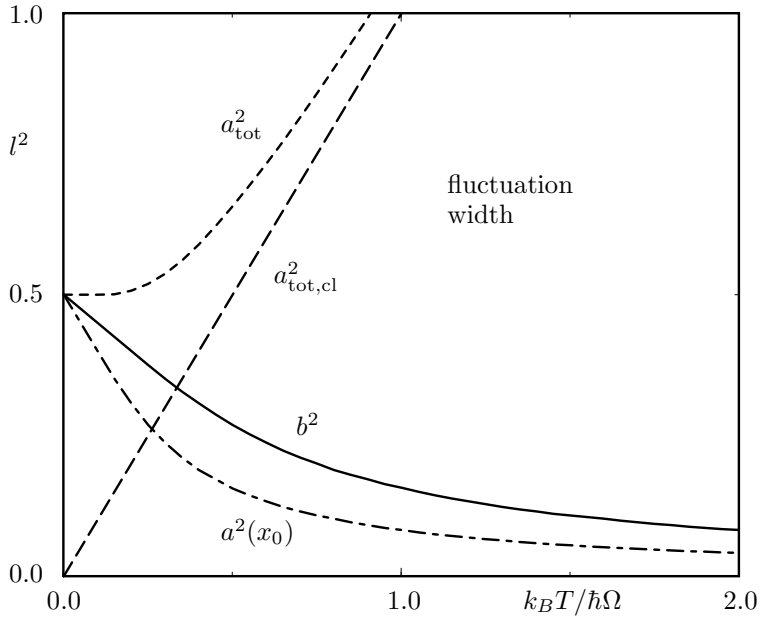

Figure 5.30 Temperature dependence of fluctuation widths of any point $x(\tau)$ on the path in a harmonic oscillator (l^2 is the generic square length in units of $\hbar/M\Omega$). The quantity a^2 (dashed) is the quantum-mechanical width, whereas $a^2(x_0)$ (dash-dotted) shares the width after separating out the fluctuations around the path average x_0. The quantity a^2_{cl} (long-dashed) is the width of the classical distribution, and b^2 (solid curve) is the fluctuation width at fixed ends which is relevant for the calculation of the density matrix by variational perturbation theory (compare Fig. 3.14).

5.23.2 Variational Perturbation Theory for Density Matrices

To obtain a variational approximation for the density matrix, we separate the full action into the harmonic trial action and a remainder

$$\mathcal{A}[x] = \mathcal{A}_{\Omega,x_m}[x] + \mathcal{A}_{\rm int}[x], \tag{5.436}$$

with an interaction

$$\mathcal{A}_{\rm int}[x(\tau)] = \int_0^{\hbar\beta} d\tau\, V_{\rm int}(x(\tau)), \tag{5.437}$$

where the interaction potential is the difference between the original one $V(x)$ and the inserted displaced harmonic oscillator:

$$V_{\rm int}(x(\tau)) = V(x(\tau)) - \frac{1}{2}M\Omega^2[x(\tau)-x_m]^2. \tag{5.438}$$

The path integral (5.424) is then expanded perturbatively around the harmonic expression (5.427) as

$$\tilde\rho(x_b,x_a) = \tilde\rho_0{}^{\Omega,x_m}(x_b,x_a)\left[1-\frac{1}{\hbar}\langle\,\mathcal{A}_{\rm int}[x]\,\rangle^{\Omega,x_m}_{x_b,x_a}+\frac{1}{2\hbar^2}\Big\langle\,\mathcal{A}^2_{\rm int}[x]\,\Big\rangle^{\Omega,x_m}_{x_b,x_a}-\ldots\right], \tag{5.439}$$

with the harmonic expectation values defined in (5.429). The sum can be evaluated as an exponential of its connected parts, going over to the cumulant expansion:

$$\tilde{\rho}(x_b,x_a)=\tilde{\rho}_0{}^{\Omega,x_m}(x_b,x_a)\exp\left[-\frac{1}{\hbar}\langle\,\mathcal{A}_{\rm int}[x]\,\rangle^{\Omega,x_m}_{x_b,x_a,c}+\frac{1}{2\hbar^2}\Big\langle\,\mathcal{A}^2_{\rm int}[x]\,\Big\rangle^{\Omega,x_m}_{x_b,x_a,c}-\ldots\right], \tag{5.440}$$

where the cumulants are defined as usual [see (3.485), (3.486)]. The series (5.440) is truncated after the N-th term, resulting in the N-th order approximant for the quantum statistical density matrix

$$\tilde{\rho}_N{}^{\Omega,x_m}(x_b,x_a)=\tilde{\rho}_0{}^{\Omega,x_m}(x_b,x_a)\exp\left[\sum_{n=1}^{N}\frac{(-1)^n}{n!\hbar^n}\,\langle\,\mathcal{A}^n_{\rm int}[x]\,\rangle^{\Omega,x_m}_{x_b,x_a,c}\right], \tag{5.441}$$

which explicitly depends on the two variational parameters Ω and x_m.

By analogy with classical statistics, where the Boltzmann distribution in configuration space is controlled by the classical potential $V(x)$ according to [recall (2.354)]

$$\tilde{\rho}_{\rm cl}(x)=\sqrt{\frac{M}{2\pi\hbar^2\beta}}\exp\left[-\beta V(x)\right], \tag{5.442}$$

we shall now work with the alternative type of *effective classical potential* $\tilde{V}^{\rm eff,cl}(x_a,x_b)$ introduced in Subsection 3.25.4. It governs the unnormalized density matrix [see Eq. (3.837)]

$$\tilde{\rho}(x_b,x_a)=\sqrt{\frac{M}{2\pi\hbar^2\beta}}\exp\left[-\beta\tilde{V}^{\rm eff,cl}(x_b,x_a)\right]. \tag{5.443}$$

Variational approximations to $\tilde{V}^{\rm eff,cl}(x_b,x_a)$ of Nth order are obtained from (5.427), (5.441), and (5.443) as a cumulant expansion

$$\begin{aligned}\tilde{W}_N^{\Omega,x_m}(x_b,x_a) &= \frac{1}{2\beta}\ln\frac{\sinh\hbar\beta\Omega}{\hbar\beta\Omega}+\frac{M\Omega}{2\hbar\beta\sinh\hbar\beta\Omega}\left\{(\tilde{x}_b^2+\tilde{x}_a^2)\cosh\hbar\beta\Omega-2\tilde{x}_b\tilde{x}_a\right\}\\ &- \frac{1}{\beta}\sum_{n=1}^{N}\frac{(-1)^n}{n!\hbar^n}\,\langle\,\mathcal{A}^n_{\rm int}[x]\,\rangle^{\Omega,x_m}_{x_b,x_a,c}.\end{aligned} \tag{5.444}$$

They have to be optimized in the variational parameters Ω and x_m for a pair of endpoints x_b,x_a. The result is denoted by $\tilde{W}_N(x_b,x_a)$. The optimal values $\Omega(x_a,x_b)$ and $x_m(x_a,x_b)$ are denoted by $\Omega_N(x_a,x_b),x_m^N(x_a,x_b)$. The Nth-order approximation for the normalized density matrix is then given by

$$\rho_N(x_b,x_a)=Z_N^{-1}\tilde{\rho}_N{}^{\Omega_N^2,x_m^N}(x_b,x_a), \tag{5.445}$$

where the corresponding partition function reads

$$Z_N=\int_{-\infty}^{\infty}dx_a\,\tilde{\rho}_N{}^{\Omega_N^2,x_m^N}(x_a,x_a). \tag{5.446}$$

In principle, one could also optimize the entire ratio (5.445), but this would be harder to do in practice. Moreover, the optimization of the unnormalized density matrix is the only option, if the normalization diverges due to singularities of the potential, for example in the hydrogen atom

5.23.3 Smearing Formula for Density Matrices

In order to calculate the connected correlation functions in the variational perturbation expansion (5.441), we must find efficient formulas for evaluating expectation values (5.429) of any power of the interaction (5.437)

$$\begin{aligned}\langle\, \mathcal{A}^n_{\rm int}[x]\,\rangle^{\Omega,x_m}_{x_b,x_a} &= \frac{1}{\tilde\rho_0{}^{\Omega,x_m}(x_b,x_a)}\int\limits_{\tilde x_a,0}^{\tilde x_b,\hbar\beta}\mathcal{D}\tilde x\,\prod_{l=1}^{n}\left[\int_0^{\hbar\beta}d\tau_l\,V_{\rm int}(\tilde x(\tau_l)+x_m)\right]\\ &\times\ \exp\left\{-\frac{1}{\hbar}\mathcal{A}_{\Omega,x_m}[\tilde x+x_m]\right\}.\end{aligned}\tag{5.447}$$

This can be done by an extension of the smearing formula (5.30). For this we rewrite the interaction potential as

$$V_{\rm int}(\tilde x(\tau_l)+x_m)=\int\limits_{-\infty}^{\infty}dz_l\,V_{\rm int}(z_l+x_m)\int\limits_{-\infty}^{\infty}\frac{d\lambda_l}{2\pi}e^{i\lambda_l z_l}\exp\left[-\int_0^{\hbar\beta}d\tau\,i\lambda_l\delta(\tau-\tau_l)\tilde x(\tau)\right],\tag{5.448}$$

and introduce a current

$$J(\tau)=\sum_{l=1}^{n}i\hbar\lambda_l\delta(\tau-\tau_l),\tag{5.449}$$

so that (5.447) becomes

$$\langle\, \mathcal{A}^n_{\rm int}[x]\,\rangle^{\Omega,x_m}_{x_b,x_a}=\frac{1}{\tilde\rho_0{}^{\Omega,x_m}(x_b,x_a)}\prod_{l=1}^{n}\left[\int_0^{\hbar\beta}d\tau_l\int_{-\infty}^{\infty}dz_lV_{\rm int}(z_l+x_{\rm min})\int_{-\infty}^{\infty}\frac{d\lambda_l}{2\pi}e^{i\lambda_l z_l}\right]K^{\Omega,x_m}[j].\tag{5.450}$$

The kernel $K^{\Omega,x_m}[j]$ represents the generating functional for all correlation functions of the displaced harmonic oscillator

$$K^{\Omega,x_m}[j]=\int\limits_{\tilde x_a,0}^{\tilde x_b,\hbar\beta}\mathcal{D}\tilde x\,\exp\left\{-\frac{1}{\hbar}\int_0^{\hbar\beta}d\tau\left[\frac{m}{2}\dot{\tilde x}^2(\tau)+\frac{1}{2}M\Omega^2\tilde x^2(\tau)+j(\tau)\tilde x(\tau)\right]\right\}.\tag{5.451}$$

For zero current j, this generating functional reduces to the Euclidean harmonic propagator (5.427):

$$K^{\Omega,x_m}[j=0]=\tilde\rho_0{}^{\Omega,x_m}(x_b,x_a),\tag{5.452}$$

and the solution of the functional integral (5.451) is given by (recall Section 3.1)

$$\begin{aligned}K^{\Omega,x_m}[j]\ =\ \tilde\rho_0{}^{\Omega,x_m}(x_b,x_a)\exp\Bigg[&-\frac{1}{\hbar}\int_0^{\hbar\beta}d\tau\,j(\tau)\,x_{\rm cl}(\tau)\\ &+\frac{1}{2\hbar^2}\int_0^{\hbar\beta}d\tau\int_0^{\hbar\beta}d\tau'\,j(\tau)\,G^{(2)}_{\Omega^2}(\tau,\tau')\,j(\tau')\Bigg],\end{aligned}\tag{5.453}$$

where $x_{\rm cl}(\tau)$ denotes the classical path (5.431) and $G^{(2)}_{\Omega^2}(\tau,\tau')$ the harmonic Green function with Dirichlet boundary conditions (3.389), to be written here as

$$G^{(2)}_{\Omega^2}(\tau,\tau') = \frac{\hbar}{2M\Omega}\frac{\cosh\Omega(|\tau-\tau'|-\hbar\beta)-\cosh\Omega(\tau+\tau'-\hbar\beta)}{\sinh\hbar\beta\Omega}. \tag{5.454}$$

The expression (5.453) can be simplified by using the explicit expression (5.449) for the current j. This leads to a generating functional

$$K^{\Omega,x_m}[j] = \tilde{\rho}_0{}^{\Omega,x_m}(x_b,x_a)\,\exp\left(-i\boldsymbol{\lambda}^T\mathbf{x}_{\rm cl}-\frac{1}{2}\boldsymbol{\lambda}^T G\,\boldsymbol{\lambda}\right), \tag{5.455}$$

where we have introduced the n-dimensional vectors $\boldsymbol{\lambda}=(\lambda_1,\ldots,\lambda_n)$ and $\mathbf{x}_{\rm cl}=(x_{\rm cl}(\tau_1),\ldots,x_{\rm cl}(\tau_n))^T$ with the superscript T denoting transposition, and the symmetric $n\times n$-matrix G whose elements are $G_{kl}=G^{(2)}_{\Omega^2}(\tau_k,\tau_l)$. Inserting (5.455) into (5.450), and performing the integrals with respect to $\lambda_1,\ldots,\lambda_n$, we obtain the n-th order smearing formula for the density matrix

$$\begin{aligned}\langle\,\mathcal{A}^n_{\rm int}[x]\,\rangle^{\Omega,x_m}_{x_b,x_a} &= \prod_{l=1}^{n}\left[\int_0^{\hbar\beta}d\tau_l\int_{-\infty}^{\infty}dz_l\,V_{\rm int}(z_l+x_m)\right]\\ &\times\frac{1}{\sqrt{(2\pi)^n\det G}}\exp\left\{-\frac{1}{2}\sum_{k,l=1}^{n}\left[z_k-x_{\rm cl}(\tau_k)\right]G^{-1}_{kl}\left[z_l-x_{\rm cl}(\tau_l)\right]\right\}.\end{aligned} \tag{5.456}$$

The integrand contains an n-dimensional Gaussian distribution describing both thermal and quantum fluctuations around the harmonic classical path $x_{\rm cl}(\tau)$ of Eq. (5.431) in a trial oscillator centered at x_m, whose width is governed by the Green functions (5.454).

For closed paths with coinciding endpoints ($x_b=x_a$), formula (5.456) leads to the n-th order smearing formula for particle densities

$$\rho(x_a)=\frac{1}{Z}\tilde{\rho}(x_a,x_a)=\frac{1}{Z}\oint\mathcal{D}x\,\delta(x(\tau=0)-x_a)\,\exp\{-\mathcal{A}[x]/\hbar\}, \tag{5.457}$$

which can be written as

$$\begin{aligned}\langle\,\mathcal{A}^n_{\rm int}[x]\,\rangle^{\Omega,x_m}_{x_a,x_a} &= \frac{1}{\rho_0^{\Omega,x_m}(x_a)}\prod_{l=1}^{n}\left[\int_0^{\hbar\beta}d\tau_l\int_{-\infty}^{\infty}dz_l\,V_{\rm int}(z_l+x_m)\right]\\ &\times\frac{1}{\sqrt{(2\pi)^{n+1}\det a^2}}\exp\left(-\frac{1}{2}\sum_{k,l=0}^{n}z_k\,a^{-2}_{kl}\,z_l\right),\end{aligned} \tag{5.458}$$

with $z_0=\tilde{x}_a$. Here a denotes a symmetric $(n+1)\times(n+1)$-matrix whose elements $a^2_{kl}=a^2(\tau_k,\tau_l)$ are obtained from the harmonic Green function for periodic paths $G^{(2)}_{\Omega^2}(\tau,\tau')$ of Eq. (3.304):

$$a^2(\tau,\tau')\equiv\frac{\hbar}{M}G^{(2)}_{\Omega^2}(\tau,\tau')=\frac{\hbar}{2M\Omega}\frac{\cosh\Omega(|\tau-\tau'|-\hbar\beta/2)}{\sinh\hbar\beta\Omega/2}. \tag{5.459}$$

The diagonal elements $a^2 = a(\tau,\tau)$ are all equal to the fluctuation square width (5.24).

Both smearing formulas (5.456) and (5.458) allow us to calculate all harmonic expectation values for the variational perturbation theory of density matrices and particle densities in terms of ordinary Gaussian integrals. Unfortunately, in many applications containing nonpolynomial potentials, it is impossible to solve neither the spatial nor the temporal integrals analytically. This circumstance drastically increases the numerical effort in higher-order calculations.

5.23.4 First-Order Variational Approximation

The first-order variational approximation gives usually a reasonable estimate for any desired quantity. Let us investigate the classical and the quantum-mechanical limit of this approximation. To facilitate the discussion, we first derive a new representation for the first-order smearing formula (5.458) which allows a direct evaluation of the imaginary time integral. The resulting expression will depend only on temperature, whose low- and high-temperature limits can easily be extracted.

Alternative First-Order Smearing Formula

For simplicity, we restrict ourselves to the case of particle densities and allow only symmetric potentials $V(x)$ centered at the origin. If $V(x)$ has only one minimum at the origin, then also x_m will be zero. If $V(x)$ has several symmetric minima, then x_m goes to zero only at sufficiently high temperatures as in Section 5.7.

To first order, the smearing formula (5.458) reads

$$\langle\, \mathcal{A}_{\rm int}[x]\,\rangle^{\Omega}_{x_a,x_a} = \frac{1}{\rho_0^{\Omega}(x_a)} \int_0^{\hbar\beta} d\tau \int_{-\infty}^{\infty} \frac{dz}{2\pi} V_{\rm int}(z)\, \frac{1}{\sqrt{a_{00}^2 - a_{01}^2}} \exp\left\{ -\frac{1}{2} \frac{(z^2+x_a^2)a_{00} - 2z x_a a_{01}}{a_{00}^2 - a_{01}^2} \right\}. \tag{5.460}$$

Expanding the exponential with the help of Mehler's formula (2.297), we obtain the following expansion in terms of Hermite polynomials $H_n(x)$:

$$\langle\, \mathcal{A}_{\rm int}[x]\,\rangle^{\Omega}_{x_a,x_a} = \sum_{n=0}^{\infty} \frac{\hbar\beta}{2^n n!}\, C_\beta^{(n)}\, H_n\!\left(\frac{z}{\sqrt{2a_{00}^2}}\right) \int_{-\infty}^{\infty} \frac{dz}{\sqrt{2\pi a_{00}^2}}\, V_{\rm int}(z)\, e^{-z^2/2a_{00}^2}\, H_n\!\left(\frac{z}{\sqrt{2a_{00}^2}}\right). \tag{5.461}$$

Its temperature dependence stems from the diagonal elements of the harmonic Green function (5.459). The dimensionless functions $C_\beta^{(n)}$ are defined by

$$C_\beta^{(n)} = \frac{1}{\hbar\beta} \int_0^{\hbar\beta} d\tau \left(\frac{a_{01}^2}{a_{00}^2}\right)^n. \tag{5.462}$$

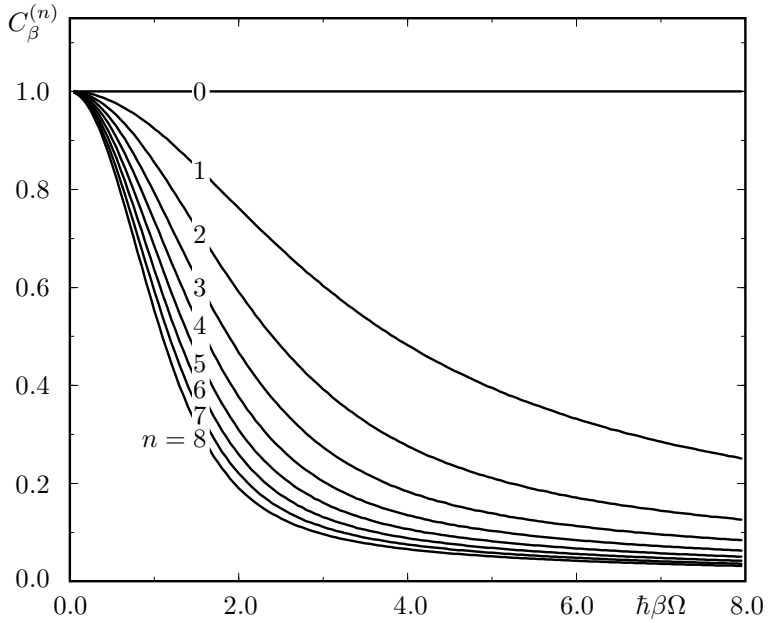

Figure 5.31 Temperature-dependence of first 9 functions $C_\beta^{(n)}$, where $\beta = 1/k_B T$.

Inserting (5.459) and performing the integral over τ, we obtain

$$C_\beta^{(n)} = \frac{1}{2^n \cosh^n \hbar\beta\Omega/2} \sum_{k=0}^{n} \binom{n}{k} \frac{\sinh \hbar\beta\Omega(n/2-k)}{\hbar\beta\Omega(n/2-k)}. \tag{5.463}$$

At high temperatures, these functions of β go to unity:

$$\lim_{\beta\to 0} C_\beta^{(n)} = 1. \tag{5.464}$$

Their zero-temperature limits are

$$\lim_{\beta\to\infty} C_\beta^{(n)} = \begin{cases} 1, & n = 0, \\ \dfrac{2}{\hbar\beta\Omega n}, & n > 0. \end{cases} \tag{5.465}$$

According to (5.444), the first-order approximation to the new effective potential is given by

$$\tilde{W}_1^\Omega(x_a) = \frac{1}{2\beta} \ln \frac{\sinh \hbar\beta\Omega}{\hbar\beta\Omega} + \frac{M\Omega}{\hbar\beta} x_a^2 \tanh \frac{\hbar\beta\Omega}{2} + V_{a^2}^\Omega(x_a), \tag{5.466}$$

with the smeared interaction potential

$$V_{a^2}^\Omega(x_a) = \frac{1}{\hbar\beta} \left\langle \mathcal{A}_{\rm int}[x] \right\rangle_{x_a,x_a}^\Omega. \tag{5.467}$$

It is instructive to discuss separately the limits $\beta \to 0$ and $\beta \to \infty$ to see the effects of pure classical and pure quantum fluctuations.

a) Classical Limit of Effective Classical Potential

In the classical limit $\beta \to 0$, the first-order effective classical potential (5.466) reduces to

$$\tilde{W}_1^{\Omega,\mathrm{cl}}(x_a) = \frac{1}{2}M\Omega^2 x_a^2 + \lim_{\beta\to 0} V_{a^2}^{\Omega}(x_a). \tag{5.468}$$

The second term is determined by inserting the high-temperature limit of the total fluctuation width (5.26):

$$a_{\mathrm{tot,cl}}^2 = \frac{k_B T}{M\Omega^2}, \tag{5.469}$$

and of the polynomials (5.464) into the expansion (5.461), leading to

$$V_{a^2}^{\Omega}(x_a) \underset{T\to\infty}{\approx} \sum_{n=0}^{\infty} \frac{1}{2^n n!} H_n\left(\sqrt{\frac{M\Omega^2\beta}{2}}x_a\right) \int_{-\infty}^{\infty} \frac{dz}{\sqrt{2\pi/M\Omega^2\beta}} V_{\mathrm{int}}(z) e^{-M\Omega^2\beta z^2/2} H_n\left(\frac{M\Omega^2\beta}{2}z\right). \tag{5.470}$$

Then we make use of the completeness relation for Hermite polynomials

$$\frac{1}{\sqrt{\pi}} e^{-x^2} \sum_{n=0}^{\infty} \frac{1}{2^n n!} H_n(x)\, H_n(x') = \delta(x - x'), \tag{5.471}$$

which may be derived from Mehler's formula (2.297) in the limit $b \to 1^-$, to reduce the smeared interaction potential $V_{a^2}^{\Omega}(x_a)$ to the pure interaction potential (5.438):

$$\lim_{\beta\to 0} V_{a^2}^{\Omega}(x_a) = V_{\mathrm{int}}(x_a). \tag{5.472}$$

Recalling (5.438) we see that the first-order effective classical potential (5.468) approaches the classical one:

$$\lim_{\beta\to 0} \tilde{W}_1^{\Omega,\mathrm{cl}}(x_a) = V(x_a). \tag{5.473}$$

This is a consequence of the vanishing fluctuation width b^2 of the paths around the classical orbits. This property is universal to all higher-order approximations to the effective classical potential (5.444). Thus all correction terms with $n > 1$ must disappear in the limit $\beta \to 0$,

$$\lim_{\beta\to 0} \frac{-1}{\beta} \sum_{n=2}^{\infty} \frac{(-1)^n}{n!\hbar^n} \left\langle \mathcal{A}_{\mathrm{int}}^n[x] \right\rangle_{x_a,x_a,c}^{\Omega} = 0. \tag{5.474}$$

b) Zero-Temperature Limit

At low temperatures, the first-order effective classical potential (5.466) becomes

$$\tilde{W}_1^{\Omega,\mathrm{qm}}(x_a) = \frac{\hbar\Omega}{2} + \lim_{\beta\to\infty} V_{a^2}^{\Omega}(x_a). \tag{5.475}$$

The zero-temperature limit of the smeared potential in the second term defined in (5.467) follows from Eq. (5.461) by taking into account the limiting procedure for the polynomials $C_\beta^{(n)}$ in (5.465) and the zero-temperature limit of the total fluctuation width (5.26), which is equal to the zero-temperature limit of $a^2(x_0)$: $a^2_{\rm tot,0} \underset{T=0}{=} a^2_{\rm tot} = \hbar/2M\Omega$. Thus we obtain with $H_0(x) = 1$ and the inverse length $\kappa \equiv 1/\lambda_\Omega = \sqrt{M\Omega/\hbar}$ [recall (2.303)]:

$$\lim_{\beta\to\infty} V^\Omega_{a^2}(x_a) = \int\limits_{-\infty}^{\infty} dz\, \sqrt{\frac{\kappa^2}{\pi}} H_0(\kappa z)^2 \exp\{-\kappa^2 z^2\}\, V_{\rm int}(z). \tag{5.476}$$

Introducing the harmonic eigenvalues

$$E^\Omega_n = \hbar\Omega\left(n + \frac{1}{2}\right), \tag{5.477}$$

and the harmonic eigenfunctions [recall (2.301) and (2.302)]

$$\psi^\Omega_n(x) = \frac{1}{\sqrt{n!2^n}} \left(\frac{\kappa^2}{\pi}\right)^{1/4} e^{-\frac{1}{2}\kappa^2 x^2}\, H_n(\kappa x), \tag{5.478}$$

we can re-express the zero-temperature limit of the first-order effective classical potential (5.475) with (5.476) by

$$\tilde{W}^{\Omega,{\rm qm}}_1(x_a) = E^\Omega_0 + \langle\, \psi^\Omega_0 \,|\, V_{\rm int} \,|\, \psi^\Omega_0 \,\rangle. \tag{5.479}$$

This is recognized as the first-order Rayleigh-Schrödinger perturbative result for the ground state energy.

For the discussion of the quantum-mechanical limit of the first-order normalized density,

$$\rho^\Omega_1(x_a) = \frac{\tilde{\rho}_1{}^\Omega(x_a)}{Z} = \rho^\Omega_0(x_a)\, \frac{\exp\left\{-\frac{1}{\hbar}\,\langle\, \mathcal{A}_{\rm int}[x]\,\rangle^\Omega_{x_a,x_a}\right\}}{\int_{-\infty}^{\infty} dx_a\, \rho^\Omega_0(x_a) \exp\left\{-\frac{1}{\hbar}\,\langle\, \mathcal{A}_{\rm int}[x]\,\rangle^\Omega_{x_a,x_a}\right\}}, \tag{5.480}$$

we proceed as follows. First we expand (5.480) up to first order in the interaction, leading to

$$\rho^\Omega_1(x_a) = \rho^\Omega_0(x_a)\left[1 - \frac{1}{\hbar}\left(\langle\, \mathcal{A}_{\rm int}[x]\,\rangle^\Omega_{x_a,x_a} - \int\limits_{-\infty}^{\infty} dx_a\, \rho^\Omega_0(x_a)\, \langle\, \mathcal{A}_{\rm int}[x]\,\rangle^\Omega_{x_a,x_a}\right)\right]. \tag{5.481}$$

Inserting (5.428) and (5.461) into the third term in (5.481), and assuming Ω not to depend explicitly on x_a, the x_a-integral reduces to the orthonormality relation for Hermite polynomials

$$\frac{1}{2^n n!\sqrt{\pi}} \int\limits_{-\infty}^{\infty} dx_a H_n(x_a) H_0(x_a) e^{-x_a^2} = \delta_{n0}, \tag{5.482}$$

so that the third term in (5.481) eventually becomes

$$-\int_{-\infty}^{\infty} dx_a\, \rho_0^\Omega(x_a)\, \langle\, \mathcal{A}_{\rm int}[x]\,\rangle_{x_a,x_a}^\Omega = -\beta \int_{-\infty}^{\infty} dz \sqrt{\frac{\kappa^2}{\pi}}\, V_{\rm int}(z)\, \exp\{-\kappa^2 z^2\}\, H_0(\kappa z). \quad (5.483)$$

But this is just the $n=0$ -term of (5.461) with an opposite sign, thus canceling the zeroth component of the second term in (5.481), which would have been divergent for $\beta \to \infty$.

The resulting expression for the first-order normalized density is

$$\rho_1^\Omega(x_a) = \rho_0^\Omega(x_a) \left[1 - \sum_{n=1}^{\infty} \frac{\beta}{2^n n!} C_\beta^{(n)} H_n(\kappa x_a) \int_{-\infty}^{\infty} dz \sqrt{\frac{\kappa^2}{\pi}}\, V_{\rm int}(z)\, \exp(-\kappa^2 z^2)\, H_n(\kappa z)\right]. \quad (5.484)$$

The zero-temperature limit of $C_\beta^{(n)}$ is from (5.465) and (5.477)

$$\lim_{\beta\to\infty} \beta C_\beta^{(n)} = \frac{2}{E_n^\Omega - E_0^\Omega}, \quad (5.485)$$

so that we obtain from (5.484) the limit

$$\begin{aligned} \rho_1^\Omega(x_a) &= \rho_0^\Omega(x_a) \left[1 - 2\sum_{n=1}^{\infty} \frac{1}{2^n n!} \frac{1}{E_n^\Omega - E_0^\Omega} H_n(\kappa x_a)\right. \\ &\times \left. \int_{-\infty}^{\infty} dz \sqrt{\frac{\kappa^2}{\pi}}\, V_{\rm int}(z)\, \exp\{-\kappa^2 z^2\} H_n(\kappa z)\, H_0(\kappa z)\right]. \end{aligned} \quad (5.486)$$

Taking into account the harmonic eigenfunctions (5.478), we can rewrite (5.486) as

$$\rho_1^\Omega(x_a) = |\psi_0(x_a)|^2 = [\psi_0^\Omega(x_a)]^2 - 2\psi_0^\Omega(x_a) \sum_{n>0} \psi_n^\Omega(x_a) \frac{\langle\, \psi_n^\Omega \,|\, V_{\rm int} \,|\, \psi_0^\Omega \,\rangle}{E_n^\Omega - E_0^\Omega}, \quad (5.487)$$

which is just equivalent to the harmonic first-order Rayleigh-Schrödinger result for particle densities.

Summarizing the results of this section, we have shown that our method has properly reproduced the high- and low-temperature limits. Due to relation (5.487), the variational approach for particle densities can be used to determine approximately the ground state wave function $\psi_0(x_a)$ for the system of interest.

5.23.5 Smearing Formula in Higher Spatial Dimensions

Most physical systems possess many degrees of freedom. This requires an extension of our method to higher spatial dimensions. In general, we must consider anisotropic harmonic trial systems, where the previous variational parameter Ω^2 becomes a $D \times D$ -matrix $\Omega_{\mu\nu}^2$ with $\mu, \nu = 1, 2, \ldots, D$.

a) Isotropic Approximation

An isotropic trial ansatz

$$\Omega^2_{\mu\nu} = \Omega^2 \delta_{\mu\nu} \tag{5.488}$$

can give rough initial estimates for the properties of the system. In this case, the n-th order smearing formula (5.458) generalizes directly to

$$\begin{aligned} \langle\, \mathcal{A}^n_{\rm int}[\mathbf{r}]\,\rangle^{\Omega}_{\mathbf{r}_a,\mathbf{r}_a} &= \frac{1}{\rho_0^{\Omega}(\mathbf{r}_a)} \prod_{l=1}^{n} \left[\int_0^{\hbar\beta} d\tau_l \int d^D z_l\, V_{\rm int}(\mathbf{z}_l) \right] \\ &\times \frac{1}{\sqrt{(2\pi)^{n+1} \det a^2}^D} \exp\left[-\frac{1}{2} \sum_{k,l=0}^{n} \mathbf{z}_k\, a^{-2}_{kl}\, \mathbf{z}_l \right], \end{aligned} \tag{5.489}$$

with the D-dimensional vectors $\mathbf{z}_l = (z_{1l}, z_{2l}, \ldots, z_{Dl})^T$. Note, that Greek labels $\mu, \nu, \ldots = 1, 2, \ldots, D$ specify spatial indices and Latin labels $k, l, \ldots = 0, 1, 2, \ldots, n$ refer to the different imaginary times. The vector $\mathbf{z}_0$ denotes $\mathbf{r}_a$, the matrix a^2 is the same as in Subsection 5.23.3. The harmonic density reads

$$\rho_0^{\Omega}(\mathbf{r}) = \sqrt{\frac{1}{2\pi a^2_{00}}}^D \exp\left[-\frac{1}{2\, a^2_{00}} \sum_{\mu=1}^{D} x^2_\mu \right]. \tag{5.490}$$

b) Anisotropic Approximation

In the discussion of the anisotropic approximation, we shall only consider radially-symmetric potentials $V(\mathbf{r}) = V(|\mathbf{r}|)$ because of their simplicity and their major occurrence in physics. The trial frequencies decompose naturally into a radial frequency Ω_L and a transverse one Ω_T as in (5.95):

$$\Omega^2_{\mu\nu} = \Omega^2_L \frac{x_{a\mu} x_{a\nu}}{r^2_a} + \Omega^2_T \left(\delta_{\mu\nu} - \frac{x_{a\mu} x_{a\nu}}{r^2_a} \right), \tag{5.491}$$

with $r_a = |\mathbf{r}_a|$. For practical reasons we rotate the coordinate system by $\bar{\mathbf{x}}_n = U\, \mathbf{x}_n$ so that $\bar{\mathbf{r}}_a$ points along the first coordinate axis,

$$(\bar{\mathbf{r}}_a)_\mu \equiv \bar{z}_{\mu 0} = \begin{cases} r_a, & \mu = 1, \\ 0, & 2 \le \mu \le D, \end{cases} \tag{5.492}$$

and Ω^2-matrix is diagonal:

$$\overline{\Omega^2} = \begin{pmatrix} \Omega^2_L & 0 & 0 & \cdots & 0 \\ 0 & \Omega^2_T & 0 & \cdots & 0 \\ 0 & 0 & \Omega^2_T & \cdots & 0 \\ \vdots & \vdots & \vdots & \ddots & \vdots \\ 0 & 0 & 0 & \cdots & \Omega^2_T \end{pmatrix} = U\, \Omega^2\, U^{-1}. \tag{5.493}$$

After this rotation, the *anisotropic* n-th order smearing formula in D dimensions reads

$$\begin{aligned} \langle\, \mathcal{A}^n_{\rm int}[\mathbf{r}]\,\rangle^{\Omega_{L,T}}_{\mathbf{r}_a,\mathbf{r}_a} &= \frac{1}{\rho_0^{\Omega_{L,T}}(\bar{\mathbf{r}}_a)} \prod_{l=1}^{n} \left[\int_0^{\hbar\beta} d\tau_l \int d^D \bar{z}_l\, V_{\rm int}(|\bar{\mathbf{z}}_l|) \right] (2\pi)^{-D(n+1)/2} \\ &\times (\det a^2_L)^{-1/2} (\det a^2_T)^{-(D-1)/2} e^{-\frac{1}{2} \sum_{k,l=0}^{n} \bar{z}_{1k} a_L{}^{-2}_{kl} \bar{z}_{1l}} e^{-\frac{1}{2} \sum_{\mu=2}^{D} \sum_{k,l=1}^{n} \bar{z}_{\mu k} a_T{}^{-2}_{kl} \bar{z}_{\mu l}}. \end{aligned} \tag{5.494}$$

The components of the longitudinal and transversal matrices a_L^2 and a_T^2 are

$$a_{Lkl}^2 = a_L^2(\tau_k, \tau_l), \quad a_{Tkl}^2 = a_T^2(\tau_k, \tau_l)\,, \tag{5.495}$$

where the frequency Ω in (5.459) must be substituted by the new variational parameters Ω_L, Ω_T, respectively. For the harmonic density in the rotated system $\rho_0^{\Omega_{L,T}}(\bar{\mathbf{r}})$ which is used to normalize (5.494), we find

$$\rho_0^{\Omega_{L,T}}(\bar{\mathbf{r}}) = \sqrt{\frac{1}{2\pi a_{L00}^2}}\sqrt{\frac{1}{2\pi a_{T00}^2}}^{D-1} \exp\left[-\frac{1}{2\,a_{L00}^2}\bar{x}_1^2 - \frac{1}{2\,a_{T00}^2}\sum_{\mu=2}^{D}\bar{x}_\mu^2\right]. \tag{5.496}$$

Appendix 5A Feynman Integrals for $T \neq 0$ without Zero Frequency

The Feynman integrals needed in variational perturbation theory of the anharmonic oscillator at nonzero temperature can be calculated in close analogy to those of ordinary perturbation theory in Section 3.20. The calculation proceeds as explained in Appendix 3D, except that the lines represent now the thermal correlation function (5.19) with the zero-frequency subtracted from the spectral decomposition:

$$G_{\tilde{\Omega}}^{(2)x_0}(\tau,\tau') = \frac{1}{2\tilde{\Omega}}\left[\frac{\cosh\tilde{\Omega}(|\tau-\tau'|-\hbar\beta/2)}{\sinh(\tilde{\Omega}\hbar\beta/2)}\right] - \frac{1}{\hbar\beta\tilde{\Omega}^2}.$$

With the dimensionless variable $x \equiv \hbar\beta\tilde{\omega}$, the results for the quantities a_V^{2L} defined of each Feynman diagram with L lines and V vertices as in (3.550), but now without the zero Matsubara frequency, are [compare with the results (3D.3)–(3D.11)]

$$a^2 = \frac{\hbar}{\tilde{\omega}}\frac{1}{x}\left(\frac{x}{2}\coth\frac{x}{2} - 1\right), \tag{5A.1}$$

$$a_2^4 = \left(\frac{\hbar}{\tilde{\omega}}\right)^2 \frac{1}{8x}\frac{1}{\sinh^2\frac{x}{2}}\left(4 + x^2 - 4\,\cosh x + x\sinh x\right), \tag{5A.2}$$

$$\begin{aligned} a_3^6 = {} & \left(\frac{\hbar}{\tilde{\omega}}\right)^3 \frac{1}{64x}\frac{1}{\sinh^3\frac{x}{2}}\left(-3\,x\cosh\frac{x}{2} + 2\,x^3\cosh\frac{x}{2} + 3\,x\cosh\frac{3x}{2}\right. \\ & \left. +48\,\sinh\frac{x}{2} + 6\,x^2\sinh\frac{x}{2} - 16\,\sinh\frac{3x}{2}\right), \end{aligned} \tag{5A.3}$$

$$\begin{aligned} a_2^8 = {} & \left(\frac{\hbar}{\omega}\right)^4 \frac{1}{768x^3}\frac{1}{\sinh^4\frac{x}{2}}\left(-864 + 18\,x^4 + 1152\,\cosh x + 32\,x^2\cosh x\right. \\ & -288\,\cosh 2x - 32\,x^2\cosh 2x - 288\,x\sinh x + 24\,x^3\sinh x \\ & \left. +144\,x\sinh 2x + 3\,x^3\sinh 2x\right), \end{aligned} \tag{5A.4}$$

$$\begin{aligned} a_3^{10} = {} & \left(\frac{\hbar}{\tilde{\omega}}\right)^5 \frac{1}{4096x^3}\frac{1}{\sinh^5\frac{x}{2}}\left(672\,x\cosh\frac{x}{2} - 8\,x^3\cosh\frac{x}{2} + 24\,x^5\cosh\frac{x}{2}\right. \\ & -1008\,x\cosh\frac{3x}{2} + 3\,x^3\cosh\frac{3x}{2} + 336\,x\cosh\frac{5x}{2} + 5\,x^3\cosh\frac{5x}{2} \\ & -7680\,\sinh\frac{x}{2} - 352\,x^2\sinh\frac{x}{2} + 72\,x^4\sinh\frac{x}{2} + 3840\,\sinh\frac{3x}{2} \\ & \left. +224\,x^2\sinh\frac{3x}{2} + 12\,x^4\sinh\frac{3x}{2} - 768\,\sinh\frac{5x}{2} - 64\,x^2\sinh\frac{5x}{2}\right), \end{aligned} \tag{5A.5}$$

$$
\begin{aligned}
a_3^{12} &= \left(\frac{\hbar}{\tilde{\omega}}\right)^6 \frac{1}{49152x^4}\frac{1}{\sinh^6\frac{x}{2}}\left(-107520-7360\,x^2+624\,x^4+96\,x^6\right.\\
&\quad +161280\,\cosh x+12000\,x^2\cosh x-777\,x^4\cosh x+24\,x^6\cosh x\\
&\quad -64512\,\cosh 2x-5952\,x^2\cosh 2x+144\,x^4\cosh 2x+10752\,\cosh 3x\\
&\quad -28800\,x\sinh x+1312\,x^2\cosh 3x+9\,x^4\cosh 3x+1120\,x^3\sinh x\\
&\quad +324\,x^5\sinh x+23040\,x\sinh 2x-320\,x^3\sinh 2x-5760\,x\sinh 3x\\
&\quad \left.-160\,x^3\sinh 3x\right), \qquad (5A.6)\\
a_2^6 &= \left(\frac{\hbar}{\tilde{\omega}}\right)^3 \frac{1}{24x^2}\frac{1}{\sinh^2\frac{x}{2}}\left(-24-4\,x^2+24\cosh x+x^2\cosh x-9\,x\sinh x\right),\\
a_3^8 &= \left(\frac{\hbar}{\tilde{\omega}}\right)^4 \frac{1}{288x^2}\frac{1}{\sinh^3\frac{x}{2}}\left(45\,x\cosh\frac{x}{2}-6\,x^3\cosh\frac{x}{2}-45\,x\cosh\frac{3x}{2}\right.\\
&\quad \left.-432\,\sinh\frac{x}{2}-54\,x^2\sinh\frac{x}{2}+144\,\sinh\frac{3x}{2}+4\,x^2\sinh\frac{3x}{2}\right), \qquad (5A.7)\\
a_{3'}^{10} &= \left(\frac{\hbar}{\tilde{\omega}}\right)^5 \frac{1}{2304x^3}\frac{1}{\sinh^4\frac{x}{2}}\left(-3456-414\,x^2-6\,x^4+4608\,\cosh x+\right.\\
&\quad 496\,x^2\cosh x-1152\,\cosh 2x-82\,x^2\cosh 2x-1008\,x\sinh x-\\
&\quad \left.16\,x^3\sinh x+504\,x\sinh 2x+5\,x^3\sinh 2x\right). \qquad (5A.8)
\end{aligned}
$$

Six of these integrals are the analogs of those in Eqs. (3.550). In addition there are the three integrals a_2^6, a_3^8, and $a_{3'}^{10}$, corresponding to the three diagrams

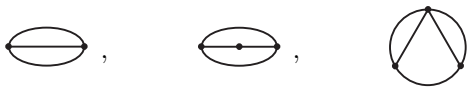 (5A.9)

respectively, which are needed in Subsection 5.14.2. They have been calculated with zero Matsubara frequency in Eqs. (3D.8)–(3D.11).

In the low-temperature limit where $x = \Omega\hbar\beta \to \infty$, the x-dependent factors in Eqs. (5A.1)–(5A.8) converge towards the same constants (3D.13) as those with zero Matsubara frequency, and the same limiting relations hold as in Eqs. (3.553) and (3D.14).

The high-temperature limits $x \to 0$, however, are quite different from those in Eq. (3D.16). The present Feynman integrals all vanish rapidly for increasing temperatures. For L lines and V vertices, $\hbar\beta(1/\tilde{\omega})^{V-1}a_V^{2L}$ goes to zero like $\beta^V(\beta/12)^L$. The first V factors are due to the V-integrals over τ, the second are the consequence of the product of $n/2$ factors a^2. Thus a_V^{2L} behaves like

$$
a_V^{2L} \propto \left(\frac{\hbar}{\tilde{\omega}}\right)^L x^{V-1+L}. \qquad (5A.10)
$$

Indeed, the x-dependent factors in (5A.1)–(5A.8) vanish now like

$$
\begin{aligned}
&x/12,\quad x^3/720,\quad x^5/30240,\\
&x^5/241920,\quad x^7/11404800,\quad 193x^8/47551795200,\\
&x^4/30240,\quad x^6/1814400,\quad x^7/59875200, \qquad (5A.11)
\end{aligned}
$$

respectively. When expanding (5A.1)–(5A.8) into a power series, the lowest powers cancel each other. For the temperature behavior of these Feynman integrals see Fig. 5.32. We have plotted the reduced Feynman integrals $\hat{a}_V^{2L}(x)$ in which the low-temperature behaviors (3.553) and (3D.14) have been divided out of a_V^{2L}.

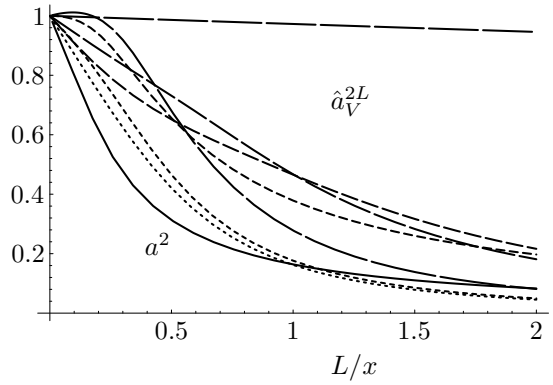

Figure 5.32 Plot of the reduced Feynman integrals $\hat{a}_V^{2L}(x)$ as functions of $L/x = Lk_BT/\hbar\omega$. The integrals (3D.4)–(3D.11) are indicated by decreasing dash-lenghts. Compare Fig. 3.16.

The integrals (5A.2) and (5A.3) for a_2^4 and a_3^6 can be obtained from the integral (5A.1) for a^2 via the operation

$$\frac{\hbar^n}{n!}\left(-\frac{\partial}{\partial\tilde{\omega}^2}\right)^n = \frac{\hbar^n}{n!}\left(-\frac{1}{2\tilde{\omega}}\frac{\partial}{\partial\tilde{\omega}}\right)^n, \tag{5A.12}$$

with $n = 1$ and $n = 2$, respectively. This is derived following the same steps as in Eqs. (3D.18)–(3D.20). The absence of the zero Matsubara frequency does not change the argument.

Also, as in Eqs. (5.195)–(3D.21), the same type of expansion allows us to derive the three integrals from the one-loop diagram (3.549).

Appendix 5B Proof of Scaling Relation for Extrema of W_N

Here we prove the scaling relation (5.215), according to which the derivative of the Nth approximation W_N to the ground state energy can be written as [14]

$$\frac{d}{d\Omega}W_N^\Omega = \left(\frac{g}{\Omega^3}\right)^N p_N(\sigma), \tag{5B.1}$$

where $p_N(\sigma)$ is a polynomial of order N in the scaling variable $\sigma = \Omega(\Omega^2-1)/g$.

For the sake of generality, we consider an anharmonic oscillator with a potential gx^P whose power P is arbitrary. The ubiquitous factor $1/4$ accompanying g is omitted, for convenience. The energy eigenvalue of the ground state (or any excited state) has an Nth order perturbation expansion

$$E_N(g) = \omega\sum_{l=0}^{N} E_l\left(\frac{g}{\omega^{(P+2)/2}}\right)^l, \tag{5B.2}$$

where E_l are rational numbers. After the replacement (5.188), the series is re-expanded at fixed r in powers of g up to order N, and we obtain

$$W_N^\Omega = \Omega\sum_{l=0}^{N} \varepsilon_l(\sigma)\left(\frac{g}{\Omega^{(P+2)/2}}\right)^l, \tag{5B.3}$$

with the re-expansion coefficients [compare (5.207)]

$$\varepsilon_l(\sigma) = \sum_{j=0}^{l} E_j \binom{(1-\frac{P+2}{2}j)/2}{l-j}(-\sigma)^{l-j}. \tag{5B.4}$$

Here σ is a scaling variable for the potential gx^P generalizing (5.208) (note that it is four times as big as the previous σ, due to the different normalization of g):

$$\sigma \equiv \frac{\Omega^{(P-2)/2}(\Omega^2 - \omega^2)}{g}. \tag{5B.5}$$

We now show that the derivative $dW_N(g,\Omega)/d\Omega$ has the following scaling form generalizing (5B.1):

$$\frac{dW_N^\Omega}{d\Omega} = \left(\frac{g}{\Omega^{(P+2)/2}}\right)^N p_N(\sigma), \tag{5B.6}$$

where $p_N(\sigma)$ is the following polynomial of order N in the scaling variable σ:

$$\begin{aligned} p_N(\sigma) &= -2\frac{d\varepsilon_{N+1}(\sigma)}{d\sigma} \\ &= 2\sum_{j=0}^{N} E_j \begin{pmatrix} (1-\frac{P+2}{2}j)/2 \\ N+1-j \end{pmatrix} (N+1-j)\,(-\sigma)^{N-j}. \end{aligned} \tag{5B.7}$$

The proof starts by differentiating (5B.3) with respect to Ω, yielding

$$\frac{dW_N^\Omega}{d\Omega} = \sum_{l=0}^{N}\left[\varepsilon_l(\sigma) - \frac{P+2}{2}l\varepsilon_l(\sigma) + \Omega\frac{d\varepsilon_l}{d\Omega}\right]\left(\frac{g}{\Omega^{(P+2)/2}}\right)^l. \tag{5B.8}$$

Using the chain rule of differentiation we see from (5B.4) that

$$\Omega\frac{d\varepsilon_l}{d\Omega} = \left[2\frac{\Omega^{(P+2)/2}}{g} + \frac{P-2}{2}\sigma\right]\frac{d\varepsilon_l}{d\sigma}, \tag{5B.9}$$

and (5B.8) can be rewritten as

$$\frac{dW_N^\Omega}{d\Omega} = \sum_{l=0}^{N}\left[\left(1-\frac{P+2}{2}l\right)\varepsilon_l(\sigma) + \left(2\frac{\Omega^{(P+2)/2}}{g} + \frac{P-2}{2}\sigma\right)\frac{d\varepsilon_l}{d\sigma}\right]\left(\frac{g}{\Omega^{(P+2)/2}}\right)^l. \tag{5B.10}$$

After rearranging the sum, this becomes

$$\begin{aligned} \frac{dW_N^\Omega}{d\Omega} &= 2\frac{d\varepsilon_0}{d\sigma}\left(\frac{g}{\Omega^{(P+2)/2}}\right)^{-1} \\ &+ \sum_{l=0}^{N-1}\left[\left(1-\frac{P+2}{2}l\right)\varepsilon_l + \frac{P-2}{2}\sigma\frac{d\varepsilon_l}{d\sigma} + 2\frac{d\varepsilon_{l+1}}{d\sigma}\right]\left(\frac{g}{\Omega^{(P+2)/2}}\right)^l \\ &+ \left[\left(1-\frac{P+2}{2}N\right)\varepsilon_N + \frac{P-2}{2}\sigma\frac{d\varepsilon_N}{d\sigma}\right]\left(\frac{g}{\Omega^{(P+2)/2}}\right)^N. \end{aligned} \tag{5B.11}$$

The first term vanishes trivially since ε_0 happens to be independent of σ. The sum in the second line vanishes term by term:

$$\left(1-\frac{P+2}{2}l\right)\varepsilon_l + \frac{P-2}{2}\sigma\frac{d\varepsilon_l}{d\sigma} + 2\frac{d\varepsilon_{l+1}}{d\sigma} = 0, \qquad l = 1\ldots N-1. \tag{5B.12}$$

To see this we form the derivative

$$2\frac{d\varepsilon_{l+1}}{d\sigma} = 2\sum_{j=0}^{l} E_j \begin{pmatrix} (1-\frac{P+2}{2}j)/2 \\ l+1-j \end{pmatrix} (j-l-1)\,(-\sigma)^{l-j}, \tag{5B.13}$$

and use the identity

$$2\left(\begin{array}{c}(1-\frac{P+2}{2}j)/2\\ l+1-j\end{array}\right)=\frac{\frac{P-2}{2}j+2l-1}{j-l-1}\left(\begin{array}{c}(1-\frac{P+2}{2}j)/2\\ l-j\end{array}\right) \tag{5B.14}$$

to rewrite (5B.13) as

$$2\frac{d\varepsilon_{l+1}}{d\sigma}=\sum_{j=0}^{l}E_j\left(\begin{array}{c}(1-\frac{P+2}{2}j)/2\\ l-j\end{array}\right)\left(\frac{P-2}{2}j+2l-1\right)(-\sigma)^{l-j}, \tag{5B.15}$$

implying

$$\frac{P-2}{2}\sigma\frac{d\varepsilon_l}{d\sigma}=\sum_{j=0}^{l}E_j\left(\begin{array}{c}(1-\frac{P+2}{2}j)/2\\ l-j\end{array}\right)\frac{P-2}{2}(l-j)(-\sigma)^{l-j}. \tag{5B.16}$$

By combining this with (5B.4), (5B.13), we obtain Eq. (5B.12) which proves that the second line in (5B.11) vanishes.

Thus we are left with the last term on the right-hand side of Eq. (5B.11). Using (5B.12) for $l=N$ leads to

$$\frac{dW_N^\Omega}{d\Omega} \;=\; -2\left(\frac{g}{\Omega^{(P+2)/2}}\right)^N\frac{d\varepsilon_{N+1}(\sigma)}{d\sigma}. \tag{5B.17}$$

When expressing $d\varepsilon_{N+1}(\sigma)/d\sigma$ with the help of (5B.4), we arrive at

$$\frac{dW_N^\Omega}{d\Omega} \;=\; 2\left(\frac{g}{\Omega^{(P+2)/2}}\right)^N\sum_{j=0}^{N}E_j\left(\begin{array}{c}(1-\frac{P+2}{2}j)/2\\ N+1-j\end{array}\right)(N+1-j)\,(-\sigma)^{N-j}. \tag{5B.18}$$

This proves the scaling relation (5B.6) with the polynomial (5B.7).

The proof can easily be extended to physical quantities $Q_N(g)$ with a different physical dimension α, which have an expansion

$$Q_N(g)=\omega^\alpha\sum_{l=0}^{N}E_l\left(\frac{g}{\omega^{(P+2)/2}}\right)^l, \quad \alpha\neq 1, \tag{5B.19}$$

rather than (5B.2). In this case the quantity $[Q_N(g)]^{1/\alpha}$ has again an expansion like (5B.2). By rewriting $Q_N(g)$ as $\{[Q_N(g)]^{1/\alpha}\}^\alpha$ and forming the derivative using the chain rule we see that the derivative vanishes whenever the polynomial $p_N(\sigma)$ vanishes, which is formed from $[Q_N(g)]^{1/\alpha}$ as in Eq. (5B.7).

Appendix 5C Second-Order Shift of Polaron Energy

For brevity, we introduce the dimensionless variable $\rho\equiv\omega\Delta\tau$ and

$$F[\rho]\equiv -2\Gamma^2\bar{G}^{\Omega,\Gamma}(\rho,0). \tag{5C.1}$$

Going to natural units with $\hbar=M=\omega=1$, Feynman's variational energy (5.395) takes the form

$$E_0=\frac{3}{4\Gamma}(\Gamma-\Omega)^2-\frac{1}{\sqrt{\pi}}\Gamma\int_0^\infty d\rho\, e^{-\rho}F^{-1/2}(\rho). \tag{5C.2}$$

The second-order correction (5.406) reads

$$\begin{aligned}\Delta E_0^{(2)}=&-\frac{41^2}{\pi}\Gamma^2 I+\frac{1}{2\Gamma\sqrt{\pi}}(\Gamma^2-\Omega^2)\int_0^\infty d\rho\, e^{-\rho}F^{-1/2}(\rho)-\frac{3}{16\Gamma^3}(\Gamma^2-\Omega^2)^2\\ &-\frac{1}{4\sqrt{\pi}}(\Gamma^2-\Omega^2)\int_0^\infty d\rho\, e^{-\rho}F^{-3/2}(\rho)\left\{\left(1+\frac{\Omega^2}{\Gamma}\right)\left(1-e^{-\Gamma\rho}\right)+\frac{\Gamma^2-\Omega^2}{\Gamma}\rho e^{-\Gamma\rho}\right\},\end{aligned} \tag{5C.3}$$

where I denotes the integral

$$I = \frac{1}{4}\int_0^\infty \int_0^\infty \int_0^\infty d\rho_1 d\rho_2 d\rho_3 e^{-\rho_1} F^{-1/2}(\rho_1) e^{-\rho_2} F^{-1/2}(\rho_2) \left(\frac{\arcsin Q}{Q} - 1\right), \tag{5C.4}$$

with

$$\begin{aligned} Q &= Q_1 \quad \text{for} \quad \rho_3 - \rho_2 + \rho_1 \geq 0 \quad \text{and} \quad \rho_3 - \rho_2 \geq 0, \\ Q &= Q_2 \quad \text{for} \quad \rho_3 - \rho_2 + \rho_1 \geq 0 \quad \text{and} \quad \rho_3 - \rho_2 < 0, \\ Q &= Q_3 \quad \text{for} \quad \rho_3 - \rho_2 + \rho_1 < 0 \quad \text{and} \quad \rho_3 - \rho_2 < 0, \end{aligned} \tag{5C.5}$$

and

$$Q_1 = \frac{1}{2} F^{-1/2}(\rho_1^2) F^{-1/2}(\rho_2^2) \frac{\Gamma^2 - \Omega^2}{\Gamma} e^{-\Gamma\rho_3}(1 - e^{-\Gamma\rho_1})(e^{\Gamma\rho} - 1), \tag{5C.6}$$

$$\begin{aligned} Q_2 = {} & \frac{1}{2} F^{-1/2}(\rho_1) F^{-1/2}(\rho_2) \\ & \times \left\{ \frac{\Gamma^2 - \Omega^2}{\Gamma} \left[e^{-\Gamma(\rho_2 - \rho_3)} - e^{-\Gamma\rho_3}(1 + e^{-\Gamma(\rho_1 - \rho_2)} - e^{-\Gamma\rho_1}) \right] - 2\Omega^2(\rho_2 - \rho_3) \right\}, \end{aligned} \tag{5C.7}$$

$$\begin{aligned} Q_3 = {} & \frac{1}{2} F^{-1/2}(\rho_1) F^{-1/2}(\rho_2) \\ & \times \left\{ \frac{\Gamma^2 - \Omega^2}{\Gamma} \left[-e^{-\Gamma\rho_3}(1 - e^{-\Gamma\rho_1}) - e^{-\Gamma(\rho_2 - \rho_3)}(e^{\Gamma\rho_1} - 1) \right] - 2\Omega^2\rho_1 \right\}. \end{aligned} \tag{5C.8}$$

Notes and References

The first-order variational approximation to the effective classical partition function $V^{\text{eff cl}}(x_0)$ presented in this chapter was developed in 1983 by
R.P. Feynman and H. Kleinert, Phys. Rev. A **34**, 5080 (1986) (`http://www.physik.fu-berlin.de/~kleinert/159`).
For further development see:
H. Kleinert, Phys. Lett. A **118**, 195 (1986) (*ibid.*`http/148`); B **181**, 324 (1986) (*ibid.*`http/151`);
W. Janke and B.K. Chang, Phys. Lett. B **129**, 140 (1988);
W. Janke, in *Path Integrals from meV to MeV*, ed. by V. Sa-yakanit et al., World Scientific, Singapore, 1990.
A detailed discussion of the accuracy of the approach in comparison with several other approximation schemes is given by
S. Srivastava and Vishwamittar, Phys. Rev. A **44**, 8006 (1991).

For a similar, independent development containing applications to simple quantum field theories, see
R. Giachetti and V. Tognetti, Phys. Rev. Lett. **55**, 912 (1985); Int. J. Magn. Mater. **54-57**, 861 (1986);
R. Giachetti, V. Tognetti, and R. Vaia, Phys. Rev. B **33**, 7647 (1986); Phys. Rev. A **37**, 2165 (1988); Phys. Rev. A **38**, 1521, 1638 (1988);
Physica Scripta **40**, 451 (1989). R. Giachetti, V. Tognetti, A. Cuccoli, and R. Vaia, lecture presented at the XXVI Karpacz School of Theoretical Physics, Karpacz, Poland, 1990.
See also
R. Vaia and V. Tognetti, Int. J. Mod. Phys. B **4**, 2005 (1990);
A. Cuccoli, V. Tognetti, and R. Vaia, Phys. Rev. B **41**, 9588 (1990); A **44**, 2743 (1991);
A. Cuccoli, A. Maradudin, A.R. McGurn, V. Tognetti, and R. Vaia, Phys. Rev. D **46**, 8839 (1992).

The variational approach has solved some old problems in quantum crystals by extending in a simple way the classical methods into the quantum regime. See
V.I. Yukalov, Mosc. Univ. Phys. Bull. **31**, 10-15 (1976);
S. Liu, G.K. Horton, and E.R. Cowley, Phys. Lett. A **152**, 79 (1991);
A. Cuccoli, A. Macchi, M. Neumann, V. Tognetti, and R. Vaia, Phys. Rev. B **45**, 2088 (1992).

The systematic extension of the variational approach was developed by
H. Kleinert, Phys. Lett. A **173**, 332 (1993) (quant-ph/9511020).
See also
J. Jaenicke and H. Kleinert, Phys. Lett. A **176**, 409 (1993) (*ibid.*`http/217`);
H. Kleinert and H. Meyer, Phys. Lett. A **184**, 319 (1994) (hep-th/9504048).

A similar convergence mechanism was first observed within an order-dependent mapping technique in the seminal paper by
R. Seznec and J. Zinn-Justin, J. Math. Phys. **20**, 1398 (1979).
For an introduction into various resummation procedures see
C.M. Bender and S.A. Orszag, *Advanced Mathematical Methods for Scientists and Engineers*, McGraw-Hill, New York, 1978.

The proof of the convergence of the variational perturbation expansion to be given in Subsection 17.10.5 went through the following stages: First a weak estimate was found for the anharmonic integral:
I.R.C. Buckley, A. Duncan, H.F. Jones, Phys. Rev. **D 47**, 2554 (1993);
C.M. Bender, A. Duncan, H.F. Jones, Phys. Rev. **D 49**, 4219 (1994).
This was followed by a similar extension to the quantum-mechanical case:
A. Duncan and H.F. Jones, Phys. Rev. D **47**, 2560 (1993);
C. Arvanitis, H.F. Jones, and C.S. Parker, Phys.Rev. D **52**, 3704 (1995) (hep-ph/9502386);
R. Guida, K. Konishi, and H. Suzuki, Ann. Phys. 241, 152 (1995) (hep-th/9407027).

The exponentially fast convergence observed in the calculation of the strong-coupling coefficients of Table 5.9 was, however, not explained. The accuracy in the table was reached by working up to the order 251 with 200 digits in Ref. [13].

The analytic properties of the strong-coupling expansion were studied by
C.M. Bender and T.T. Wu, Phys. Rev. **184**, 1231 (1969); Phys. Rev. Lett. **27**, 461 (1971); Phys. Rev. D **7**, 1620 (1973); *ibid.* D **7**, 1620 (1973);
C.M. Bender, J. Math. Phys. **11**, 796 (1970);
T. Banks and C.M. Bender, J. Math. Phys. **13**, 1320 (1972);
J.J. Loeffel and A. Martin, Cargèse Lectures on Physics (1970);
D. Bessis ed., Gordon and Breach, New York 1972, Vol. 5, p.415;
B. Simon, Ann. Phys. (N.Y.) **58**, 76 (1970); Cargèse Lectures on Physics (1970), D. Bessis ed., Gordon and Breach, New York 1972, Vol. 5, p. 383.

The problem of tunneling at low barriers (*sliding*) was solved by
H. Kleinert, Phys. Lett. B **300**, 261 (1993) (*ibid.*`http/214`).
See also Chapter 17. Some of the present results are contained in
H. Kleinert, *Pfadintegrale in Quantenmechanik, Statistik und Polymerphysik*, B.-I. Wissenschaftsverlag, Mannheim, 1993.

A variational approach to tunneling is also used in chemical physics:
M.J. Gillan, J. Phys. C **20**, 362 (1987);
G.A. Voth, D. Chandler, and W.H. Miller, J. Chem. Phys. **91**, 7749 (1990);
G.A. Voth and E.V. OGorman, J. Chem. Phys. **94**, 7342 (1991);
G.A. Voth, Phys. Rev. A **44**, 5302 (1991).

Variational approaches without the separate treatment of x_0 have been around in the literature

for some time:
T. Barnes and G.I. Ghandour, Phys. Rev. D **22**, 924 (1980);
B.S. Shaverdyan and A.G. Usherveridze, Phys. Lett. B **123**, 316 (1983);
K. Yamazaki, J. Phys. A **17**, 345 (1984);
H. Mitter and K. Yamazaki, J. Phys. A **17**, 1215 (1984);
P.M. Stevenson, Phys. Rev. D **30**, 1712 (1985); D **32**, 1389 (1985);
P.M. Stevenson and R. Tarrach, Phys. Lett. B **176**, 436 (1986);
A. Okopinska, Phys. Rev. D **35**, 1835 (1987); D **36**, 2415 (1987);
W. Namgung, P.M. Stevenson, and J.F. Reed, Z. Phys. C **45**, 47 (1989);
U. Ritschel, Phys. Lett. B **227**, 44 (1989); Z. Phys. C **51**, 469 (1991);
M.H. Thoma, Z. Phys. C **44**, 343 (1991);
I. Stancu and P.M. Stevenson, Phys. Rev. D **42**, 2710 (1991);
R. Tarrach, Phys. Lett. B **262**, 294 (1991);
H. Haugerud and F. Raunda, Phys. Rev. D **43**, 2736 (1991);
A.N. Sissakian, I.L. Solovtsov, and O.Y. Shevchenko, Phys. Lett. B **313**, 367 (1993).

Different applications of variational methods to density matrices are given in
V.B. Magalinsky, M. Hayashi, and H.V. Mendoza, J. Phys. Soc. Jap. **63**, 2930 (1994);
V.B. Magalinsky, M. Hayashi, G.M. Martinez Peña, and R. Reyes Sánchez, Nuovo Cimento B **109**, 1049 (1994).

The particular citations in this chapter refer to the publications

[1] H. Kleinert, Phys. Lett. A **173**, 332 (1993) (quant-ph/9511020).

[2] The energy eigenvalues of the anharmonic oscillator are taken from
F.T. Hioe, D. MacMillan, and E.W. Montroll, Phys. Rep. **43**, 305 (1978); W. Caswell, Ann. Phys. (N.Y.) **123**, 153 (1979); R.L. Somorjai, and D.F. Hornig, J. Chem. Phys. **36**, 1980 (1962).
See also
K. Banerjee, Proc. Roy. Soc. A **364**, 265 (1978);
R. Balsa, M. Plo, J.G. Esteve, A.F. Pacheco, Phys. Rev. D **28**, 1945 (1983);
and most accurately
F. Vinette and J. Cizek, J. Math. Phys. **32**, 3392 (1991);
E.J. Weniger, J. Cizek, J. Math. Phys. **34**, 571 (1993).

[3] R.P. Feynman, *Statistical Mechanics*, Benjamin, Reading, 1972, Section 3.5.

[4] M. Hillary, R.F. O'Connell, M.O. Scully, and E.P. Wigner, Phys. Rep. **106**, 122 (1984).

[5] H. Kleinert, Phys. Lett. A **118**, 267 (1986) (*ibid.*`http/145`).

[6] For a detailed discussion of the effective classical potential of the Coulomb system see
W. Janke and H. Kleinert, Phys. Lett. A **118**, 371 (1986) (*ibid.*`http/153`).

[7] C. Kouveliotou et al., Nature **393**, 235 (1998); Astroph. J. **510**, L115 (1999);
K. Hurley et al., Astroph. J. **510**, L111 (1999);
V.M. Kaspi, D. Chakrabarty, and J. Steinberger, Astroph. J. **525**, L33 (1999);
B. Zhang and A.K. Harding, (astro-ph/0004067).

[8] The perturbation expansion of the ground state energy in powers of the magnetic field B was driven to high orders in
J.E. Avron, B.G. Adams, J. Cizek, M. Clay, M.L. Glasser, P. Otto, J. Paldus, and E. Vrscay, Phys. Rev. Lett. **43**, 691 (1979);
B.G. Adams, J.E. Avron, J. Cizek, P. Otto, J. Paldus, R.K. Moats, and H.J. Silverstone, Phys. Rev. A **21**, 1914 (1980).
This was possible on the basis of the dynamical group O(4,1) and the tilting operator (13.186) found by the author in his Ph.D. thesis. See

H. Kleinert, *Group Dynamics of Elementary Particles*, Fortschr. Physik **6**, 1 (1968) (*ibid.*http/1);
H. Kleinert, *Group Dynamics of the Hydrogen Atom*, Lectures in Theoretical Physics, edited by W.E. Brittin and A.O. Barut, Gordon and Breach, N.Y. 1968, pp. 427-482 (*ibid.*http/4).

[9] Precise numeric calculations of the ground state energy of the hydrogen atom in a magnetic field were made by
H. Ruder, G. Wunner, H. Herold, and F. Geyer, *Atoms in Strong Magnetic Fields* (Springer-Verlag, Berlin, 1994).

[10] M. Bachmann, H. Kleinert, and A. Pelster, Phys. Rev. A **62**, 52509 (2000) (quant-ph/0005074), Phys. Lett. A **279**, 23 (2001) (quant-ph/000510).

[11] L.D. Landau and E.M. Lifshitz, *Quantum Mechanics*, Pergamon, London, 1965.

[12] J.C. LeGuillou and J. Zinn-Justin, Ann. Phys. (N.Y.) **147**, 57 (1983).

[13] W. Janke and H. Kleinert, Phys. Rev. Lett. **75**, 2787 (1995) (quant-ph/9502019).

[14] The high accuracy became possible due to a scaling relation found in
W. Janke and H. Kleinert, Phys. Lett. A **199**, 287 (1995) (quant-ph/9502018).

[15] For the proof of the exponentially fast convergence see
H. Kleinert and W. Janke, Phys. Lett. A **206**, 283 (1995) (quant-ph/9502019);
R. Guida, K. Konishi, and H. Suzuki, Ann. Phys. **249**, 109 (1996) (hep-th/9505084).
The proof will be given in Subsection 17.10.5.

[16] The oscillatory behavior around the exponential convergence shown in Fig. 5.22 was explained in
H. Kleinert and W. Janke, Phys. Lett. A **206**, 283 (1995) (quant-ph/9502019)
in terms of the convergence radius of the strong-coupling expansion (see Section 5.15).

[17] H. Kleinert, Phys. Rev. D **60** , 085001 (1999) (hep-th/9812197); Phys. Lett. B **463**, 69 (1999) (cond-mat/9906359).
See also Chapters 19–20 in the textbook
H. Kleinert and V. Schulte-Frohlinde, *Critical Properties of* Φ^4*-Theories*, World Scientific, Singapore 2001 (*ibid.*http/b8)

[18] H. Kleinert, Phys. Lett. A **207**, 133 (1995).

[19] See for example the textbooks
H. Kleinert, *Gauge Fields in Condensed Matter*, Vol. I Superflow and Vortex Lines, Vol. II Stresses and Defects, World Scientific, Singapore, 1989 (*ibid.*http/b1).

[20] R.P. Feynman, Phys. Rev. **97**, 660 (1955).

[21] S. Höhler and A. Müllensiefen, Z. Phys. *157*, 159 (1959); M.A. Smondyrev, Theor. Math. Fiz. *68*, 29 (1986); O.V. Selyugin and M.A. Smondyrev, Phys. Stat. Sol. (b) *155*, 155 (1989).

[22] N.N. Bogoliubov (jun) and V.N. Plechko, Teor. Mat. Fiz. [Sov. Phys.-Theor. Math. Phys.], **65**, 423 (1985); Riv. Nuovo Cimento *11*, 1 (1988).

[23] S.J. Miyake, J. Phys. Soc. Japan, **38**, 81 (1975).

[24] J.E. Avron, I.W. Herbst, B. Simon, Phys. Rev. A **20**, 2287 (1979).

[25] I.D. Feranshuk and L.I. Komarov, J. Phys. A: Math. Gen. **17**, 3111 (1984).

[26] H. Kleinert, W. Kürzinger, and A. Pelster, J. Phys. A: Math. Gen. **31**, 8307 (1998) (quant-ph/9806016).

[27] H. Kleinert, Phys. Lett. A **173**, 332 (1993) (quant-ph/9511020).

[28] H. Kleinert, Phys. Rev. D **57**, 2264 (1998) and Addendum: Phys. Rev. D **58**, 107702 (1998).

[29] F.J. Wegner, Phys. Rev. B **5**, 4529 (1972); B *6*, 1891 (1972).

[30] H. Kleinert, Phys. Lett. A **207**, 133 (1995) (quant-ph/9507005).

[31] J. Rössler, J. Phys. Stat. Sol. **25**, 311 (1968).

[32] J.T. Marshall and L.R. Mills, Phys. Rev. B *2*, 3143 (1970).

[33] Higher-order smearing formulas for nonpolynomial interactions were derived in
H. Kleinert, W. Kürzinger and A. Pelster, J. Phys. A **31**, 8307 (1998) (quant-ph/9806016).

[34] The polaron problem is solved in detail in the textbook
R.P. Feynman, *Statistical Mechanics*, Benjamin, New York, 1972, Chapter 8.
Extensive numerical evaluations are found in
T.D. Schultz, Phys. Rev. **116**, 526 (1959);
See also
M. Dineykhan, G.V. Efimov, G. Ganbold, and S.N. Nedelko, *Oscillator Representation in Quantum Physics*, Springer, Berlin, 1995.
An excellent review article is
J.T. Devreese, *Polarons*, Review article in Encyclopedia of Applied Physics, **14**, 383 (1996) (cond-mat/0004497).
This article contains ample references on work concerning polarons in magnetic fields, for instance
F.M. Peeters, J.T. Devreese, Phys. Stat. Sol. B **110**, 631 (1982); Phys. Rev. B **25**, 7281, 7302 (1982);
Xiaoguang Wu, F.M. Peeters, J.T. Devreese, Phys. Rev. B **32**, 7964 (1985);
F. Brosens and J.T. Devreese, Phys. Stat. Sol. B **145**, 517 (1988).
For discussion of the validity of the Jensen-Peierls inequality (5.10) in the presence of a magnetic field, see
J.T. Devreese and F. Brosens, Solid State Communs. **79**, 819 (1991); Phys. Rev. B **45**, 6459 (1992); Solid State Communs. **87**, 593 (1993);
D. Larsen in *Landau Level Spectroscopy*, Vol. 1, G. Landwehr and E. Rashba (eds.), North Holland, Amsterdam, 1991, p. 109.
The paper
D. Larsen, Phys. Rev. B **32**, 2657 (1985)
shows that the variational energy can lie lower than the exact energy.
The review article by Devreese contains numerous references on bipolarons, small polarons, and polaronic excitations. For instance:
J.T. Devreese, J. De Sitter, M.J. Goovaerts, Phys. Rev. B **5**, 2367 (1972);
L.F. Lemmens, J. De Sitter, J.T. Devreese, Phys. Rev. B **8**, 2717 (1973);
J.T. Devreese, L.F. Lemmens, J. Van Royen, Phys. Rev. B **15**, 1212 (1977);
J. Thomchick, L.F. Lemmens, J.T. Devreese, Phys. Rev. B **14**, 1777 (1976);
F.M. Peeters, Xiaoguang Wu, J.T. Devreese, Phys. Rev. B **34**, 1160 (1986);
F.M. Peeters, J.T. Devreese, Phys. Rev. B **34**, 7246 (1986); B **35**, 3745 (1987);
J.T. Devreese, S.N. Klimin, V.M. Fomin, F. Brosens, Solid State Communs. **114**, 305 (2000).
There exists also a broad collection of articles in
E.K.H. Salje, A.S. Alexandrov, W.Y. Liang (eds.), *Polarons and Bipolarons in High-T_c Superconductors and Related Materials*, Cambridge University Press, Cambridge, 1995.
A generalization of the harmonic trial path integral (5.356), in which the exponential function $e^{-\Omega|\tau-\tau'|}$ at zero temperature is replaced by $f(|\tau-\tau'|)$, has been proposed by
M. Saitoh, J. Phys. Soc. Japan. **49**, 878 (1980),
and further studied by
R. Rosenfelder and A.W. Schreiber, Phys. Lett. A **284**, 63 (2001) (cond-mat/0011332).

In spite of a much higher numerical effort, this generalization improves the ground state energy only by at most 0.1 % (the weak-coupling expansion coefficient −0.012346 in (5.396) is changed to −0.012598, while the strong-coupling coefficients in (5.399) remain unchanged at this level of accuracy. For the effective mass, the lowest nontrivial weak-coupling coefficient of 1^2 in (5.402) is changed by 0.0252 % while the strong-coupling coefficients in (5.403) remain unchanged at this level of accuracy.